A study on growth by tri-halide vapor phase epitaxy for III-nitride and III-sesqui oxide semiconductors

Kentaro Ema

Department of Applied Chemistry

Graduate School of Engineering

Tokyo University of Agriculture and Technology

Contents

Chapter 1. Introduction 5

1.1. **History of crystal growth technique** 5

1.2. **The problem of HVPE and the merit of THVPE** 5

1.3. **Consist of this thesis** 6

Part I 8

Chapter 2. Introduction 9

1.4. **III-nitride semiconductors** 9

1.5. **Progress of III-nitride application** 10

1.6. **The problem of InGaN devices** 11

1.7. **Investigation toward fabrication of InGaN quasi-substrate** 12

1.8. **Outline of Part I** 13

Reference 14

Chapter 3. Experimental procedure and purpose 17

3.1. **Growth technique of InGaN** 17

3.2. **Investigation of InGaN growth by HVPE and THVPE** 18

3.3. **Consideration by thermodynamics for generation of the sources of THVPE** 19

3.4. **Previous studies and problems** 24

3.5. **Purpose of this work** 25

Reference 27

Chapter 4. Influence of intermediate layers on thick InGaN growth using Tri-Halide Vapor Phase Epitaxy 28

4.1. **Introduction** 28

4.2. **Experimental** 29

4.3. Results and discussion 31
4.4. Conclusion 40
4.5. Acknowledgments 40
Reference 42
Chapter 5. Growth of Lattice-Relaxed InGaN Thick Films on Patterned Sapphire Substrates by Tri-Halide Vapor Phase Epitaxy 45
5.1. Introduction 45
5.2. Experimental 47
5.3. Results and discussion 48
5.4. Conclusion 60
5.5. Acknowledgments 61
Reference 62
Chapter 6. Conclusion of Part I 65
Part II 67
Chapter 7. Introduction 68
7.1. III-sesqui oxide semiconductors 68
7.2. Recent progress in β-Ga_2O_3 69
7.3. The problem of β-Ga_2O_3 devices 71
7.4. Outline of Part II 72
Reference 73
Chapter 8. Experimental procedure 76
8.1. Growth technique of β-Ga_2O_3 76
8.2. Investigation of Ga_2O_3 growth by HVPE and THVPE 77
8.3. Consideration by thermodynamics for generation of the sources of THVPE 86

Reference 89

Chapter 9. Homo- and hetero-epitaxial growth of *β*-Gallium Oxide via $GaCl_3$-O_2-N_2 system 91

9.1. Introduction 91

9.2. Experimental 92

9.3. Results and discussion 94

9.4. Conclusion 101

9.5. Acknowledgments 102

Reference 103

Chapter 10. Conclusion of Part II 107

Chapter 11. Discussion throughout Part I and Part II 108

11.1. Reactivity of raw materials 108

11.2. Adsorption behavior of metal trichloride 108

Reference 112

Chapter 12. Conclusion entire this thesis 113

Acknowledgments 115

List of the papers related to this research 116

List of international conference presentations 117

Other contributed presentations 118

Awards 119

Chapter 1. Introduction

1.1. History of crystal growth technique

Semiconductive materials have made great progress in the recent half a century. At first, silicon (Si) and germanium (Ge) were developed for diodes, thyristors, transistors. After Si, various compound semiconductors such as gallium arsenide (GaAs), indium phosphide (InP), and gallium nitride (GaN) and so on were widely developed for the high-frequency device and light-emitting devices. And today, for next-generation power electric devices, GaN, silicon carbide (SiC), and gallium oxide (Ga_2O_3) are now developing.

Along with the progress of semiconductive materials, crystal growth techniques for compound semiconductors have also been developed. Epitaxial wafers of compound semiconductors are commercially fabricated by vapor phase epitaxy (VPE), such as metal-organic vapor phase epitaxy (MOVPE) and halide vapor phase epitaxy (HVPE). MOVPE is a VPE method using metal-organics as precursors and is widely utilized for the growth of compound semiconductors, but HVPE is used for few materials such as GaN and Ga_2O_3 commercially.

1.2. The problem of HVPE and the merit of THVPE

HVPE is a relatively new method using metal monochlorides such as gallium monochloride (GaCl) for the growth of bulk GaN and Ga_2O_3 wafers. Other metal monochlorides, aluminum

monochloride (AlCl) and indium monochloride (InCl), have unique reactivity, e.g., AlCl reacts with quartz reactor. On the other hand, InCl hardly reacted with nitrogen precursor. To expand the possibility of HVPE, tri-halide vapor phase epitaxy (THVPE) using metal trichlorides as precursors of III-nitrides has been suggested. The HVPE method using metal monochloride still has some problems. For example, in GaN, it is challenging to grow an ultra-thick film due to the problem that the diameter shrinks during growth, and in Ga_2O_3, the raw material molecules undergo a gas phase reaction due to the large driving force of growth, reported to cause killer defects. In order to solve these problems, this study proposes the THVPE method using metal trichloride as the raw material molecule. By using metal trichloride as raw material, the issue of GaN diameter reduction can be solved, and InN growth, which was difficult with monochloride, can be achieved, and a mixed crystal substrate of AlN, GaN, and InN can be fabricated. It has also been suggested that the driving force can be widely controlled in the growth of Ga_2O_3, and it is expected that the particle that causes killer defects will be suppressed. By applying THVPE using metal trichloride, the HVPE method can be expected to be applied to more compound semiconductors and has the potential to be commercially used in a wide range of compound semiconductors. Therefore, in this study, in order to expand the industrial application of the HVPE method, the THVPE method is expected to be used to fabricate a mixed crystal substrate of InGaN, which is one of the mixed crystals of nitride semiconductors, and to apply Ga_2O_3 to power devices.

1.3. Consist of this thesis

In this study, to overcome the problems on the growth of InGaN and Ga_2O_3 (details are described later.), THVPE-InGaN and -Ga_2O_3 growth was performed, and the possibility of THVPE was

investigated. This thesis is made of two parts of the growth by THVPE for InGaN and Ga_2O_3. Part I describes the growth of InGaN by THVPE for the fabrication of InGaN quasi-substrate, aiming to further improvement of the InGaN-based light-emitting devices. Using the THVPE method for the growth of InGaN, high-speed growth and high crystalline quality are available compared with the conventional method such as MOVPE. Part II describes the first growth of β-Ga_2O_3 by THVPE for resolving the problems of the growth by HVPE.

Part I

Chapter 2. Introduction

1.4. III-nitride semiconductors

III-nitrides such as AlN, GaN, and InN have the same crystal structure of wurtzite and largely different bandgap energy, 6.2 eV of AlN, 3.4 eV of GaN, and 0.62 eV of InN, respectively.[1-5] AlN and GaN are called wide gap semiconductors (or ultra-wide gap semiconductors) and are expected for next-generation power electronic devices[1,2] due to their superior physical properties such as a high withstand voltage, high electron mobility, and high thermal conductivity, to conventional semiconductive materials, for example, Si, Ge, or GaAs. GaN has already been widely used for various applications such as high-brightness blue light-emitting diodes (LEDs)[3] and high-speed power chargers. InN has high electron mobility, and it is expected for high-frequency devices.[5] Furthermore, these III-nitrides can form alloy crystals such as AlGaN, InGaN, or AlInN, and they can be controlled the bandgap energy by changing their composition in themselves. Especially, InGaN is a ternary alloy semiconductor of InN and GaN, and it can emit and absorb all the visible light by changing the solid composition of InN in itself. Therefore, InGaN is widely used for active layers in high brightness blue LEDs and blue-violet laser diodes (LDs).

Table 2.1. Crystal structure and bandgap of III nitrides.

	AlN	GaN	InN
crystal structure	wurtzite	wurtzite	wurtzite
a	3.112 Å	3.189 Å	3.537 Å
c	4.982 Å	5.185 Å	5.703 Å
α β	120°	120°	120°
γ	90°	90°	90°
Bandgap	6.2 eV	3.4 eV	0.69 eV

1.5. Progress of III-nitride application

Group-III nitride semiconductors, GaN and its related materials, are expected to be applied for optical and electrical devices due to their superior physical property. In particular, InGaN, a ternary alloy of GaN and InN, is focused on as a promising material that can emit and absorb all the visible light by changing the solid composition of InN in itself. Actually, high brightness blue LEDs and blue-violet LDs have been realized using InGaN as an active layer. There are three breakthrough technologies in the invention of the blue LED, high-quality GaN single crystal, p-type GaN layer, and InGaN growth for light emitting layer. First, the breakthrough of realization of high-quality GaN single crystal was realized by introducing a low-temperature AlN buffer layer on a sapphire substrate by I. Akasaki, and H. Amano et al.[6] Second, p-type GaN layer was also realized by electron beam irradiation of Mg-doped GaN by I. Akasaki, and H. Amano et al. [7]. Finally, InGaN growth for light emitting layer was realized by T. Matsuoka et al.,

NIPPON TELEGRAPH AND TELEPHONE CORPORATION (NTT), and T. Nagatomo et al., Shibaura Institute of Technology, at almost the same time by achieving the world's first InGaN crystal with an In composition of 40% or more.[8,9] The points of the technology established by Matsuoka et al. were replacing the carrier gas that carries the raw materials with nitrogen from conventional hydrogen, increasing the supply ratio of the ammonia gas approximately 100 times, and lowering the growth temperature. Furthermore, all three breakthroughs were surprisingly achieved in the late 1980s and early 1990s. Then, in 1993, the world's first blue LED was commercialized by Nakamura et al., Nichia Corporation.[10,11] For these achievements, I. Akasaki, H. Amano, and S. Nakamura were awarded the Nobel Prize in Physics in 2014. Recently, InGaN-based LEDs have been taking place of incandescent light bulbs and fluorescent lamps, and InGaN-based LDs are utilized for recording on Blu-ray Discs, which enable to record larger volume than conventional compact discs (CDs) and digital video discs (DVDs). Additionally, in 2019, a car called All GaN Vehicle using GaN devices as a headlamp, high beam lamp, converter, an inverter, and battery charger was demonstrated by Institute of Materials and Systems for Sustainability (IMaSS), Nagoya University at Tokyo Motor Show 2019.[12] GaN and its related materials have been applied not only for light-emitting devices but also for electronic devices.

1.6. The problem of InGaN devices

InGaN-based light-emitting devices are widely utilized as light sources. However, a decrease in the luminous efficiency of light-emitting devices called the green gap is a serious issue.[13] The optical devices using InGaN have low luminous efficacy in the long-wavelength region caused by the internal electric field derived from self and piezo polarization called quantum-confined

Stark effect (QCSE)[14] due to lattice mismatch in the InGaN/GaN quantum well and the degradation of crystalline quality due to misfit dislocations at the InGaN/GaN interface. Although the entire visible region emission has recently been achieved by InGaN multiple quantum wells (MQWs) grown on an N-polar GaN substrate,[15] the luminous efficiency of the long-wavelength region was still low. Eu doped GaN has a sharp peak of emission around 2.0 eV which is red luminescence at the wavelength of 621 nm.[16] However, Eu doped GaN is inferior in terms of mass production because Eu is one of the rare metals and high cost.

1.7. Investigation toward fabrication of InGaN quasi-substrate

One approach to solve the problem is the fabrication of InGaN quasi-substrate with high crystalline quality. Using the thick InGaN layer as a quasi-substrate, lattice mismatch between the light-emitting layer and the substrate can be reduced. Recently, several reports on buffer layer have been carried out either by molecular beam epitaxy (MBE) or metal-organic vapor phase epitaxy (MOVPE) using an InGaN graded buffer layer,[17] for example, stress relaxed InGaN buffer layer by the generation of misfit dislocations between the GaN substrate and InGaN layer,[18] and an InGaN buffer layer grown on sputtered InGaN directly deposited on sapphire.[19] There are also other growth techniques such as an InGaN layer grown on a GaN template using droplet elimination by radical-beam irradiation,[20] a porous GaN substrate,[21] an InGaN quasi-substrate called InGaNOS by Smart Cut method,[22] and InGaN platelet which is hexagonal InGaN sub-micrometer platelets having an extension of a few hundred nanometers by selective area MOVPE.[23]However, the driving forces for InN deposition by MOVPE and MBE are quite small. Since this small driving force leads to a small growth rate and

compositionally unstable nature in InGaN alloys, fabrication of high crystalline quality thick InGaN layers is difficult by these growth methods.[24-30]

1.8. Outline of Part I

In this thesis of Par I, the first lattice-relaxed thick InGaN growth by THVPE is studied. Part I of this thesis consists of 5 chapters and the contents are as follows:

Chapter 2 describes the details of the experimental procedure and equipment. Selective generation of metal tri-chlorides inside the reactor is discussed by thermodynamic analysis. the author optimized the generation condition of metal tri-chlorides.

In chapter 3, the lattice-relaxed thick InGaN grown on an N-polar freestanding GaN substrate by THVPE is described. The lattice relaxation of the InGaN layer is controlled by the double intermediate InGaN layer, one is grown at a low speed, and the other is grown at a high speed.

Chapter 4 describes the lattice-relaxed thick InGaN with high crystalline quality grown on the pattered sapphire substrates (PSSs). An important role of the GaN intermediate layer between the InGaN epilayer and the PSS to obtain high crystalline quality InGaN layer is described here.

Finally, chapter 5 serves as the summarization and conclusion of Part I.

Reference

[1] M. Feneberg, R.A.R. Leute, B. Neuschl, and K. Thonke, Phys. Rev. B **82**, 075208 (2010).

[2] R. Dingle, D.D. Sell, S.E. Stokowski, and M. Ilegems, Phys. Rev. B **4**, 1211 (1971).

[3] V.Y. Davydov, A.A. Klochikhin, V.V. Emtsev, D.A. Kurdyukov, S.V. Ivanov, V.A. Vekshin, F. Bechstedt, J. Furthmüller, J. Aderhold, J. Graul, A.V. Mudryi, H. Harima, A. Hashimoto, A. Yamamoto, and E.E. Haller, Physca Status Solidi B **234**, 787 (2002).

[4] J. Wu, W. Walukiewicz, K.M. Yu, J.W. Ager III, E.E. Haller, H. Lu, W.J. Schaff, Y. Saito, Y. Nanishi, Appl. Phys. Lett. **80**, 3967 (2002).

[5] T. Matsuoka, H. Okamoto, M. Nakao, H. Harima, E. Kurimoto, Appl. Phys. Lett. **81**, 1246 (2002).

[6] H. Amano, N. Sawaki, I. Akasaki, and Y. Toyoda, Appl. Phys. Lett. **48**, 353 (1986).

[7] H. Amano, M. Kito, K. Hiramatsu, and I. Akasaki, Jpn. J. Appl. Phys. **28**, 2112 (1989).

[8] T. Matsuoka, N. Yoshimoto, T. Sasaki, and A. Katsui, J. Electronic Materials **21**, (1992).

[9] T. Nagatomo, T. Kuboyama, H. Minamino, and O. Otomo, Jpn. J. Appl. Phys. **28**, 1334, (1989).

[10] S. Nakamura, M. Senoh, and T. Mukai, Appl. Phys, Lett. **62**, 2390, (1993).

[11] S. Nakamura, M. Senoh, and T. Mukai, Jpn. J. Appl. Phys. **32**, 8, (1993).

[12] All GaN Vehicle https://www.gan-vehicle.jp/

[13] M.R. Krames, O.B. Shchekin, R.M. Mach, G.O. Mueller, L. Zhou, G. Harbers, and M.G. Craford, J. Disp. Technol. **3**, 160 (2007).

[14] T. Takeuchi, S. Sota, M. Katsuragawa, M. Komori, H. Takeuchi, H. Amano, and I. Akasaki, Jpn. J. Appl. Phys. **36**, L382 (1997).

[15] J. Heikenfeld, M. Garter, D. S. Lee, R. Birkhahn, and A. J. Steckl, Appl. Phys. Lett. **75**, 1189 (1999).

[16] S. Ichikawa, K. Shiomi, T. Morikawa, D. Timmerman, Y. Sasaki, J. Tatebayashi, and Y. Fujiwara, Appl. Phys. Express **14**, 031008 (2021).

[17] K. Hestroffer, F. Wu, H. Li, C. Lund, S. Keller, J.S. Speck, and U.K. Mishra, Semicond. Sci. Technol. **30**, 105015 (2015).

[18] C. Lund, K. Hestroffer, N. Hatui, S. Nakamura, S.P. DenBaars, U.K. Mishra, and S. Keller, Appl. Phys. Express **10**, 111001 (2017).

[19] I.L. Koslow, M.T. Hardy, P.S. Hsu, P.Y. Dang, F. Wu, A. Romanov, Y.R. Wu, E.C. Young, S. Nakamura, J.S. Speck, and S.P. DenBaars, Appl. Phys. Lett. **101**, 121106 (2012).

[20] T. Ohata, Y. Honda, M. Yamaguchi, and H. Amano, Jpn. J. Appl. Phys. **52**, 08JB11 (2013).

[21] S.S. Pasayat, R. Ley, C. Gupta, M.S. Wong, C. Lynsky, Y. Wang, M.J. Gordon, S. Nakamura, S.P. Denbaars, S. Keller, and U.K. Mishra, Appl. Phys. Lett. **116**, 111101 (2020).

[22] T. Yamaguchi, N. Uematsu, T. Araki, T. Honda, E. Yoon, and Y. Nanishi, J. Cryst. Growth **377**, 123 (2013).

[23] A. Even, G. Laval, O. Ledoux, P. Ferret, D. Sotta, E. Guiot, F. Levy, I. C. Robin, and A. Dussaigne, Appl. Phys. Lett. **110**, 262103 (2017).

[24] A. Koukitu, N. Takahashi, T. Taki, and H. Seki, Jpn. J. Appl. Phys. **35**, L673 (1996).

[25] A. Koukitu, N. Takahashi, T. Taki, and H. Seki, J. Cryst. Growth **170**, 306 (1996).

[26] A. Koukitu, and H. Seki, Jpn. J. Appl. Phys. **36**, L750 (1997).

[27] A. Koukitu, N. Takahashi, and H. Seki, Jpn. J. Appl. Phys. **36**, L1136 (1997).

[28] A. Koukitu, and H. Seki, J. Cryst. Growth **189/190**, 13 (1998).

[29] A. Koukitu, T. Taki, N. Takahashi, and H. Seki, J. Cryst. Growth **197**, 99 (1999).

[30] A. Koukitu, N. Takahashi, and H. Seki, J. Cryst. Growth **221**, 743 (2000).

Chapter 3. Experimental procedure and purpose

3.1. Growth technique of InGaN

There are various methods for GaN growth including the liquid phase epitaxy (LPE) and vapor phase epitaxy (VPE). For the bulk GaN growth, the ammonothermal method and Na flux method are used as LPE[1,2] and halide vapor phase epitaxy (HVPE) is used as VPE.[3] However, InGaN cannot be grown by these methods. In an equilibrium system like LPE, the phase separation occurs and the region having different In composition is formed.[4] This is caused by the immiscibility between GaN and InN.[5] Therefore, InGaN growth is possible in a quasi-equilibrium system like VPE. A conventional method for the growth of InGaN is metal-organic vapor phase epitaxy (MOVPE) using organic metals such as tri-ethyl gallium (TEGa) and tri-methyl indium (TMIn) as group III precursors. Typical LED structures are fabricated by MOVPE.[6] However, the growth rate of MOVPE-InGaN is too low to fabricate InGaN templates or free-standing InGaN substrates. Molecular beam epitaxy (MBE), which needs a high vacuum and large equipment, is inferior on thick InGaN growth. In the case of HVPE, according to thermodynamics analysis, the driving force of InN growth using indium mono-chloride is much small and the reaction does not undergo (discussed below). In order to obtain thick InGaN layer for InGaN substrate, a new growth method to overcome these issue is required.

3.2. Investigation of InGaN growth by HVPE and THVPE

Our previous study has proposed the InGaN growth by tri-halide vapor phase epitaxy(THVPE). In the growth by THVPE, metal tri-chlorides are used as sources of group-III, and NH_3 are used as sources of group-V, respectively. **Figure 2.1.** shows the temperature dependence of the equilibrium constant of InGaN and Ga_2O_3 growth by THVPE compared with by HVPE. In the case of InGaN growth, the four kinds of combination of the raw material are considered, GaCl-InCl-NH_3, $GaCl_3$-InCl-NH_3, GaCl-$InCl_3$-NH_3, and $GaCl_3$-$InCl_3$-NH_3 systems. In the cases of GaCl-InCl-NH_3 and $GaCl_3$-InCl-NH_3 systems, the reaction of InCl and NH_3 does not undergo due to the low equilibrium constant at all, and InN does not grow at any temperatures. In the case of the GaCl-$InCl_3$-NH_3 system, it is considered the trans-chlorine reaction occurs, and $GaCl_3$ and InCl are generated, resulting in InN does not grow. Finally, only in the case of $GaCl_3$-$InCl_3$-NH_3 systems, InGaN could be grown at a high temperature where it is advantageous for the crystal growth with high crystalline quality. The chemical reaction formula of GaN and InN growth by HVPE and THVPE is described as follows:

$$\mathrm{GaCl} + \mathrm{NH_3} \rightleftarrows \mathrm{GaN} + \mathrm{HCl} + \mathrm{H_2} \qquad (2\text{-}1)$$

$$\mathrm{InCl} + \mathrm{NH_3} \rightleftarrows \mathrm{InN} + \mathrm{HCl} + \mathrm{H_2} \qquad (2\text{-}2)$$

$$\mathrm{GaCl_3} + \mathrm{NH_3} \rightleftarrows \mathrm{GaN} + 3\mathrm{HCl} \qquad (2\text{-}3)$$

$$\mathrm{InCl_3} + \mathrm{NH_3} \rightleftarrows \mathrm{InN} + 3\mathrm{HCl} \qquad (2\text{-}4)$$

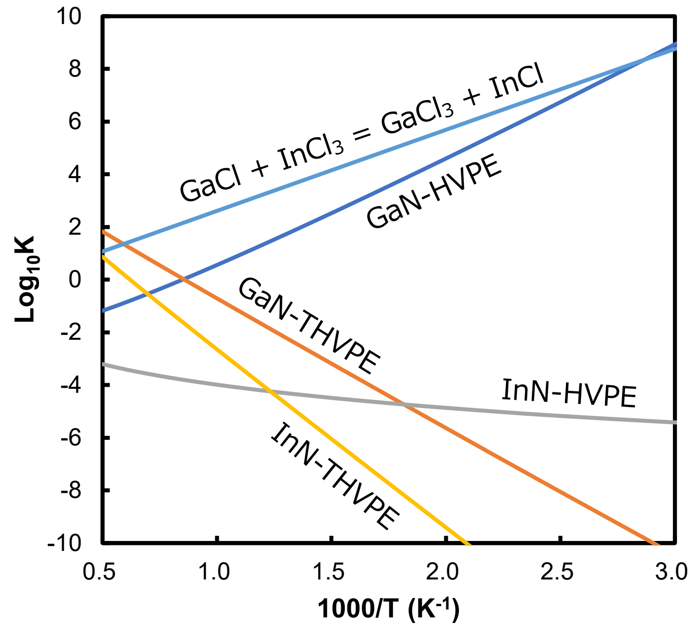

Figure 3.1. The dependence of the equilibrium constant of each reaction on the temperature.

3.3. Consideration by thermodynamics for generation of the sources of THVPE

Figure 2.2. shows the schematics of the generation of group-III precursors by a one-step reaction, and **figure 2.3.** shows the thermodynamics analysis of the temperature dependence of the partial pressure of possible gaseous species in the source zone. In the case of the one-step reaction, it is clearly found that the main products are the metal mono-chlorides almost the entire temperature. A certain amount of gaseous metals (Ga and In) are produced from the surface of the liquid metals as followed by the vapor pressure of them. Therefore, input Cl_2 reacted with gaseous metals priority, and metal mono-chlorides are generated without generation of metal tri-chlorides from the reaction between metal mono-chlorides and Cl_2. Therefore, by the one-step reaction, it is impossible that metal trichlorides are obtained. On the other hand, **figure 2.4.** shows the schematics of the generation of group-III precursors by a two-step reaction using two separated

chambers, one contains metals and is supplied 1st chlorine and the other is only supplied 2nd chlorine. **Figure 2.5.** shows the thermodynamic analysis of the reaction for metal tri-chlorides generation compared with a one-step reaction and a two-step reaction in the source zone. However, in the case of a two-step reaction, it is found that the main products are the metal tri-chlorides at the temperature between 400°C and 900°C. In the 1st chamber, metal mono-chlorides were generated via reaction of metals and Cl_2, and only metal mono-chlorides are introduced into the 2nd chamber. Next, in the 2nd chamber, metal tri-chlorides are generated by the reaction of metal mono-chlorides and 2nd Cl_2. The reactions occurring in the source zone are as follows;

$$\mathrm{M} + \frac{1}{2}\mathrm{Cl_2} \rightarrow \mathrm{MCl} \quad (2\text{-}5)$$

$$\mathrm{MCl} + \mathrm{Cl_2} \rightarrow \mathrm{MCl_3} \quad (2\text{-}6)$$

where M is metal Ga or In. In addition, thermodynamic analysis shows $GaCl_3$ is prior to GaCl the entire temperature till 1200°C, on the other hand, $InCl_3$ is prior to InCl till the temperature of approximately 1000°C. Therefore, the author adopted the temperature of 800°C at the source zone in InGaN growth .

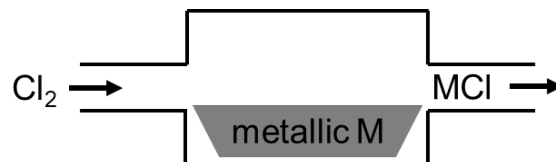

Figure 3.2. The schematics of one-step reaction of the generation of gallium and indium precursors. M is gallium or indium.

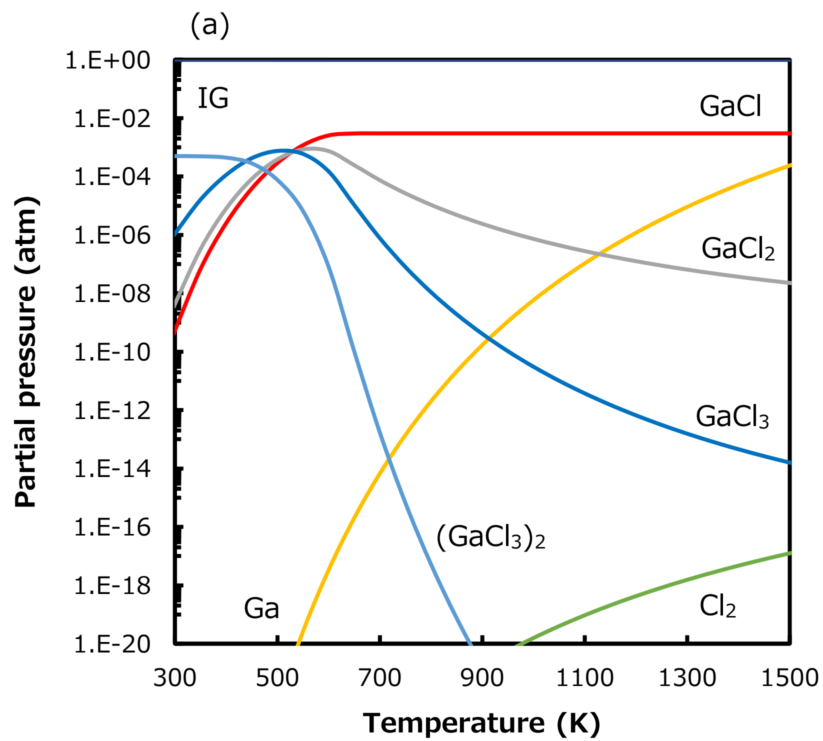

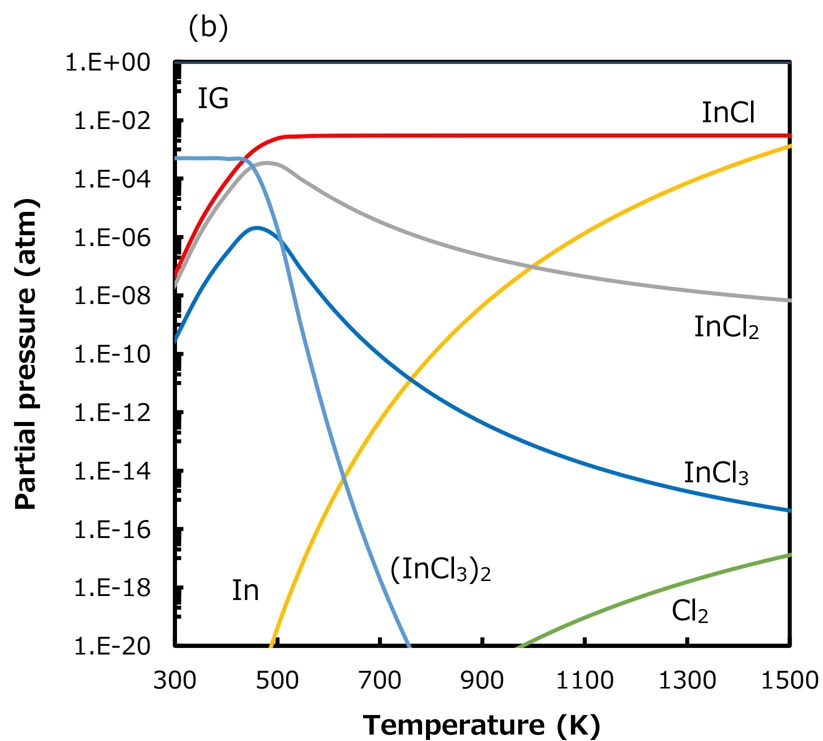

Figure 3.3. The temperature dependence of partial pressure of each gaseous species at one-step reaction of the generation of (a) gallium and (b) indium precursors.

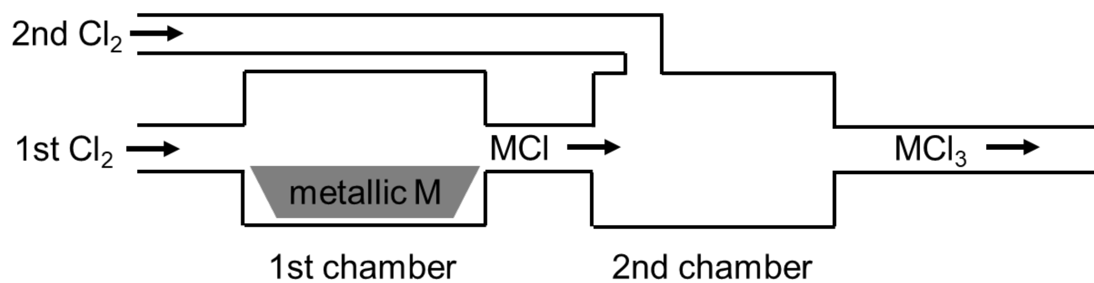

Figure 3.4. The schematics of two-step reaction of the generation of gallium and indium precursors. M is gallium or indium.

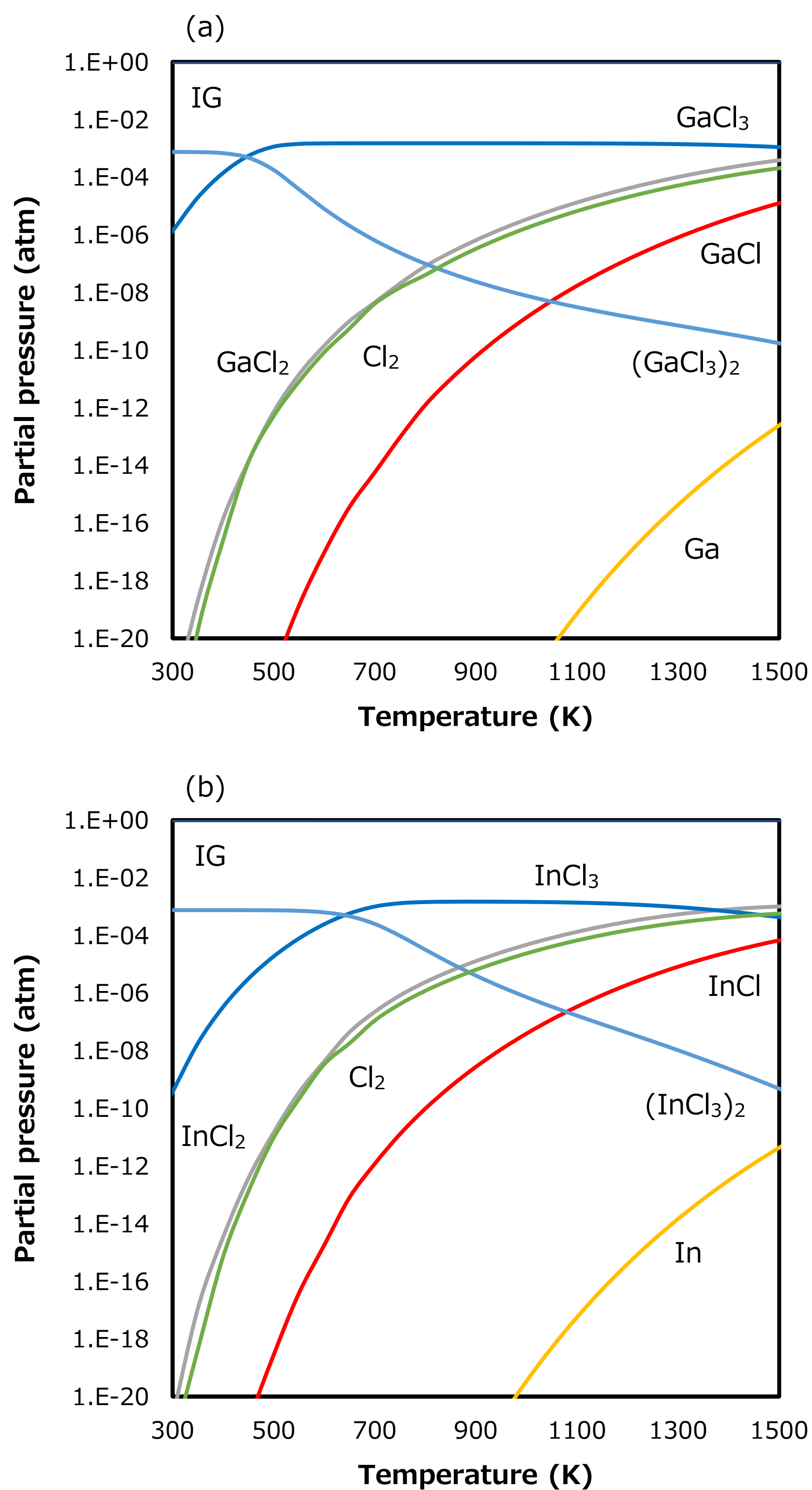

Figure 3.5. The temperature dependence of partial pressure of each gaseous species at two-step reaction of the generation of (a) gallium and (b) indium precursors.

3.4. Previous studies and problems

Previously, our group has proposed thick InGaN growth by THVPE. Our previous study showed that the bulkiness of the THVPE precursors causes unique adsorption behavior on the N-polar GaN substrate and THVPE-InGaN growth has plane selectivity. Then, the growth rate of InGaN on an N-polar GaN substrate of 15.6 μm/h was realized. The In composition could be widely controlled by changing the growth temperature between 650°C and 950°C, and moreover, thick (> 10 μm), high crystalline quality $In_{0.05}Ga_{0.95}N$ growth could be achieved. However, the thick $In_{0.05}Ga_{0.95}N$ layer remains lattice-matched with a GaN bulk substrate. In other words, the *a*-axis of the InGaN layer was the same as that of the GaN substrate.

On the heteroepitaxy, the epilayer grows strained by the substrate at the initial stage. However, when the thickness of the epilayer reaches certain values, the dislocation is introduced at the interface between the epilayer and the substrate because the epilayer could not bear the stress. This thickness is called critical thickness, and this phenomenon is called lattice relaxation. Matthews and Blakeslee theoretically calculated the critical thickness from the mechanical balance on the dislocation,[7] on the other hand, People and Bean also calculated from the energy balance stored in the dislocation.[8] The equations calculated by Matthews and Blakeslee, and People and Bean are described as follows, respectively;

$$h_c = \frac{b}{2\pi f} \cdot \frac{(1-\nu cos^2\alpha)}{(1+\nu)cos\lambda} \cdot (ln\frac{h_c}{b} + 1) \quad (2\text{-}7)$$

$$h_c = \frac{1-\nu}{1+\nu} \cdot \frac{1}{16\pi\sqrt{2}} \cdot \frac{b^2}{a} \cdot \frac{1}{f^2} \cdot ln\frac{h_c}{b} \quad (2\text{-}8)$$

where h_c is the critical thickness, b is the magnitude of buggers vector, ν is Poisson's ratio, f is

the lattice mismatch, α is the angle between dislocation and buggers vector, and λ is the angle between the slip plane and the epilayer-substrate interface. According to these equations, the critical thickness of the InGaN epilayer with In composition of 10% grown on the GaN substrate is several dozen of nanometers. However, our previous study reported several micrometers thick of InGaN epilayer with a coherent state on the GaN substrate. Using the InGaN thick layer as a quasi-substrate for optoelectronic devices, the lattice relaxation of InGaN must be required. On the other hand, the relaxation state of InGaN divides three-state, fully relax, partially relax, and coherent (strained). The relaxation ratio of the InGaN layer against the GaN substrate oriented to the *c*-plane is given by the following equation.

$$R = \frac{a_{epi} - a_{GaN}}{a_{InGaN} - a_{GaN}} \quad (2\text{-}9)$$

Where R is the relaxation ratio, a_{epi} is the real in-plane lattice constant of the InGaN epilayer, a_{InGaN} is the ideal in-plane lattice constant of InGaN, and a_{GaN} is the ideal in-plane lattice constant of GaN. In order to obtain the lattice relaxed InGaN layer with a high crystalline quality, controlling the relaxation ratio is needed.

3.5. Purpose of this work

In this study, to fabricate InGaN quasi-substrate, the lattice-relaxation of the InGaN epilayer was investigated by two approaches, one is inserting the intermediate InGaN layers between InGaN epilayer and the N-polar GaN substrate to occur the lattice-relaxation gradually, and the other is using sapphire substrates having larger lattice-mismatch than GaN substrates to occur the lattice-

relaxation intentionally.

Reference

[1] T. Hashimoto, K. Fujito, M. Saito, J.S. Speck, and S. Nakamura, Jpn. J. Appl. Phys. **44**, L1570 (2005).

[2] M. Imanishi, K. Murakami, T. Yamada, K. Kakinouchi, K. Nakamura, T. Kitamura, K. Okumura, M. Yoshimura, and Y. Mori, Appl. Phys. Express **12**, 045508 (2019).

[3] K. Fujito, S. Kubo, H. Nagaoka, T. Mochizuki, H. Namita, and S. Nagao, J. Cryst. Growth **311**, 3011 (2009).

[4] N.A. El-Masry, E.L. Piner, and S.X. Liu, Appl. Phys. Lett. **72**, 40 (1998).

[5] A. Wakahara, T. Tokuda, X.Z. Dang, S. Noda, and A. Sasaki, Appl. Phys. Lett. **71**, 906 (1997).

[6] I. Ho, and G.B. Stringfellow, Appl. Phys. Lett. **69**, 2701 (1996).

[7] J.W. Matthews, and A.E. Blakeslee, J. Cryst. Growth **27**, 118 (1974).

[8] R. People, and J. C. Bean, Appl. Phys. Lett. **47**, 322 (1985).

Chapter 4. Influence of intermediate layers on thick InGaN growth using Tri-Halide Vapor Phase Epitaxy

4.1. Introduction

$In_xGa_{1-x}N$ is a ternary alloy semiconductor of InN and GaN, and it can emit and absorb all the visible light by changing the solid composition of InN in itself. Therefore, InGaN is widely used for active layers in high brightness blue light-emitting diodes (LEDs) and blue-violet laser diodes (LDs). However, degradation of the crystalline quality of the InGaN epilayer called the green gap is a serious issue[1]. The optical devices using InGaN have low luminous efficacy in the long-wavelength region caused by internal electric field derived from piezo polarization due to lattice mismatch in the InGaN/GaN quantum well and degradation of crystalline quality due to misfit dislocations at the InGaN/GaN interface. Although the entire visible region emission has recently been achieved by InGaN multiple quantum wells (MQWs) grown on an N-polar GaN substrate[2], the luminous efficiency of the long-wavelength region was still low.

One approach to solve the problem is the fabrication of InGaN quasi-substrate with high crystalline quality. Using the thick InGaN layer as a quasi-substrate, lattice mismatch between the light-emitting active layer and the substrate can be relieved. Recently, several reports on buffer layer have been carried out either by molecular beam epitaxy (MBE) or metal-organic vapor phase epitaxy (MOVPE) using an InGaN graded buffer layer[3,4], for example, stress relaxed InGaN buffer layer by the generation of misfit dislocations between the GaN substrate and InGaN layer[5], and an InGaN buffer layer grown on sputtered InGaN directly deposited on

sapphire[6]. There are also other growth techniques such as an InGaN layer grown on a GaN template using droplet elimination by radical-beam irradiation[7], or an InGaN quasi-substrate called InGaNOS[8]. However, the driving forces for InN deposition by MOVPE and MBE are quite small. Since this small driving force leads to a small growth rate and compositionally unstable nature in InGaN alloys, fabrication of high crystalline quality thick InGaN layers is difficult by these growth methods [9-15].

Recently, we proposed thick InGaN growth with high crystalline quality using Tri-Halide Vapor Phase Epitaxy (THVPE). According to the thermodynamic analyses for InGaN growth, metal trichlorides ($GaCl_3$ and $InCl_3$) are suitable for the growth of InGaN alloys with a high growth rate[16-20]. In fact, the growth rate of InGaN on a GaN substrate of 15.6 μm/h was realized[21]. Moreover, thick (> 10 μm), high crystalline quality $In_{0.05}Ga_{0.95}N$ growth could be achieved[22]. However, the thick $In_{0.05}Ga_{0.95}N$ layer remains lattice-matched with a GaN bulk substrate. In other words, the *a*-axis of the InGaN layer was the same as that of the GaN substrate. In order to use the InGaN thick layer as a quasi-substrate for optoelectronic devices, the method for the lattice relaxation of InGaN must be required. In this work, the relationship of growth rate on the surface morphology and lattice relaxation of the InGaN layer was investigated, and then, by changing the growth rate to control the lattice relaxation, the influence of double intermediate layers on the growth of lattice relaxed InGaN layers with In composition of 5% using THVPE was investigated.

4.2. Experimental

InGaN epilayers were grown in a cold-wall type horizontal quartz reactor by THVPE using metal trichlorides ($GaCl_3$ and $InCl_3$) as group-III sources[21,22]. The partial pressure of ammonia, as a

source of group V (P^0_V), was fixed at 4.0×10^{-2} atm in a total pressure of 1.0 atm using N_2 as carrier gas without H_2 gas[23,24]. The total flow rate was 18000 sccm. InGaN layers for all samples were grown on the $(000\bar{1})$ free-standing GaN substrate at 840°C. GaN growth by THVPE has plane selectivity, namely, it can be grown on the $(000\bar{1})$ (N-polar, -c) GaN substrate but cannot be grown on the (0001) (Ga-polar, +c) GaN substrate. This phenomenon was discussed elsewhere[21,25].

At first, two InGaN layers were grown with different growth condition, one is at a low growth rate with $InCl_3$ partial pressure (P^0_{In}) of 4.75×10^{-4} atm, $GaCl_3$ partial pressure (P^0_{Ga}) of 0.25×10^{-4} atm and group III supply ratio ($R_{In} = P^0_{In} / (P^0_{In} + P^0_{Ga})$) of 0.95 and the other is at a high growth rate with $InCl_3$ partial pressure (P^0_{In}) of 2.85×10^{-3} atm, $GaCl_3$ partial pressure (P^0_{Ga}) of 0.15×10^{-3} atm and R_{In} of 0.95, in order to investigate the relationship of growth rate and relaxation. Next, the growth condition of the intermediate InGaN layers for fully relaxed InGaN growth was optimized. The first InGaN layer was grown with the thickness from approximately 50 nm to 400 nm with $InCl_3$ partial pressure (P^0_{In}) of 6.75×10^{-5} atm, $GaCl_3$ partial pressure (P^0_{Ga}) of 0.75×10^{-5} atm and R_{In} of 0.90, and then, second InGaN layer was grown with the fixed thickness of approximately 2.0 μm with $InCl_3$ partial pressure (P^0_{In}) of 3.60×10^{-4} atm, $GaCl_3$ partial pressure (P^0_{Ga}) of 0.40×10^{-4} atm and R_{In} of 0.90, and finally, the topmost InGaN layer was grown with the thickness from approximately 1.0 μm to 3.0 μm with $InCl_3$ partial pressure (P^0_{In}) of 7.5×10^{-5} atm, $GaCl_3$ partial pressure (P^0_{Ga}) of 2.5×10^{-5} atm and R_{In} of 0.75. All samples were fabricated after growing GaN homo-epilayer to prepare a reproducible surface at 1050°C for 60 min with the $GaCl_3$ partial pressure of 5.0×10^{-5} atm.

InGaN layers were analyzed by X-ray diffraction (XRD). The indium solid composition and the relaxation ratio of InGaN epilayers were estimated from reciprocal space mapping (RSM) measurements around the $\bar{1}\bar{1}2\bar{4}$ diffraction by XRD. To confirm the In composition, the optical

characteristics were also measured by cathodoluminescence (CL) measurements at room temperature. The surface morphology and epilayer thickness were observed by field emission - scanning electron microscopy (FE-SEM).

4.3. Results and discussion

4.3.1. Low growth rate and high growth rate InGaN growth on N-polar GaN substrates.

First, in order to confirm the influence of growth rate on the surface morphology and lattice relaxation of the InGaN layer, two kinds of InGaN layer were grown by THVPE with low growth rate and high growth rate. The thickness of each layer was adjusted at approximately 11μm by changing the growth time. Figure 1 shows the bird's eye view SEM images of these two InGaN layers. At a low growth rate, a 10.9-μm-thick InGaN epilayer with a mirror-like surface was obtained. On the other hand, at a high growth rate, 11.2-μm-thick InGaN epilayer with a rough and finger-like structure was obtained.

Figure 2 shows the X-ray RSM at $\overline{1}\overline{1}2\overline{4}$ diffraction of InGaN layers grown with low growth rate and high growth rate. Two lines are drawn in each figure ((a) and (b)). One is a vertical line which is the same Q_x value of GaN substrate, and the other is a diagonal line connecting the coordinates of GaN and InN. When the peak of RSM measurement of the InGaN epilayer lies on the vertical line, it means this InGaN epilayer has the same Q_x value and coherently grew on the GaN substrate. Conversely, when the peak lies on the diagonal line, the InGaN epilayer has its own Q_x value and grew with fully relaxed. If the peak lies between these two lines, the InGaN epilayer grew with partially relaxed. The same lines are also drawn in figure 4 and figure 6. Since the only single peak of the GaN was observed, the GaN homo-epilayer grown before the growth of InGaN layers has the same lattice constant with the GaN substrate according to RSM in figure

2, figure 4, and figure 6. At a low growth rate, the Q_x value of the InGaN epilayer showed almost the same as that of the GaN substrate. This means that the InGaN epilayer grown with a low growth rate had almost the same a-axis lattice constant as the GaN substrate. On the other hand, at a high growth rate, the peak of the InGaN layer shifted to the partially relaxed region. It means that the InGaN epilayer grown at a high growth rate had its own *a*-axis lattice constant different from the GaN substrate. The estimated In the composition of both samples with low growth rate and high growth rate was 4.8% and 4.5%, respectively, and the estimated relaxation ratio of these two samples were 16% and 57%, respectively.

According to the RSM, a thick InGaN layer having a smooth surface at a low growth rate was coherently grown on the $(000\bar{1})$ GaN substrate. This result was completely different from any other previously reported results, both experimental and calculated[26-28]. Further investigation is needed to provide an accurate description of this phenomenon. On the other hand, at a high growth rate, the thick InGaN layer was partially relaxed. Generally, it is well known that the higher the growth rate is, the less the crystalline quality gets due to the generation of defects such as dislocations. This unique characteristic that the growth rate of InGaN epilayer grown by THVPE strongly influences lattice relaxation suggested that it is possible to control the relaxation ratio of the InGaN epilayer by controlling the growth rate of the InGaN layer using THVPE. Furthermore, it is possible to grow a fully relaxed InGaN layer on the intermediate InGaN layers using several InGaN layers grown at different growth rates as intermediate layers.

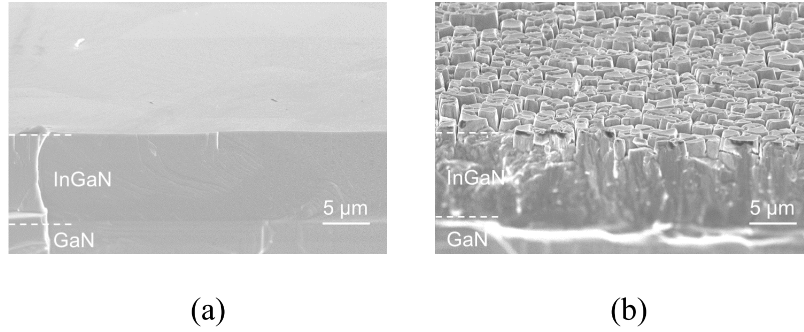

(a) (b)

Figure 4.1. The bird's eye view SEM images of thick InGaN layer (a) with a low growth rate for 360 minutes and (b) with a high growth rate for 60 minutes.

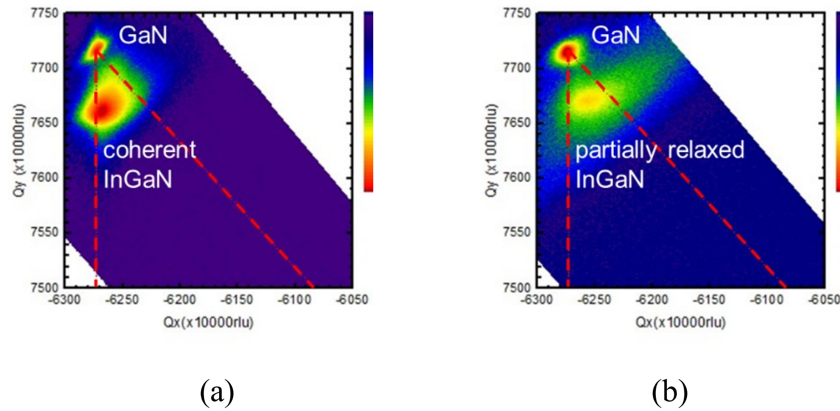

(a) (b)

Figure 4.2. The RSM measurements around the $\overline{1}\overline{1}2\overline{4}$ diffraction of thick InGaN layer (a) with a low growth rate for 360 minutes and (b) with a high growth rate for 60 minutes. Two lines are drawn in each figure ((a) and (b)). One is a vertical line which is the same Q_x value of GaN substrate, and the other is a diagonal line connecting the coordinates of GaN and InN. When the peak of RSM measurement of the InGaN epilayer lies on the vertical line, it means this InGaN epilayer has the same Q_x value and coherently grew on the GaN substrate. Conversely, when the peak lies on the diagonal line, the InGaN epilayer has its own Q_x value and grew with fully relaxed. If the peak lies between these two lines, the InGaN epilayer grew with partially relaxed. The same lines are also drawn in figure 4 and figure 6.

4.3.2. Optimization of intermediate InGaN layers

The thickness of the first InGaN layers grown with a low growth rate was varied to optimize the relaxation ratio under the fixed thickness of the second InGaN layer. The first InGaN layer was coherently grown on the GaN substrate with a low growth rate, following the second InGaN layer was grown with a high growth rate. The role of the first InGaN layer was to control the lattice relaxation of the second InGaN layer. Figure 3 shows the bird's eye view and cross-sectional SEM images of two InGaN layers with the different thickness of the first layer from 50 nm to 400 nm. As seen from the figures, cracking and peeling were observed in the sample of the 50-nm-thick first layer. It was considered that cracking and peeling were caused by compressive stress between the GaN substrate and the InGaN epilayers. In this case, the first InGaN layer was too thin to bear the stress. It was conceived that the stress could be decreased by increasing the thickness of the first layer.

Figure 4 shows the X-ray RSM around the $\overline{1}\overline{1}2\overline{4}$ diffraction of the three samples of InGaN layers grown on the GaN substrates. It was found that the Q_x value changed with the increase of the first InGaN thickness. In addition, it was observed that the peaks of the sample with the first layer thickness of 50 nm are divided into three positions, that is, the coherent position, the partially relaxed position, and the fully relaxed position. As for the samples with the first layer thickness of 200 nm and 400 nm, the peaks of the InGaN layer exist at the partially relaxed position and fully relaxed position. The estimated In composition of the sample of the first layer thickness of 50 nm, 200 nm, and 400 nm was 10.8%, 11.3%, and 10.1% at the partially relaxed position, respectively, and 15.7%, 16.5%, and 16.7% at the fully relaxed position, respectively. The estimated relaxation ratio of each sample was 59%, 32%, and 25% at the partially relaxed position, respectively. According to the RSM measurements, it was found that the position of the

peak of the InGaN layer differs for each sample due to the difference in the thickness of the first InGaN layer. As cracking and peeling were observed in the sample of 50-nm-thick first layer, it was suggested that lattice relaxation occurred in the second InGaN layer, so the peaks at the partially relaxed position and fully relaxed position were second InGaN layer. In the case of 200 nm and 400 nm, there seems to be no peak at the coherent position in the RSM, however, since the growth rate of the first InGaN layer was too low to relax, and the peak of the first InGaN layer was slightly overlapped by that of the second InGaN layer and so thin compared with the second InGaN layer that has weaker intensity, it was thought that the first InGaN layer was coherently grown on GaN substrate. However, since no cracking or peeling was observed, the stress at the second InGaN layer was gradually released. The peak at the partially relaxed position of the sample of the first layer thickness of 400 nm slightly shifted to the coherent region compared with that of 200 nm. Generally speaking, on InGaN growth on a GaN substrate, the thicker the InGaN layer gets, the more lattice relaxation proceeds[26,29,30]. However, in this study, it was considered that lattice relaxation proceeded for the sample of 400 nm less than the sample of 200 nm. This is explained by the difference in the thickness of the first layer of these two samples. The thin first layer could not bear the stress between the GaN substrate and the second InGaN epilayer, so the cracking and peeling were generated and the second InGaN layer drastically relaxed. On the other hand, the thick first layer could bear the stress and the second InGaN layer gradually relaxed. Thus, the partial relaxation proceeded at the sample of 50-nm-thick first layer more than at that of 400-nm-thick, and it was found that the partially relaxed peak position of the sample of 200-nm-thick first layer was lattice-matched to a-axis length of the $In_{0.05}Ga_{0.95}N$. The peak of the fully relaxed position will be discussed below. For the reasons above, the sample of 200-nm-thick first layer, crack free and a-axis lattice-matched with 5% InGaN, was chosen as the intermediate layer for the fully relaxed $In_{0.05}Ga_{0.95}N$ growth.

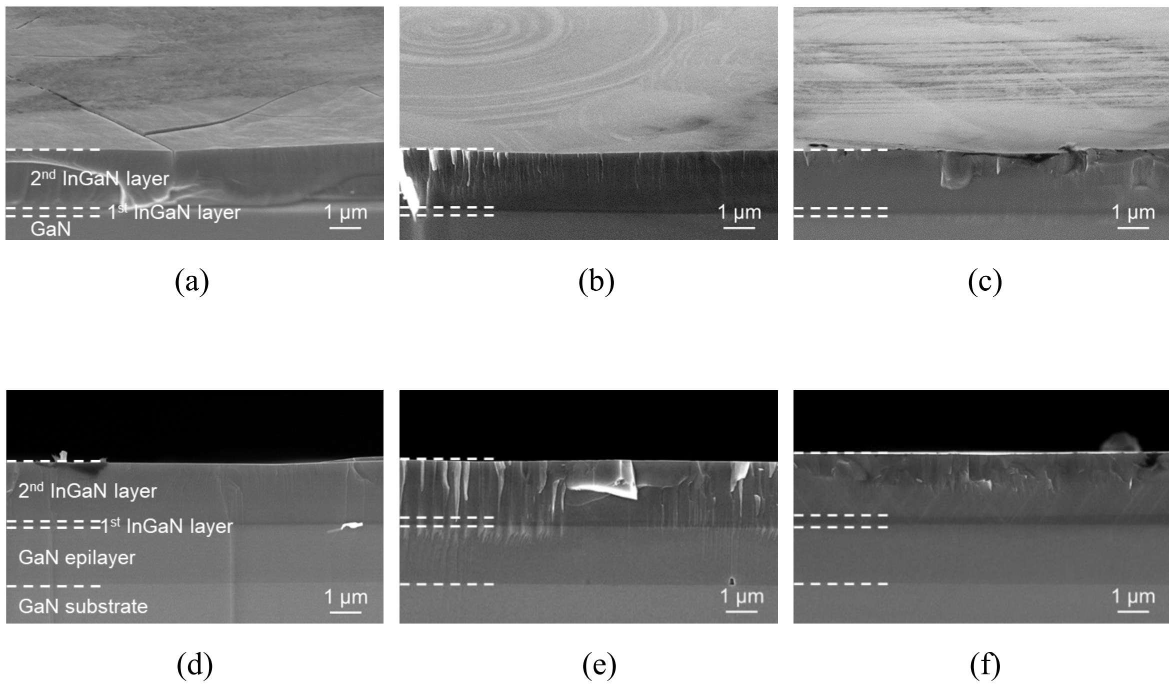

Figure 4.3. The bird's eye view SEM images and the cross-sectional SEM images of two InGaN layers grown on a $(000\bar{1})$ GaN substrate with a low growth rate with the thickness of (a), (d) 50 nm, (b), (e) 200 nm and (c), (f) 400 nm and with a high growth rate with the thickness of 2.0 μm all three samples.

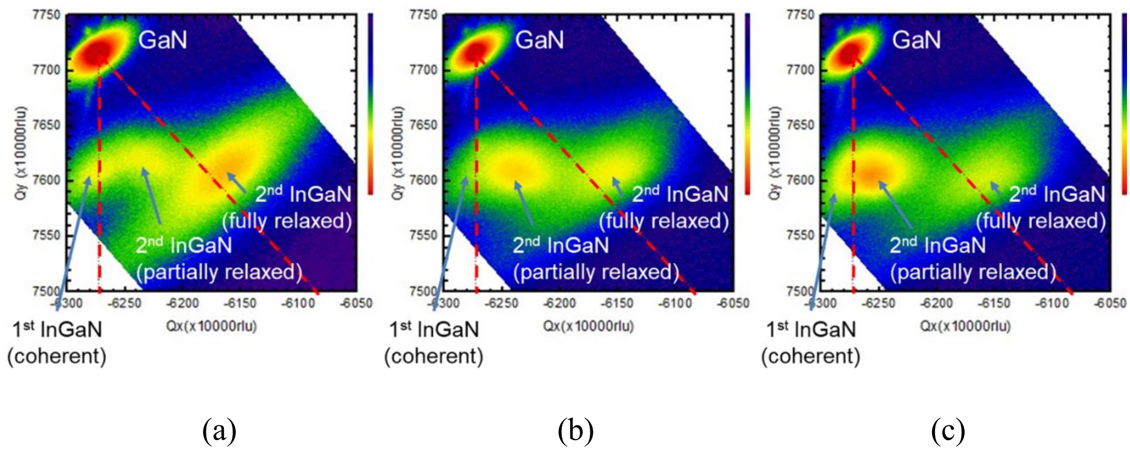

Figure 4.4. The RSM measurements around the $\bar{1}\bar{1}2\bar{4}$ diffraction of two InGaN layers grown

on a $(000\bar{1})$ GaN substrate with a low growth rate with the thickness of (a) 50 nm, (b) 200 nm, and (c) 400 nm and with a high growth rate with the thickness of 2.0 μm all three samples.

4.3.3. Growth of the relaxed thick $In_{0.05}Ga_{0.95}N$

$In_{0.05}Ga_{0.95}N$ was grown on the double intermediate InGaN layers. As shown in figure 5, surface morphology was drastically improved compared with the sample directly grown on the GaN substrate seen in figure 1(b). The thickness of the topmost InGaN layer was approximately 1.1 μm for 60 min growth. The thickness of the topmost layer linearly increased to 2.0 μm in the sample grown for 120 minutes and 3.0 μm in the sample grown for 180 minutes. The surface morphology of the topmost InGaN layer was maintained for 180 minutes of growth.

The RSM around the $\bar{1}\bar{1}2\bar{4}$ diffraction was shown in figure 6. In addition to the peak of the GaN substrate and the InGaN epilayer at the partially relaxed position, a peak was observed at the fully relaxed position with an estimated In composition of 4.8%. As shown in figure 7, the near band edge emission peaking at around 394 nm was observed by CL measurement, which corresponds to the In composition of 6.3% by using the bowing parameter of 1.3[31]. Thus, we succeeded to grow a smooth surface, fully relaxed and thick $In_{0.05}Ga_{0.95}N$ layer by controlling the relaxation ratio of intermediate InGaN layers. Based on the results of RSM measurements, since the value of Q_x in the figure are substantially equal to that of the topmost InGaN layer and the intermediate InGaN layer, it was found that the topmost InGaN layer was grown with lattice-matched on the intermediate InGaN layers. The peak at the fully relaxed position with In composition of 16.5% observed in the sample grown only the intermediate layers disappeared. If the relaxation proceeds in the growth process of the high growth rate intermediate InGaN layer, it is considered that the same peak is observed in figure 6. However, such a peak was not observed

in this sample. It was considered that in the sample in which only the intermediate layer was grown, the relaxation of the high growth rate intermediate layer proceeded during the cooling process after the growth of the intermediate layer. When InGaN is grown on the GaN substrate, compressive stress is accumulated in the InGaN layer due to not only the effect of lattice mismatch but also the large difference in the thermal expansion coefficient between GaN and InN[32]. At the interface between InGaN and GaN, it was thought that compressive stress increased during the cooling process, resulting in a state where relaxation is more likely to proceed. In our case, it was considered that the tensile stress was generated to compensate for the compressive stress, and cracking and peeling were suppressed because In composition of the intermediate InGaN layers is higher than that of the topmost $In_{0.05}Ga_{0.95}N$ layer. From now on, in order to control the lattice relaxation more accurately, it is necessary to study not only the crystal growth condition but also the cooling process.

As shown in figure 5, there was a region where decomposition occurred in the high growth rate intermediate layer. Because this was not observed in the sample shown in figure 3, it was thought that thermal decomposition proceeded during the growth of the topmost InGaN layer due to the higher In composition and low thermal stability at a high temperature around 840 ºC[33,34]. Moreover, since the peak intensity of the topmost InGaN layer observed in the RSM was also small, the crystalline quality of the topmost InGaN layer was thought not to be high. However, since the topmost layer was not decomposed and grown steadily, by optimizing growth condition, it was suggested that a fully relaxed InGaN thick layer could be obtained by inserting the double intermediate InGaN layers with low growth rate and high growth rate.

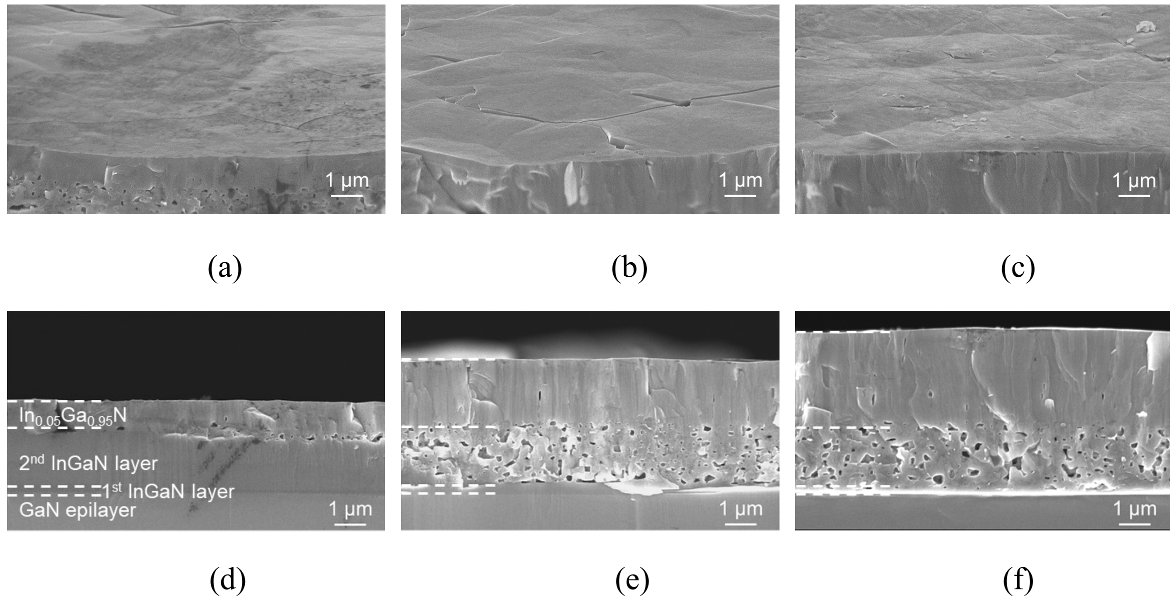

Figure 4.5. The bird's eye view SEM images and the cross-sectional SEM images of three InGaN layers, 200-nm-thick first intermediate layer with a low growth rate, 2.0-μm-thick second intermediate layer with a high growth rate, and the topmost layer for (a), (d) 60 minutes, (b), (e) 120 minutes and (c), (f) 180 minutes.

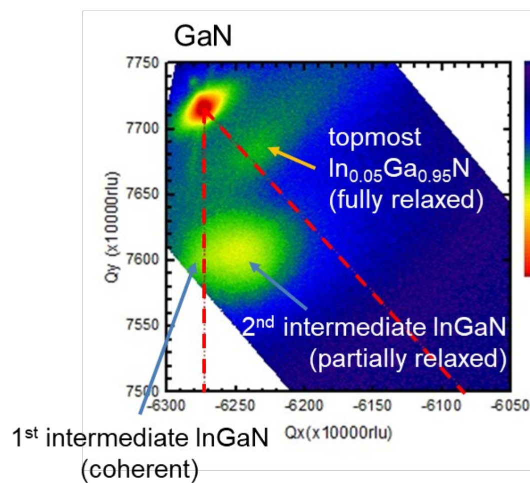

Figure 4.6. The RSM measurements around the $\overline{1}\overline{1}2\overline{4}$ diffraction of three InGaN layers, 200-nm-thick first intermediate layer with a low growth rate, 2.0-μm-thick second intermediate layer with a high growth rate, and the topmost layer for 60 minutes.

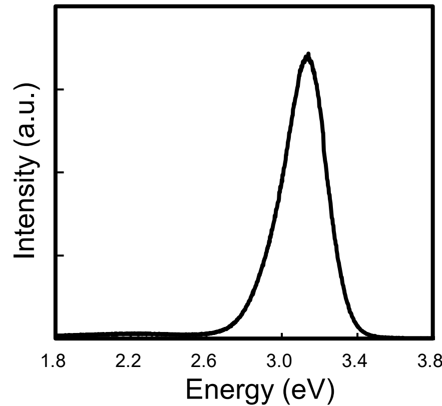

Figure 4.7. The CL measurements of three InGaN layers, 200-nm-thick first intermediate layer with a low growth rate, 2.0-µm-thick second intermediate layer with a high growth rate, and the topmost layer for 60 minutes.

4.4. Conclusion

The influence of intermediate InGaN layers for relaxed InGaN growth using THVPE was investigated. It was found that the difference in growth rate influenced the relaxation ratio of the InGaN layer. We had succeeded to control the relaxation by changing the thickness of the intermediate layer grown with a low growth rate. Moreover, a smooth surface, fully relaxed and thick $In_{0.05}Ga_{0.95}N$ layer was obtained by inserting partially relaxed double intermediate InGaN layers which are grown with low growth rate and high growth rate.

4.5. Acknowledgments

The authors would like to thank Mr. N. Matsumoto and Ms. M. Kawabe of Tokyo University of

Agriculture and Technology for their assistance with the experiments and characterization. This work was partially supported Grants-in-Aid for Scientific Research No. 16K04945 and No. 16H06417 from the Japan Society for the Promotion of Science.

Reference

[1] M.R. Krames, O.B. Shchekin, R.M. Mach, G.O. Mueller, L. Zhou, G. Harbers, and M.G. Craford, J. Disp. Technol. **3**, 160 (2007).

[2] K. Shojiki, T. Tanikawa, J.H. Choi, S. Kuboya, T. Hanada, R. Katayama, and T. Matsuoka, Appl. Phys. Express **8**, 061005 (2015).

[3] K. Hestroffer, F. Wu, H. Li, C. Lund, S. Keller, J.S. Speck, and U.K. Mishra, Semicond. Sci. Technol. **30**, 105015 (2015).

[4] C. Lund, K. Hestroffer, N. Hatui, S. Nakamura, S.P. DenBaars, U.K. Mishra, and S. Keller, Appl. Phys. Express **10**, 111001 (2017).

[5] I.L. Koslow, M.T. Hardy, P.S. Hsu, P.Y. Dang, F. Wu, A. Romanov, Y.R. Wu, E.C. Young, S. Nakamura, J.S. Speck, and S.P. DenBaars, Appl. Phys. Lett. **101**, 121106 (2012).

[6] T. Ohata, Y. Honda, M. Yamaguchi, and H. Amano, Jpn. J. Appl. Phys. **52**, 08JB11 (2013).

[7] T. Yamaguchi, N. Uematsu, T. Araki, T. Honda, E. Yoon, and Y. Nanishi, J. Cryst. Growth **377**, 123 (2013).

[8] A. Even, G. Laval, O. Ledoux, P. Ferret, D. Sotta, E. Guiot, F. Levy, I. C. Robin, and A. Dussaigne, Appl. Phys. Lett. **110**, 262103 (2017).

[9] A. Koukitu, N. Takahashi, T. Taki, and H. Seki, Jpn. J. Appl. Phys. **35**, L673 (1996).

[10] A. Koukitu, N. Takahashi, T. Taki, and H. Seki, J. Cryst. Growth **170**, 306 (1996).

[11] A. Koukitu, and H. Seki, Jpn. J. Appl. Phys. **36**, L750 (1997).

[12] A. Koukitu, N. Takahashi, and H. Seki, Jpn. J. Appl. Phys. **36**, L1136 (1997).

[13] A. Koukitu, and H. Seki, J. Cryst. Growth **189/190**, 13 (1998).

[14] A. Koukitu, T. Taki, N. Takahashi, and H. Seki, J. Cryst. Growth **197**, 99 (1999).

[15] A. Koukitu, N. Takahashi, and H. Seki, J. Cryst. Growth **221**, 743 (2000).

[16] Y. Kumagai, Y. Kubota, T. Nagashima, T. Kinoshita, R. Dalmau, R. Schlesser, B. Moody, J. Xie, H. Murakami, A. Koukitu, and Z. Sitar, Appl. Phys. Express **5**, 055504 (2012).

[17] Y. Kumagai, K. Takemoto, T. Hasegawa, A. Koukitu, and H. Seki, J. Cryst. Growth **231**, 57 (2001).

[18] K. Hanaoka, H. Murakami, Y. Kumagai, and A. Koukitu, J. Cryst. Growth **318**, 441 (2011).

[19] N. Takahashi, R. Matsumoto, A. Koukitu, and H. Seki, Jpn. J. Appl. Phys. **36**, L601 (1997).

[20] N. Takahashi, R. Matsumoto, A. Koukitu, and H. Seki, J. Cryst. Growth **189/190**, 37 (1998).

[21] T. Hirasaki, K. Asano, M. Banno, M. Ishikawa, F. Sakuma, H. Murakami, Y. Kumagai, and A. Koukitu, Jpn. J. Appl. Phys. **53**, 05FL02 (2014).

[22] T. Hirasaki, M. Eriksson, Q.T. Thieu, F. Karlsson, H. Murakami, Y. Kumagai, B. Monemar, P.O. Holtz, and A. Koukitu, J. Cryst Growth **456**, 145 (2016).

[23] A. Koukitu, M. Mayumi, and Y. Kumagai, J. Cryst. Growth **246**, 230 (2002).

[24] M. Mayumi, F. Satoh, Y. Kumagai, K. Takemoto, and A. Koukitu, J. Cryst. Growth **237**, 1143 (2002).

[25] K. Iso, N. Takekawa, K. Matsuda, K. Hikida, N. Hayashida, H. Murakami, and A. Koukitu Appl. Phys. Express **9**, 105501 (2016).

[26] D. Holec, P.M.F.J. Costa, M.J. Kappers, and C.J. Humphreys, J. Cryst. Growth **303**, 314 (2007).

[27] M. Leyer, J. Stellmach, Ch. Meissner, M. Pristovsek, and M. Kneissl, J. Cryst. Growth **310**, 4913 (2008).

[28] W. Zhao, L. Wang, J. Wang, Z. Hao, and Y. Luo, J. Cryst. Growth **327**, 202 (2011).

[29] A.D. Bykhovski, B.L. Gelmont, and M.S. Shur, J. Appl. Phys. **81**, 6332 (1997).

[30] Y. Kawaguchi, M. Shimizu, M. Yamaguchi, K. Hiramatsu, N. Sawaki, W. Taki, H. Tsuda,

N. Kuwano, K. Oki, T. Zheleva, and R.F. Davis, J. Cryst. Growth **189/190**, 24 (1998).

[31] G. Orsal, Y. El. Gmili, N. Fressengeas, J. Streque, R. Djerboub, T. Moudakir, S. Sundaram, A. Ougazzaden, and J.P. Salvestrini, Opt. Mater. Express **4**(5), 1030–1041 (2014).

[32] H. Iwanaga, A. Kunishige, and S. Takeuchi, J. Mater. Sci. **35**, 2451 (2000).

[33] A. Yamamoto, T.M. Hasan, K. Kodama, N. Shigekawa, and M. Kuzuhara, J. Cryst. Growth **419**, 64 (2015).

[34] G.T. Thaler, D.D. Koleske, S.R. Lee, K.H.A. Bogart, and M.H. Crawford, J. Cryst. Growth **312**, 1817 (2010).

Chapter 5. Growth of Lattice-Relaxed InGaN Thick Films on Patterned Sapphire Substrates by Tri-Halide Vapor Phase Epitaxy

5.1. Introduction

Group-III nitride semiconductors, GaN and its related materials, are expected to be applied for optical and electrical devices owing to their superior physical properties. In particular, InGaN, a ternary alloy of GaN and InN, is focused on as a promising material that can emit and absorb all the visible light by changing the solid composition of InN in itself. High-brightness blue light-emitting diodes and blue-violet laser diodes have been realized using InGaN as light-emitting active layers. However, especially in In-rich regions, the degradation of the crystalline quality of InGaN epilayers grown on GaN substrates is a severe issue for achieving high-efficiency light-emitting devices with a longer wavelength. To overcome this problem, several approaches have been proposed, the use of InGaN platelets fabricated by the in-situ annealing of the InGaN pyramids grown on a masked substrate,[1] the porous GaN substrate to grow the InGaN layer with a lattice-relaxed state,[2] and InGaNOS, which is a quasi-substrate fabricated by Smart Cut process using mesa patterned structures.[3] High crystalline quality InGaN layers lattice-matched with light-emitting layers are required for further developments with respect to InGaN-based light-emitting devices.

Previously, several studies for fabricating the InGaN quasi-substrate have been reported. We have proposed thick InGaN growth for fabricating the InGaN quasi-substrate by tri-halide vapor

phase epitaxy (THVPE), a method using metal trichlorides as precursors. The thermodynamic analysis revealed the possibility of higher temperature growth of InGaN by THVPE compared with by metalorganic vapor phase epitaxy (MOVPE).[4-6] We have succeeded in the high-speed InGaN growth at 15.6 μm/h,[7] and 10.9-μm-thick, high-quality $In_{0.05}Ga_{0.95}N$ grown on an N-polar freestanding GaN substrate were obtained at 930°C by THVPE.[8] Recently, several studies on the growth of InGaN on the N-polar GaN substrate were carried out owing to its unique physical or chemical properties, which are different from Ga-polar, e.g., polarization,[9] thermal stability,[10] and impurity incorporation.[11,12] Our focus on using the N-polar GaN substrate is the unique adsorption behavior of adatoms. Our previous study showed that the bulkiness of the THVPE precursors causes unique adsorption behavior on the N-polar GaN substrate[8] and THVPE-InGaN growth (especially GaN growth) has plane selectivity [7,13]. However, the thick InGaN layer was coherently grown, having almost the same *a*-axis length as the GaN substrate. As for the $In_xGa_{1-x}N$ growth on the GaN substrate by THVPE, the lattice mismatch between the substrate crystal and epilayer is relatively small in the region wherein In composition is small ($x < 0.10$), and it has been found that the *a*-axis lattice constant of the InGaN epilayer is easily constrained by the substrate crystal. Fabricating the desired InGaN quasi-substrate for optoelectronic devices, the InGaN epilayer must have a relaxed *a*-axis lattice constant that is not strained by the substrate crystal. Previously, we reported the relationship between the InGaN growth rate and lattice relaxation, and a smooth surface, fully relaxed, and thick $In_{0.05}Ga_{0.95}N$ layer was obtained by inserting the partially relaxed double intermediate InGaN layers with the In composition of approximately 10% that are grown with a low and a high growth rate.[14] However, the intermediate InGaN layers had low thermal stability, and in a long-time growth, thermal decomposition occurred in the intermediate InGaN layers. To grow lattice-relaxed

InGaN epilayers having their relaxed *a*-axis lattice constant free from the restraint of substrates, it is necessary to grow them on substrates having larger lattice mismatch with the InGaN epilayer. In this study, lattice-relaxed InGaN layers were grown by THVPE on sapphire substrates having a larger lattice mismatch than GaN substrates with InGaN epilayers. Furthermore, there are many reports on GaN growth on patterned sapphire substrates (PSSs), and it is well known that the GaN growth on PSSs reduces dislocation densities in GaN epilayers.[15-18] However, there are no reports on thick InGaN growth on PSSs by THVPE. The bulkiness of THVPE precursors may cause unique adsorption behavior on PSSs. Therefore, to obtain lattice-relaxed InGaN epilayers with high crystalline quality, growth on a PSS was also performed.

5.2. Experimental

InGaN layers were grown on an N-polar GaN substrate, a *c*-plane sapphire substrate, and a *c*-plane PSS using $InCl_3$ and $GaCl_3$ as group-III precursors, and NH_3 as the group-V precursor. N_2 gas was used as the carrier gas throughout the entire growth sequence.[19,20] All InGaN layers were grown at the same condition except the substrates. The growth temperature was fixed at 930°C during InGaN growth. The partial pressures of group III precursors and NH_3 were fixed at 7.75×10^{-4} and 2.4×10^{-2} atm, respectively. The input ratio of $InCl_3$ in group-III precursors ($R_{In} = P_{InCl3}/(P_{InCl3} + P_{GaCl3})$) was 0.968, and the InGaN growth time was 60 min. Before the growth on a sapphire substrate, the nitridation of the sapphire surface was performed for 20 min at 1020°C using H_2 gas and the partial pressure of NH_3 was 4.0×10^{-2} atm to obtain reproductivity independent the surface state of the sapphire substrate.[21,22] Moreover, further investigation was carried out by inserting the GaN intermediate layer between an InGaN epilayer and a PSS (GaN/PSS) that was grown at the $GaCl_3$ partial pressure of 5.0×10^{-5} atm and NH_3 partial

pressure of 1.6×10^{-2} atm at a growth temperature of 1030°C. The thickness dependence of the GaN intermediate layer on the InGaN epilayer was also investigated by changing the growth time for 45, 90, 135 min.

InGaN layers were analyzed by X-ray diffraction (XRD) using PANalytical X'Pert PRO MRD. The indium solid composition and relaxation ratio of InGaN epilayers were estimated from reciprocal space mapping (RSM) measurements around the $\bar{1}01\bar{5}$ diffraction by XRD, and the crystalline quality of the InGaN epilayers was evaluated using the full width at half maximum (FWHM) of the XRD ω-rocking curve (XRC) measurements around the $000\bar{4}$ symmetrical reflection and around the $10\bar{1}\bar{2}$ skew-symmetrical reflection. The stress acting on the GaN epilayer was evaluated by Raman spectroscopy using JASCO NRS-3100. To confirm the In composition and In inhomogeneity, the optical characteristics were also measured by photoluminescence (PL) measurements using KIMMON He-Cd laser IK3452R-F (325 nm, 45 mW) at room temperature. The surface morphology and thickness of the epilayers were observed by JEOL JSM-6700F field emission-scanning electron microscope (FE-SEM).

5.3. Results and discussion

5.3.1. Lattice-relaxed InGaN growth on a GaN substrate, a sapphire substrate, and a PSS by THVPE

The InGaN layers were grown directly on an N-polar GaN substrate, a *c*-plane sapphire substrate, and a *c*-plane PSS. Figure 1 shows the RSM around the $\bar{1}01\bar{5}$ diffraction of these InGaN epilayers. The peak of the InGaN epilayer grown on a GaN substrate (shown in Figure 1 (a)) lay on the vertical line, and it was found that the InGaN epilayer had the same Q_x value as the GaN

substrate, namely the same *a*-axis lattice constant. The estimated *a*-axis lattice constants of GaN and InGaN were 3.1907 and 3.1907 Å, respectively, and the estimated *c*-axis lattice constants were 5.1840 and 5.2426 Å, respectively. In other words, the InGaN epilayer grown on a GaN substrate was strained by the substrate. On the other hand, the peaks of the InGaN epilayer grown on a sapphire substrate and a PSS (shown in Figure 1 (b) and (c)) lay on the diagonal lines connecting the bulk GaN $\bar{1}01\bar{5}$ and InN $\bar{1}01\bar{5}$ in reciprocal space, and the InGaN epilayer had relaxed *a*-axis lattice constant. The estimated *a*-axis lattice constant of each InGaN epilayer was 3.22(43) Å and 3.22(25) Å, respectively, and the estimated *c*-axis lattice constant was 5.23(17) Å and 5.22(73) Å, respectively, indicating that the lattice-relaxed InGaN layer was obtained on a sapphire substrate and a PSS. The estimated In compositions were 7.5% for the InGaN epilayer grown on the GaN substrate, 9.8% for that grown on the sapphire substrate, and 9.0% for that grown on the PSS. It was considered that this difference in the In composition between the growth on a GaN substrate and sapphire substrates was due to the composition pulling effect by the coherent growth on the GaN substrate.[23,24] In the case of the growth on the GaN substate, the InGaN epilayer grows coherently. Thus, the In composition decreased compared with the other two samples. According to the bird's-eye-view SEM images in Figure 2, many pits and cracks were observed in the sample grown on a sapphire substrate and PSS. These cracks were generated owing to the large lattice mismatch between epilayers and substrates, and pits were also generated on these micro-cracks in the process of filling the cracks during the growth. The FWHM of XRC measurements around the $000\bar{4}$ symmetrical reflection of the InGaN epilayer grown on the GaN substrate, the sapphire substrate, and the PSS was 93, 4476, and 2961 arcsec, respectively. To grow a lattice-relaxed InGaN epilayer with a high crystalline quality, further investigation was carried out.

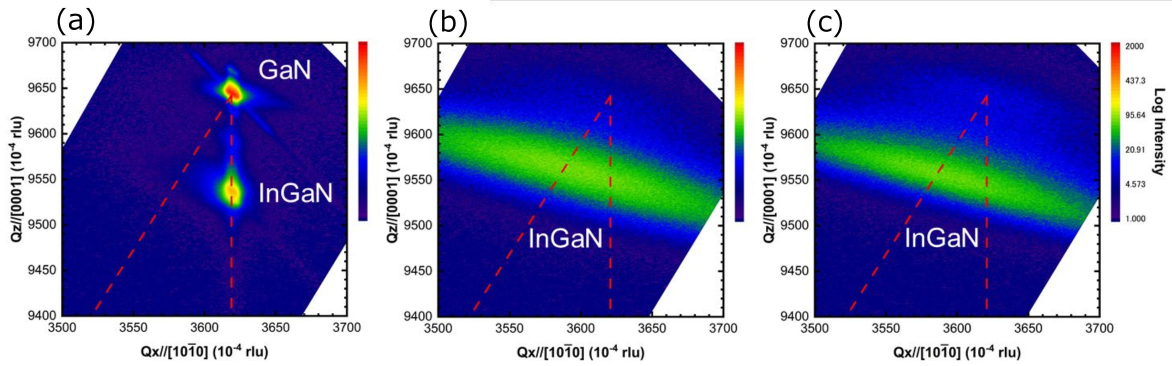

Figure 5.1. RSM around the $\bar{1}01\bar{5}$ diffraction of the three InGaN epilayers grown on (a) an N-polar freestanding GaN substrate, (b) a sapphire substrate, and (c) a PSS. Two lines are drawn in each figure. One is a vertical line which is the Q_x value of the bulk GaN $\bar{1}01\bar{5}$ in reciprocal space, and the other is a diagonal line connecting the bulk GaN $\bar{1}01\bar{5}$ and InN $\bar{1}01\bar{5}$ in reciprocal space. The same lines are also drawn in figure 5.

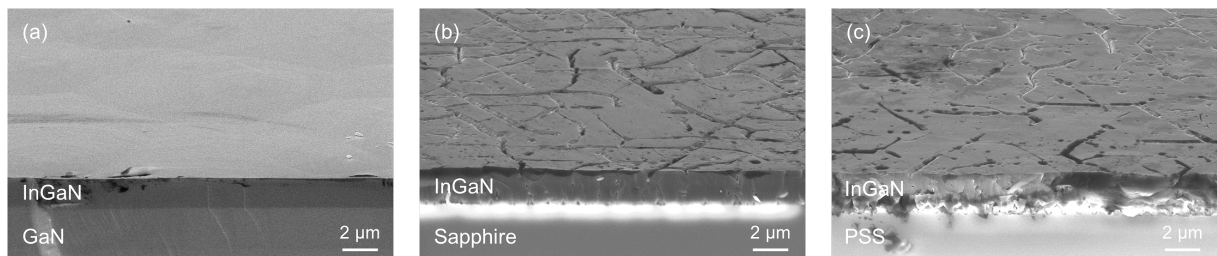

Figure 5.2. Bird's-eye-view SEM images of the InGaN epilayer grown directly on (a) an N-polar freestanding GaN substrate, (b) a sapphire substrate, and (c) a PSS. The InGaN epilayers grown on a sapphire substrate and a PSS had many cracks owing to the large lattice mismatch.

5.3.2. Influence of inserting GaN intermediate layer on the growth of InGaN

Further investigation on inserting a GaN intermediate layer between a InGaN epilayer and a PSS was carried out. Figure 3 shows the bird's-eye-view and cross-sectional SEM images of the samples of a GaN epilayer grown on a PSS and an InGaN epilayer grown on a GaN/PSS. The GaN epilayer had no cracks and smooth surface morphology (shown in Figure 3 (a)). Moreover, in the GaN epilayer, many voids were observed above the cone-shaped pattern on the PSS. On the growth of GaN using sapphire substrates, the GaN epilayer was grown with compressive strain due to the large lattice mismatch between the GaN epilayer and sapphire substrate and the difference in thermal expansion coefficient.[25] However, on the PSS, the GaN epilayer was grown over the cones with forming voids, resulting in these voids relieving the stress in the GaN epilayer. To confirm the influence of the voids, Raman spectroscopy was carried out on the GaN epilayer grown on a sapphire substrate and a PSS. Figure 4 shows the Raman Shift around the E_2 (High) of the GaN epilayer grown on a sapphire substrate and a PSS. The GaN epilayer grown on a sapphire substrate has no voids in the GaN epilayer. On the other hand, that grown on a PSS has a lot of voids. The E_2 (High) peaks of the bulk GaN and GaN epilayers grown on a sapphire substrate and a PSS are 567.8,[26,27] 570.3, 568.7 cm^{-1}, respectively. The E_2 (High) peaks of the two GaN epilayers shifted to a higher wavenumber than the bulk GaN, meaning the compressive stress acted on each GaN epilayer.[28] Furthermore, the peak shift of the GaN epilayer grown on a sapphire substrate was larger than that grown on a PSS, indicating the more significant stress acted on the GaN epilayer grown on a sapphire substrate than that grown on a PSS. Therefore, the voids formed over the corn of PSS relieved the stress acting on the GaN epilayer. Though the stress working on the GaN epilayer is considered to propagate to the following InGaN epilayer, relieving the stress acting on the GaN epilayer with the voids formed on the PSS is also considered to relieve the stress acting on the InGaN epilayer. Therefore, the GaN epilayer was

grown without any cracks on the PSS, and likewise, the InGaN epilayer grown on a GaN/PSS also had no cracks and a smooth surface.

According to the RSM measurements around the $\bar{1}01\bar{5}$ diffraction shown in Figure 5, the estimated In composition of the InGaN epilayer grown on a GaN/PSS were 8.2%, and the estimated relaxation ratio was 81.6%. The InGaN epilayer was almost fully relaxed against the GaN intermediate layer. According to the XRC measurements shown in Figure 6, the FWHM of the InGaN epilayers around the $000\bar{4}$ symmetrical reflection grown on a sapphire substrate, a PSS, and a GaN/PSS was 4476, 2961, and 850 arcsec, respectively, and that around $10\bar{1}\bar{2}$ skew-symmetrical reflection was 6382, 3233, and 967 arcsec, respectively. Compared with the InGaN epilayers grown directly on a sapphire substrate and that on a PSS, the crystalline quality was improved by utilizing a PSS. This is explained by lateral growth. The InGaN epilayer over the cone on a PSS grew in the direction of the surface perpendicular and surface lateral, and in the lateral growth region, InGaN was grown free from the stress of the sapphire substrate, resulting in a lower dislocation density. This phenomenon is well known in the growth of GaN on a PSS.[16] Moreover, compared with the InGaN epilayer grown directly on a PSS, the crystalline quality of the InGaN epilayer grown on a GaN/PSS was drastically improved. This meant that the GaN intermediate layer played as a buffer layer and relieved the stress from sapphire. Therefore, the voids formed in the GaN intermediate layer also relieved the stress acting on the interface between the GaN intermediate layer and the InGaN epilayer. The InGaN epilayer grown directly on a GaN substrate was coherently grown having the same *a*-axis lattice constant as GaN.[14] However, the InGaN epilayer grown on the GaN/PSS had a lattice-relaxed state (shown in Figure 5).

The optical characteristics were investigated by the PL measurements to confirm the In composition and In inhomogeneity. Figure 7 shows the PL spectra of the three InGaN epilayers

grown directly on a sapphire substrate, a PSS, and grown on a GaN/PSS, and Gaussian fitting profiles of InGaN grown directly on a PSS. The PL peak energies of the three InGaN epilayers grown directly on a sapphire substrate, a PSS, and grown on a GaN/PSS were 3.01, 3.11, and 3.02 eV, respectively, and the estimated In compositions were 9.6%, 7.2%, and 9.5%, respectively. The InGaN epilayer grown directly on a PSS had a slightly lower In composition than that grown directly on a sapphire substrate and grown on a GaN/PSS. This was considered to be due to the lateral growth over the cone on the PSS. It is known that the In incorporation is strongly affected by the growth direction.[29,30] In our case, the InGaN epilayer on the PSS grew in different directions depending on the regions, flat-surface region or cone-shaped region. In the flat-surface region, the InGaN epilayer was grown toward the surface perpendicular direction ($-c$ direction), but in the cone-shape region, it was grown toward the surface lateral direction (*a* or *m* direction). Gaussian fitting profiles of the sample grown directly on the PSS show two peaks which have a low In composition (Fitting 1) and a high In composition (Fitting 2). The peak of Fitting 1 (2.98 eV) was almost the same value as that grown directly on a sapphire substrate (3.01 eV) and grown on a GaN/PSS (3.02 eV), and the peak of Fitting 2 (3.13 eV) had a lower In composition, considered to be grown toward different directions by region on a PSS. Furthermore, the FWHM of the PL spectra of the InGaN epilayer grown on a PSS was 485 meV, indicating larger In inhomogeneity. On the other hand, the FWHM of the InGaN epilayer grown on a GaN/PSS was 199 meV, meaning that a more uniform and homogeneous InGaN was successfully obtained. Therefore, the In composition was different by region.

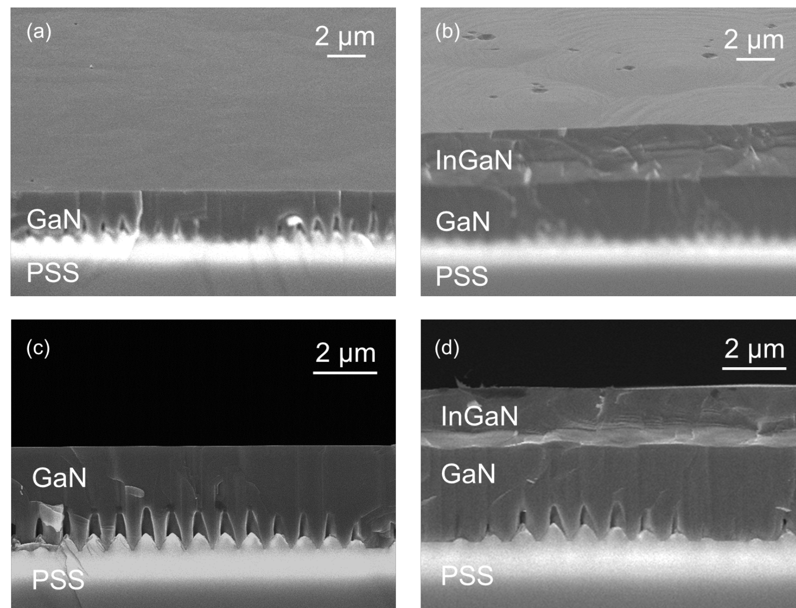

Figure 5.3. SEM images of the two samples of (a) and (c) the GaN/PSS, (b) and (d) the InGaN layer grown on the GaN/PSS. (a) and (b) are bird's-eye-view, and (c) and (d) are cross-sectional. The GaN epilayer grown on the PSS formed voids over the cone.

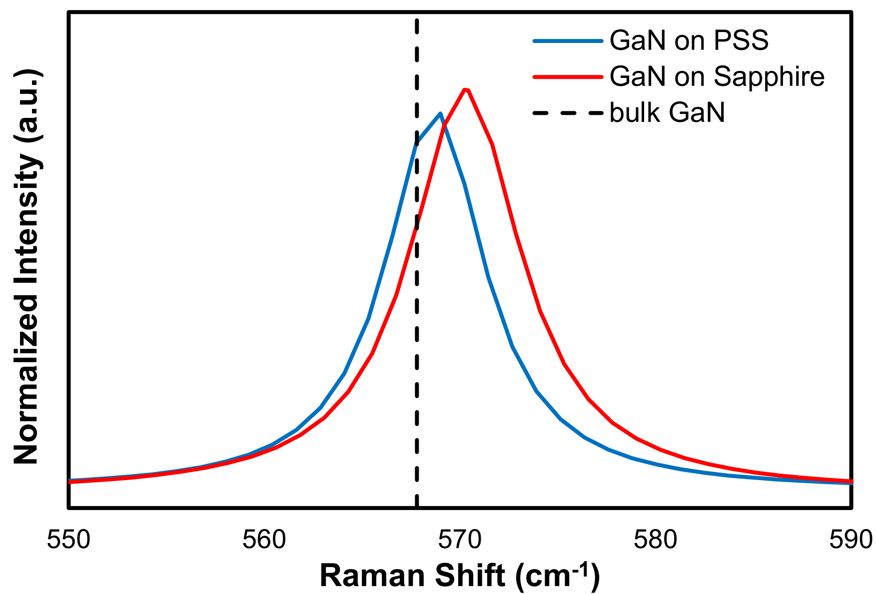

Figure 5.4. Raman shift around the E_2 (High) peak of the two GaN epilayers grown on a sapphire substrate and a PSS. The dashed line shows the E_2 (High) peak of the bulk GaN. The peak of the two GaN epilayers grown on a sapphire substrate and a PSS is 570.6 and 568.7 cm^{-1}, and the peak of the bulk GaN is 567.8 cm^{-1}.[26,27]

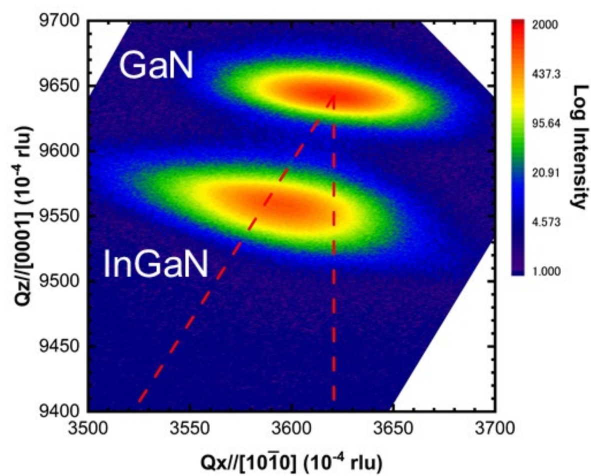

Figure 5.5. RSM around the $\bar{1}01\bar{5}$ diffraction of the InGaN epilayer grown on the GaN/PSS. The InGaN epilayer was grown with lattice-relaxed against the GaN intermediate layer.

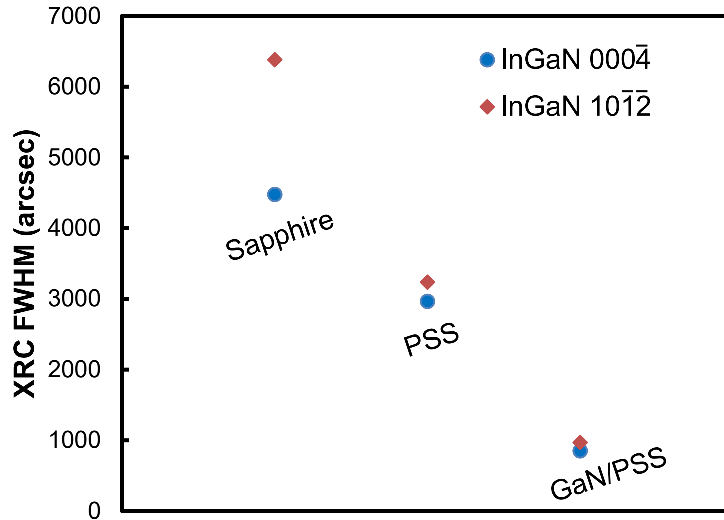

Figure 5.6. FWHMs of XRC measurements of the three InGaN epilayers around the $000\bar{4}$ symmetrical reflection and $10\bar{1}\bar{2}$ skew-symmetrical reflection. The FWHM of each reflection of the InGaN layers grown on a sapphire substrate, a PSS, and a GaN/PSS was 4476, 2961, and 850 arcsec, respectively, and 6382, 3233, and 967 arcsec, respectively.

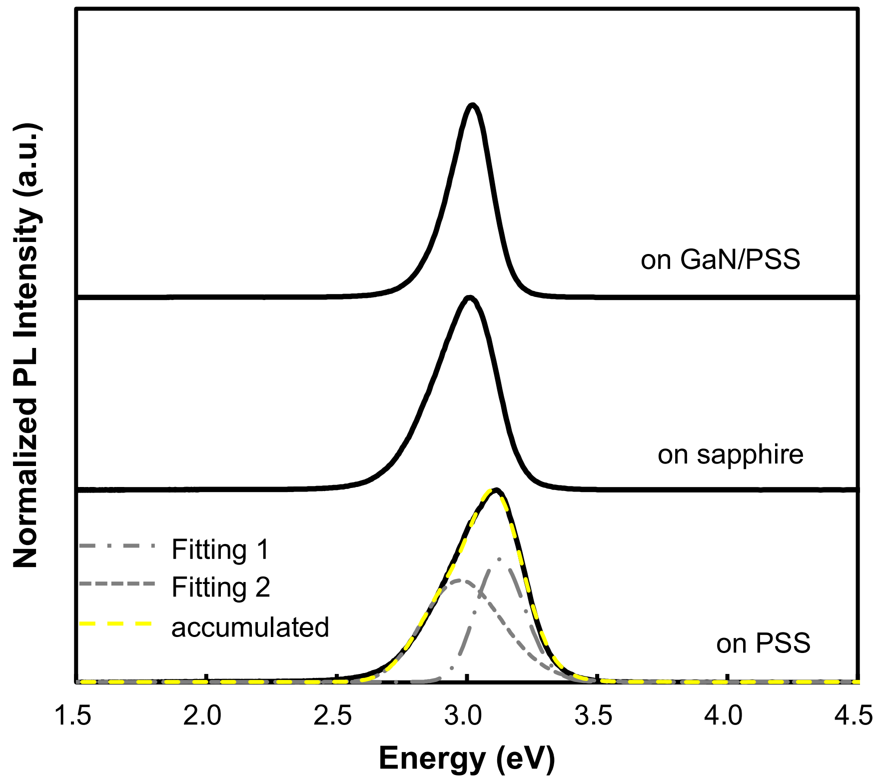

Figure 5.7. PL spectra of the two samples of the InGaN epilayers grown on a sapphire substrate, a PSS, and a GaN/PSS. Dashed lines show the Gaussian fitting profiles of the sample grown directly on a PSS. The PL peak energies of each sample were 3.11 and 3.02 eV, and the FWHMs of the PL spectra of each sample were 485 and 199 meV. Peak shifting to the higher energy was observed in the sample of the InGaN epilayer grown directly on a PSS. The fitting profiles had two peaks, 3.13 (Fitting 1) and 2.98 eV (Fitting 2).

5.3.3. Thickness dependence of the GaN intermediate layer on the crystalline quality of InGaN grown on PSSs

In order to confirm the relationship between the thickness of the GaN intermediate layer and the crystalline quality of the InGaN epilayer, further investigation was performed. Figure 8 shows the bird's-eye-view SEM images of three samples of the InGaN layers grown on GaN/PSSs, adjusting the thickness of the GaN intermediate layer to approximately 1.3, 2.7, and 4.0 μm. Several microcracks were observed in the InGaN epilayer on the GaN intermediate layer with a thickness of 1.3 μm. Because of lateral growth of InGaN caused by not filling the voids in the GaN intermediate layer, the In inhomogeneity increased in the InGaN layer, resulting in the microscopic stress acting on the InGaN epilayer. Therefore, the growth of InGaN was similar to the case of the direct growth on a PSS (shown in Figure 2 (c)). On the other hand, the InGaN epilayers grown on the 2.7-μm-thick and 4.0-μm-thick GaN intermediate layers have no cracks. As the thickness of the GaN intermediate layer increases, the surface morphology was improved. The estimated In compositions from RSM measurements around the $\bar{1}01\bar{5}$ diffraction of the InGaN epilayers grown on the 1.3-, 2.7-, and 4.0-μm-thick GaN intermediate layers were 8.1%, 8.2%, and 8.3%, respectively, and the estimated relaxation ratio of each InGaN epilayer were 86.3%, 81.0%, and 76.6%, respectively. The relaxation ratio was slightly decreased with increasing the thickness of the GaN intermediate layer. This decrease in relaxation ratio was considered to be caused by the state of the GaN intermediate layer approaching the bulk state gradually. According to the XRC measurements around the $000\bar{4}$ symmetrical reflection and $10\bar{1}\bar{2}$ skew-symmetrical reflection, the FWHM of the GaN intermediate layers grown on PSSs were 1132 and 1309 arcsec for 1.3 μm, 827 and 873 arcsec for 2.7 μm, and 681 and 735 arcsec for 4.0 μm, and that of the InGaN epilayers grown on each GaN/PSS were 1306 and 1519 arcsec for 1.3 μm, 850 and 967 arcsec for 2.7 μm, and 727 and 802 arcsec for 4.0 μm (shown in Figure

9). The crystalline quality of the GaN intermediate layer was improved with the increase in the thickness of the GaN intermediate layer, and likewise, the crystalline quality of the InGaN epilayer was also improved with the increase in the thickness of the GaN intermediate layer. Therefore, it is seen that the crystalline quality of the InGaN epilayer was improved by improving the crystalline quality of the GaN intermediate layer, and moreover, the voids formed in the GaN intermediate layer relieved the stress acting on the interface between the GaN intermediate layer and the InGaN epilayer. On the other hand, as the thickness of the GaN intermediate layer increases, the relaxation ratio decreases gradually, and it was considered the influence of the voids on the InGaN epilayer decreases. Therefore, to grow a relaxed InGaN epilayer with a high crystalline quality, adjusting the GaN intermediate layer thickness and the crystalline quality is necessary. Moreover, other approaches such as varying the shape or size of the voids by changing the growth condition or the pattern of PSS may be needed. Furthermore, in this study, all the InGaN epilayers were grown with the same condition. To obtain the InGaN epilayer with a higher crystalline quality, the growth condition of InGaN needs to optimize.

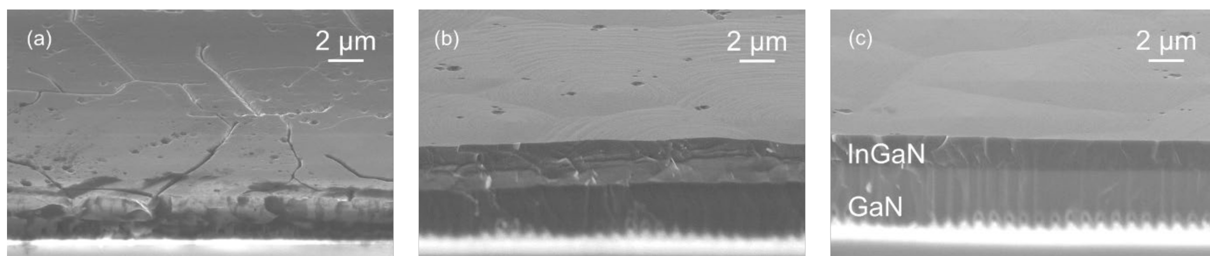

Figure 5.8. Bird's-eye-view SEM images of the three samples of the InGaN layers grown on GaN/PSSs adjusting the thickness of the GaN intermediate layer to approximately (a) 1.3, (b) 2.7, and (c) 4.0 μm. The InGaN epilayer grown on the 1.3-μm-thick GaN intermediate layer has

several microcracks. However, the InGaN epilayers grown on the 2.7- and 4.0-μm-thick GaN intermediate layer has no cracks and smooth surface morphology.

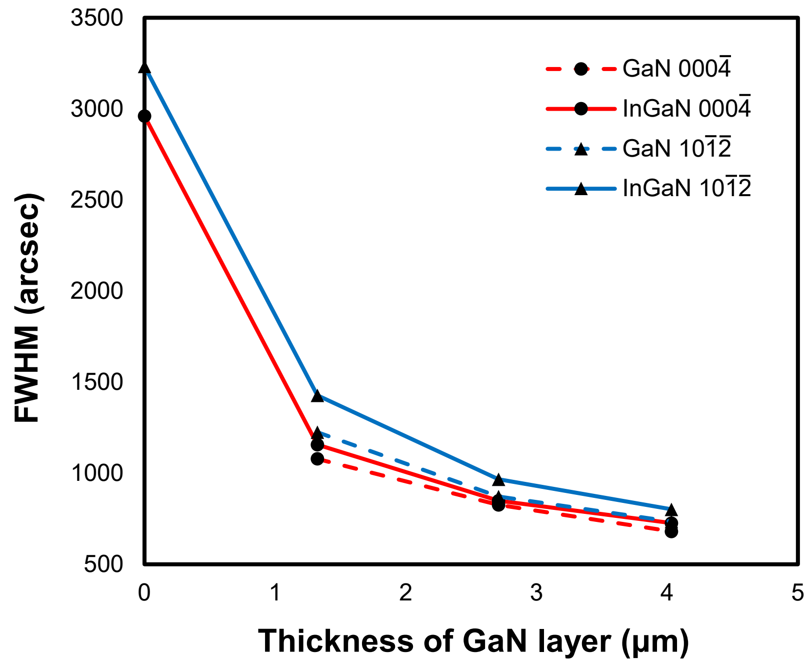

Figure 5.9. Dependence of XRC FWHMs of the GaN and InGaN epilayers around the $000\bar{4}$ symmetrical reflection and $10\bar{1}\bar{2}$ skew-symmetrical reflection on the thickness of the GaN intermediate layer. XRC FWHMs decreased with an increase in the thickness of the GaN intermediate layer.

5.4. Conclusion

In this study, the growth of lattice-relaxed InGaN by THVPE was performed using sapphire substrates having a larger lattice mismatch than GaN substrates. By inserting the GaN

intermediate layer, the lattice-relaxed InGaN was successfully obtained on the PSS with the high crystalline quality compared with the direct growth on the sapphire substrate or the PSS; note that the InGaN epilayer was grown on the PSS still needs improvements for utilizing the InGaN quasi-substrate. Moreover, the dependence of the crystalline quality of the GaN intermediate layer on the InGaN epilayer was also investigated by changing the thickness of the GaN intermediate layer. It was found that the crystalline quality of the InGaN epilayer was affected by that of the GaN intermediate layer.

5.5. Acknowledgments

Part of this work was supported by Grants-in-Aid for Scientific Research No. 16H06417 and No. 19H02614 from the Japan Society for the Promotion of Science and by the Institute of Global Innovation Research, TUAT, Japan.

Reference

[1] Z. Bi, F. Lenrick, J. Colvin, A. Gustafsson, O. Hultin, A. Nowzari, T. Lu, R. Wallenberg, R. Timm, A. Mikkelsen, B.J. Ohlsson, K. Storm, B. Monemar, and L. Samuelson, Nano Lett. **19**, 2832 (2019).

[2] S.S. Pasayat, R. Ley, C. Gupta, M.S. Wong, C. Lynsky, Y. Wang, M.J. Gordon, S. Nakamura, S.P. Denbaars, S. Keller, and U.K. Mishra, Appl. Phys. Lett. **116**, 111101 (2020).

[3] A. Even, G. Laval, O. Ledoux, P. Ferret, D. Sotta, E. Guiot, F. Levy, I. C. Robin, and A. Dussaigne, Appl. Phys. Lett. **110**, 262103 (2017).

[4] Y. Kumagai, Y. Kubota, T. Nagashima, T. Kinoshita, R. Dalmau, R. Schlesser, B. Moody, J. Xie, H. Murakami, A. Koukitu, and Z. Sitar, Appl. Phys. Express **5**, 055504 (2012).

[5] Y. Kumagai, K. Takemoto, T. Hasegawa, A. Koukitu, and H. Seki, J. Cryst. Growth **231**, 57 (2001).

[6] K. Hanaoka, H. Murakami, Y. Kumagai, and A. Koukitu, J. Cryst. Growth **318**, 441 (2011).

[7] T. Hirasaki, K. Asano, M. Banno, M. Ishikawa, F. Sakuma, H. Murakami, Y. Kumagai, and A. Koukitu, Jpn. J. Appl. Phys. **53**, 05FL02 (2014).

[8] T. Hirasaki, M. Eriksson, Q.T. Thieu, F. Karlsson, H. Murakami, Y. Kumagai, B. Monemar, P.O. Holtz, and A. Koukitu, J. Cryst. Growth **456**, 145 (2016).

[9] F. Akyol, D.N. Nath, E. Gür, P.S. Park, and S. Rajan, Jpn. J. Appl. Phys. **50**,052101 (2011).

[10] M.A. Mastro, O.M. Kryliouk, T.J. Anderson, A. Davydov, and A. Shapiro, J. Cryst. Growth **274**, 38 (2005).

[11] N.A. Fichtenbaum, T.E. Mates, S. Keller, S.P. DenBaars, and U.K. Mishra, J. Cryst. Growth **310**, 1124 (2008).

[12] T. Tanikawa, S. Kuboya, and T. Matsuoka, Phys. Status Solidi B **254**, 1600751 (2017).

[13] K. Iso, N. Takekawa, K. Matsuda, K. Hikida, N. Hayashida, H. Murakami, and A. Koukitu Appl. Phys. Express **9**, 105501 (2016).

[14] K. Ema, R. Uei, H. Murakami, and A. Koukitu, Jpn. J. Appl. Phys. **58**, SC1027 (2019).

[15] H.Y. Shin, S.K. Kwon, Y.I. Chang, M.J. Cho, and K.H. Park, J. Cryst. Growth **311**, 4167 (2009).

[16] M.T. Wang, K.Y. Liao and Y.L. Li, IEEE Photonics Technol. Lett. **23**, 962 (2011).

[17] F. Tendille, P.D. Mierry, P. Vennéguès, S. Chenot, and M. Teisseire, J. Cryst. Growth **404**, 177 (2014).

[18] H. Hu, B. Tang, H. Wan, H. Sun, S. Zhou, J. Dai, C. Chen, S. Liu, and L.J. Guo, Nano Energy **69**, 104427 (2020).

[19] A. Koukitu, M. Mayumi, and Y. Kumagai, J. Cryst. Growth **246**, 230 (2002).

[20] M. Mayumi, F. Satoh, Y. Kumagai, K. Takemoto, and A. Koukitu, J. Cryst. Growth **237**, 1143 (2002).

[21] K. Uchida, A. Watanabe, F. Yano, M. Kouguchi, T. Tanaka, and S. Minagawa, J. Appl. Phys. **79**, 3487 (1996).

[22] N. Grandjean, J. Massies, and M. Leroux, Appl. Phys. Lett. **69**, 2071 (1996).

[23] K. Hiramatsu, Y. Kawaguchi, M. Shimizu, N. Sawaki, T. Zheleva, R.F. Davis, H. Tsuda, W. Taki, N. Kuwano, and K. Oki, Materials Research Society Internet Journal of Nitride Semiconductor Research **2**, 6 (1997).

[24] Y. Inatomi, Y. Kangawa, T. Ito, T. Suski, Y. Kumagai, K. Kakimoto, and A. Koukitu, Jpn. J. Appl. Phys. **56**, 078003 (2017).

[25] H. Iwanaga, A. Kunishige, and S. Takeuchi, J. Mater. Sci. **35**, 2451 (2000).

[26] V.Yu. Davydov, Yu.E. Kitaev, I.N. Goncharuk, A.N. Smirnov, J. Graul, O. Semchinova, D. Uffmann, M.B. Smirnov, A.P. Mirgorodsky, and R.A. Evarestov, Phys Rev. B, **58**, 12899 (1998).

[27] N. Kokubo, Y. Tsunooka, F. Fujie, J. Ohara, K. Hara, S. Onda, H. Yamada, M. Shimizu, S. Harada, M Tagawa, and T. Ujihara, Appl. Phys. Express **11**, 061002 (2018).

[28] A. Hushur, M.H. Manghnani, and J. Narayan, J. Appl. Phys. **106**, 054317 (2009).

[29] Y. Zhao, Q. Yan, C.Y. Huang, S.C. Huang, P.S. Hsu, S. Tanaka, C.C. Pan, Y. Kawaguchi, K. Fujito, C.G. Van de Walle, J.S. Speck, S.P. DenBaars, S. Nakamura, and D. Feezell, Appl. Phys. Lett. **100**, 201108 (2012).

[30] D.V. Dinh, M. Pristovsek, and M. Kneissl, Phys. Status Solidi B **253**, 93 (2016).

Chapter 6. Conclusion of Part I

Previous studies on THVPE-InGaN growth revealed that the InGaN epilayer grown on a free-standing N-polar GaN substrate is strongly strained and grown coherently. Therefore, in this study, to fabricate the InGaN quasi-substrate, the growth of InGaN with the lattice-relaxed state was performed by THVPE.

One approach to solve the issue is inserting the intermediate InGaN layers between the GaN substrate and lattice-relaxed InGaN layer with changing the growth rate to proceed with the lattice-relaxation gradually. The influence of intermediate InGaN layers for relaxed InGaN growth using THVPE was investigated. It was found that the difference in growth rate influenced the relaxation ratio of the InGaN layer. We had succeeded to control the relaxation by changing the thickness of the intermediate layer grown with a low growth rate. Moreover, a smooth surface, fully relaxed and thick $In_{0.05}Ga_{0.95}N$ layer was obtained by inserting partially relaxed double intermediate InGaN layers which are grown with low growth rate and high growth rate.

The other approach is utilizing sapphire substrates having larger lattice mismatch than GaN substrates to occur the lattice-relaxation intentionally. However, it was found intentional lattice-relaxation is accompanied by crack generation. Therefore, inserting the GaN intermediate layer was tried to suppress the crack generation. By inserting the GaN intermediate layer, the lattice-relaxed InGaN was successfully obtained on the PSS with the high crystalline quality compared

with the direct growth on the sapphire substrate or the PSS. Moreover, the dependence of the crystalline quality of the GaN intermediate layer on the InGaN epilayer was also investigated by changing the thickness of the GaN intermediate layer. It was found that the crystalline quality of the InGaN epilayer was strongly affected by that of the GaN intermediate layer.

Part II

Chapter 7. Introduction

7.1. III-sesqui oxide semiconductors

III sesqui oxides such as Al_2O_3, Ga_2O_3, and In_2O_3 have several crystal structures and wide bandgap energy. Al_2O_3 shows polymorphism having a lot of phases,[1-9] and *α*-phase, corundum structure, is the most stable known as sapphire. *α*-Al_2O_3 is almost the insulating material having approximately 9 eV of bandgap energy. Therefore, *α*-Al_2O_3 is used as the insulating layer of electronic devices such as field-effect transistor (FET).[10,11] Furthermore, *α*-Al_2O_3 is used as the initial substrate for the growth of various semiconductor materials, AlN, GaN, and those related materials, due to the chemical and thermal stability. Ga_2O_3 also shows polymorphism having *α*-, *β*-, *γ*-, *δ*-, *ε*-, and *κ*-phases,[12-17] where the *β*-phase, monoclinic structure called *β*-Gallia, is the most stable among them. *β*-Ga_2O_3 is expected to be applied to next-generation electronic devices, low-loss, and high withstand voltage power devices,[18-22] due to its excellent physical properties such as a large bandgap of 4.5 eV and a high breakdown electric field [23-26]. There are also several reports that *β*-Ga_2O_3 shows promise as light-emitting devices or light-receiving devices, such as the substrate for blue LEDs or deep ultra-violet photodetectors.[27,28] In_2O_3 has two crystal structures, *α*- and *β*-phase, which is corundum and cubic (bixbyite) structure, respectively,[29,30] and cubic In_2O_3 is the most stable structure of the two. Tin doped In_2O_3 is utilized for transparent conductive films known as indium tin oxide

(ITO)[31] due to its high transparency and low resistance.

Table 7.1. Crystal structure of α-Al_2O_3, β-Ga_2O_3, and c-In_2O_3 for their most stable phase.[32,33]

	α-Al_2O_3	β-Ga_2O_3	c-In_2O_3
crystal structure	corundum	monoclinic	bixbyite
a	4.758 Å	12.21 Å	10.12 Å
b		3.03 Å	
c	12.99 Å	5.79 Å	
α	120°	90°	90°
β		103.8°	
γ	90°	90°	

7.2. Recent progress in β-Ga_2O_3

Table1 6.2. shows the physical properties of several semiconductive materials related to the electric devices. β-Ga_2O_3 is also expected for application to next-generation electronic devices, especially power electronic devices due to its large bandgap energy and high breakdown voltage. **Figure 6.1.** shows the on-resistance at a given reverse breakdown voltage.[34] It is indicated that β-Ga_2O_3 has much superior characteristics for electric devices to conventional Si and even candidate materials such as SiC or GaN. However, β-Ga_2O_3, at first, was developed for applying LEDs or their substrates.[35] Since the possibility for power devices of β-Ga_2O_3 was revealed, many studies were performed rapidly in 2010s. β-Ga_2O_3 is the most stable phase and can be grown by the melt growth technique to obtain the bulk crystal. Therefore, the β-Ga_2O_3 substrate is relatively available and possible to be cost down. The study on β-Ga_2O_3 for power devices began in 2010s by M. Higashiwaki, National Institute of Information and Communications

Technology (NICT), and A. Kuramata, Tamura Corporation at that time. They established Novel Crystal Technology, Inc. and A. Kuramata et al. succeeded in obtaining the bulk β-Ga_2O_3 crystal by edge-difined film-fed growth (EFG) method.[36] Furthermore, in 2014, Y. Kumagai, and H. Murakami et al., Tokyo University of Agriculture and Technology, achieved the homoepitaxial growth of β-Ga_2O_3 layer with high purity and high crystalline quality by HVPE first in the world[37] and demonstrated to fabricate vertical β-Ga_2O_3 Schottky barrier diodes (SBDs).[38] These achievements will be called the breakthrough of the power devices of β-Ga_2O_3 in the future. β-Ga_2O_3 based electronic devices are now developing, for example, n-Ga_2O_3 metal-semiconductor field-effect transistors (MESFETs)[39] or metal-oxide-semiconductor FETs (MOSFETs)[40] on a single-crystal β-Ga_2O_3 (010) substrate, vertical β-Ga_2O_3 Schottky barrier diodes (SBDs) using a drift layer with a record breakdown voltage of 1076 V[21], β-Ga_2O_3 SBDs with a trench MOS structure (MOSSBD) which showed reasonable forward characteristics with small reverse leakage current[22], and so on.

Table 7.2. Physical properties of several semiconductive materials related to the electric devices[41].

Material parameter	Si	GaAs	4H-SiC	GaN	β-Ga_2O_3
Bandgap (eV)	1.1	1.43	3.25	3.4	4.85
Dielectric constant	11.8	12.9	9.7	9	10
Breakdown field (MV/cm)	0.3	0.4	2.5	3.3	8
Electron mobility (cm^2/V・s)	1480	8400	1000	1250	300
Saturation velocity (10^7 cm/s)	1	1.2	2	2.5	1.8-2
Thermal conductivity (W/cm・K)	1.5	0.5	4.9	2.3	0.1-0.3
Baliga's figure of merit	1	14.7	317	846	3214

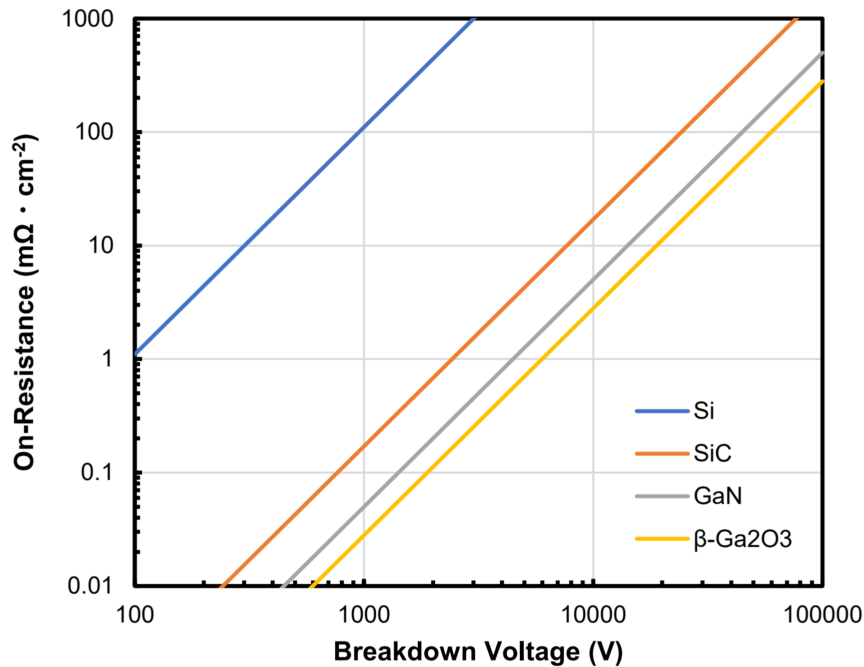

Figure 7.1. Comparison of breakdown voltage and on-resistance in candidate materials for high power electronics.[34]

7.3. The problem of β-Ga_2O_3 devices

Thermodynamic analysis predicted high temperature and high-speed growth of Ga_2O_3 by HVPE [42], and H. Murakami et al. have succeeded in the homoepitaxial growth of high purity β-Ga_2O_3 by HVPE using the GaCl-O_2-N_2 system at 1000°C [37]. K. Goto et al. have also succeeded in the fabrication of vertical β-Ga_2O_3 SBDs with excellent Schottky characteristics using an HVPE-grown drift layer [38] and linear control of the n-type carrier density in the range of 10^{15} to 10^{18} cm^{-3} by changing the Si concentration [38]. However, generally, a critical nuclear radius depends on the driving force of crystal growth, and due to the large driving force of β-Ga_2O_3 growth by HVPE, it was found that GaCl and O_2, precursors of Ga_2O_3 growth, reacted in the gas phase,

resulting in Ga_2O_3 particle formation. Furthermore, many particles were deposited on the substrate, which affects the growth mode change from two-dimensional to three-dimensional. On the other hand, β-Ga_2O_3-MBE growth is also studied widely.[43] However, the growth rate of MBE is much lower than that of HVPE, and to obtain the β-Ga_2O_3 layer having several micrometer thicknesses which are needed to fabricate power device structure is difficult. Therefore, a novel method to grow the β-Ga_2O_3 layer with several micrometer thicknesses and without any particle generation is required.

7.4. Outline of Part II

In this thesis, the first Ga_2O_3 growth by THVPE is demonstrated. This thesis consists of 4 chapters and the contents are as follows:

Chapter 7 describes the details of the experimental procedure and equipment. Selective generation of metal tri-chlorides inside the reactor is discussed by thermodynamic analysis. the author optimized the generation condition of metal tri-chlorides.

Chapter 8 discussed the possibility of Ga_2O_3 growth by THVPE. The first β-Ga_2O_3 growth using gallium tri-chloride as a precursor of gallium source on the c-plane sapphire substrate was investigated and compared with β-Ga_2O_3 growth by HVPE.

Finally, chapter 4 serves as the summarization and conclusion.

Reference

[1] J.R. Walker, and C.R.A. Catlow, and J. Phys. C: Solid State Phys. **15**, 6151 (1982).

[2] G. Oya, M. Yoshida, and Y. Sawada, Appl. Phys. Lett. **51**, 1143 (1987).

[3] Z. Zhang, R.W. Hicks, T.R. Pauly, and T.J. Pinnavaia, J. Am. Chem. Soc. **124**, 1592 (2002).

[4] S.D. Mo, Y.N. Xu, and W.Y. Ching, J. Am. Ceram. Soc. **80**, 1193 (1997).

[5] S.V. Tsybulya, and G.N. Kryukova, Powder Diffraction, **18**, 309 (2003).

[6] L. Kovarik, M. Bowden, D. Shi, J. Szanyi, and C.H.F. Peden, J. Phys. Chem. C **123**, 9454 (2019).

[7] S. Vuorinen, and J. Skogsmo, Thin Solid Films **193**, 536 (1990).

[8] S. Ruppi, and A. Larsson, Thin Solid Films **388**, 50 (2001).

[9] J.A. Kohn, G. Katz, and J.D. Broder, Am. Mineralogist **42**, 398 (1957).

[10] C.H. Shin, S.Y. Cha, H.C. Lee, W.J. Lee, B.G Yu, and D.H. Kwak, Integrated Ferroelectrics **34**, 113 (2001).

[11] X. Zhong, Y. Liua, J. Li, and Y. Wang, J. Magnetism and Magnetic Mater. **324**, 2631 (2012).

[12] R. Roy, V.G. Hill, and E.F. Osborn, J. Am. Chem. Soc. **74**, 719 (1952).

[13] K. Kaneko, S. Fujita, and T. Hitora, Jpn. J. Appl. Phys. **57**, 02CB18 (2018).

[14] H. He, R. Orlando, M.A. Blanco, R. Pandey, E. Amzallag, I. Baraille, and M. Rérat, Phys. Rev. B **74**, 195123 (2006).

[15] S.I. Stepanov, V.I. Nikolaev, V.E. Bougrov, and A.E. Romanov, Rev. Adv. Mater. Sci. **44**, 63 (2016).

[16] I. Cora, F. Mezzadri, F. Boschi, M. Bosi, M. Čaplovičová, G. Calestani, I. Dódony, B. Pécz, and R. Fornari, Cryst. Eng. Comm. **19**, 1509 (2017).

[17] A. Hashimoto, H. Sako, J. Sameshima, M. Nakamura, T. Kobayashi, S. Motoyama, and Y. Otsuka, Mater. Sci. Forum **1004**, 505 (2020).

[18] K. Sasaki, A. Kuramata, T. Masui, E.G. Víllora, K. Shimamura, and S. Yamakoshi, Appl. Phys. Express **5**, 035502 (2012).

[19] M. Higashiwaki, K. Sasaki, A. Kuramata, T. Masui, and S. Yamakoshi, Appl. Phys. Lett. **100**, 013504 (2012).

[20] M.H. Wong, K. Sasaki, A. Kuramata, S. Yamakoshi, and M. Higashiwaki, IEEE Electron Device Lett. **37**, 212 (2016).

[21] K. Konishi, K. Goto, H. Murakami, Y. Kumagai, A. Kuramata, S. Yamakoshi, and M. Higashiwaki, Appl. Phys. Lett. **110**, 103506 (2017).

[22] K. Sasaki, D. Wakimoto, Q.T. Thieu, Y. Koishikawa, A. Kuramata, M. Higashiwaki, and S. Yamakoshi, IEEE Electron Device Lett. **38**, 783 (2017).

[23] H.H. Tippins, Phys. Rev. **140**, A316 (1965).

[24] M. Mohamed, C. Janowitz, I. Unger, R. Manzke, Z. Galazka, R. Uecker, R. Fornari, J.R. Weber, J.B. Varley, C.G. Van de Walle, Appl. Phys. Lett. **97**, 211903 (2010).

[25] H. Peelaers, C.G. Van de Walle, Phys. Status Solidi B **252**, 828 (2015).

[26] T. Onuma, S. Saito, K. Sasaki, T. Masui, T. Yamaguchi, T. Honda, M. Higashiwaki, Jpn. J. Appl. Phys. **54**, 112601 (2015).

[27] Y. Kokubun, K. Miura, F. Endo, S. Nakagomi, Appl. Phys. Lett. **90**, 031912 (2007).

[28] T. Oshima, T. Okuno, S. Fujita, Jpn. J. Appl. Phys. **46**, 7217 (2007).

[29] K. Kaneko, M. Kitajima, and S. Fujita, MRS Advance **2**, 301 (2017).

[30] R. Togashi, S. Numata, M. Hayashida, T. Suga, K. Goto, A. Kuramata, S. Yamakoshi, P. Paskov, B. Monemar, and Y Kumagai, Jpn. J. Appl. Phys. **55**, 1202B3 (2016).

[31] M. Mizuhashi, Thin Solid Films **70**, 91 (1980).

[32] M. Baldini, Z. Galazka, and G. Wagner, Materials Science in Semiconductor Processing **78**, 132 (2018).

[33] M. Marezio, Acta Cryst. **20**, 723 (1966).

[34] M. Higashiwaki, K. Sasaki, A. Kuramata, T. Masui, and S. Yamakoshi, Appl. Phys. Lett., **100**, 013504 (2012).

[35] K. Shimamura, E.G. Villora, K. Domen, K. Yui, K. Aoki, and N. Ichinose, Jpn. J. Appl. Phys. **44**, L7 (2005).

[36] A. Kuramata, K. Koshi, S. Watanabe, Y. Yamaoka, T. Masui, S. Yamakoshi, Jpn. J. Appl. Phys. **55**, 1202A2 (2016).

[37] H. Murakami, K. Nomura, K. Goto, K. Sasaki, K. Kawara, Q.T. Thieu, R. Togashi, Y. Kumagai, M. Higashiwaki, A. Kuramata, Appl. Phys. Express **8**, 015503 (2014).

[38] K. Goto, K. Konishi, H. Murakami, Y. Kumagai, B. Monemar, M. Higashiwaki, A. Kuramata, S. Yamakoshi, Thin Solid Films **666**, 182 (2018).

[39] M. Higashiwaki, K. Sasaki, T. Kamimura, M.H. Wong, D. Krishnamurthy, A. Kuramata, T. Masui, and S. Yamakoshi, Appl. Phys. Lett. **103**, 123511 (2013).

[40] J.H. Park, R. McClintock, and M. Razeghi, Semicond. Sci. Technol., **34**, 08LT01 (2019).

[41] B.J. Baliga, J. Appl. Phys., **53**, 1759 (1982).

[42] K. Nomura, K. Goto, R. Togashi, H. Murakami, Y. Kumagai, A. Kuramata, S. Yamakoshi, A. Koukitu, J. Cryst. Growth **405** (2014) 19.

[43] K. Sasaki, M. Higashiwaki, A. Kuramata, T. Masui, S. Yamakoshi, J. Cryst. Growth **392**, 30 (2014).

Chapter 8. Experimental procedure

8.1. Growth technique of β-Ga_2O_3

Bulk β-Ga_2O_3 crystals are generally grown using melt growth techniques, for example, the floating zone (FZ) method,[1,2] vertical Bridgeman (VB) method,[3] Czochralski (CZ) method,[4,5] and EFG method.[6] Today, almost all commercially provided β-Ga_2O_3 substrate crystals were fabricated by Novel Crystal Technology, Inc. using EFG method. Ga_2O_3 powder was used as the source material in EFG process. The source powder was placed in a crucible made of iridium (Ir) together with an Ir die. When the temperature reached the melting point of β-Ga_2O_3, the melt moved up through a slit in the Ir die by capillary action and reached the top surface of the die. The crystal growth was initiated by placing a β-Ga_2O_3 seed crystal in contact with the melt on the top surface of the die. In the EFG method, the shape of the grown crystal is usually determined by the shape of the top surface of the die. After contacting the seed, the crystal grew on the top surface of the die. The growth direction and the principal surface were determined by setting the seed direction The growth rate reached 15 mm/h.

On the other hand, thin films of β-Ga_2O_3 were grown by VPE such as MBE,[7,8] MOVPE,[9] pulsed laser deposition (PLD),[10] and HVPE. [11-15] Thermodynamic analysis predicted high temperature and high-speed growth of Ga_2O_3 by HVPE,[14] and the homoepitaxial growth of high purity β-Ga_2O_3 by HVPE using the GaCl-O_2-N_2 system at 1000℃ were reported.[10]

However, generally, a critical nuclear radius depends on the driving force of crystal growth, and due to the large driving force of β-Ga_2O_3 HVPE growth, it was found that GaCl and O_2 reacted in the gas phase as precursors of Ga_2O_3 growth, resulting in Ga_2O_3 particle formation. Furthermore, many particles were deposited on the substrate, which affects the growth mode change from two-dimensional to three-dimensional.

On the other hand, THVPE has a relatively small driving force on Ga_2O_3 growth compared with HVPE,[14] and it is expected that β-Ga_2O_3 is grown with suppressing the gas-phase reaction. For β-Ga_2O_3 growth, it is expected that the thickness control or surface morphology are improved by THVPE due to the unique adsorption behavior of $GaCl_3$, known as N-polar GaN growth.[16,17]

8.2. Investigation of Ga_2O_3 growth by HVPE and THVPE

GaCl-O_2 and $GaCl_3$-O_2 systems are considered as HVPE- and THVPE-Ga_2O_3 growth systems, respectively. For the thermodynamic calculations, the following chemical species were selected; Ga, GaCl, $GaCl_2$, $GaCl_3$, $(GaCl_3)_2$, GaO, Ga_2O, Ga_2O_3, Cl_2, O_2, and the inert gas (IG) of N_2. The reactions of each specie in the growth zone were described as follows;

$$2\mathrm{Ga} + \frac{1}{2}\mathrm{O_2} \rightleftarrows \mathrm{Ga_2O} \tag{8-6}$$

$$2\mathrm{GaCl} + \frac{3}{2}\mathrm{O_2} \rightleftarrows \mathrm{Ga_2O_3} + \mathrm{Cl_2} \tag{8-7-1}$$

$$2\mathrm{GaCl_3} + \frac{3}{2}\mathrm{O_2} \rightleftarrows \mathrm{Ga_2O_3} + 3\mathrm{Cl_2} \tag{8-7-2}$$

and the equilibrium constant K of these reaction is shown as follows;

$$K_{7-1} = \frac{P_{GaCl}}{P_{Ga}P_{Cl2}^{\frac{1}{2}}} \tag{8-8}$$

$$K_{7-2} = \frac{P_{GaCl2}}{P_{GaCl}P_{Cl2}^{\frac{1}{2}}} \tag{8-9}$$

$$K_{7-3} = \frac{P_{GaCl3}}{P_{GaCl2}P_{Cl2}^{\frac{1}{2}}} \tag{8-10}$$

$$K_{7-4} = \frac{P_{(GaCl3)2}}{P_{GaCl3}^{2}} \tag{8-11}$$

$$K_{7-5} = \frac{P_{GaO}}{P_{Ga}P_{O2}^{\frac{1}{2}}} \tag{8-12}$$

$$K_{7-6} = \frac{P_{Ga2O}}{P_{Ga}^{2}P_{O2}^{\frac{1}{2}}} \tag{8-13}$$

$$K_{7-7-1} = \frac{a_{Ga2O3}P_{Cl2}}{P_{GaCl}P_{O2}^{\frac{3}{2}}} \tag{8-14-1}$$

$$K_{7-7-2} = \frac{a_{Ga2O3}P_{Cl2}^{3}}{P_{GaCl3}P_{O2}^{\frac{3}{2}}} \tag{8-14-2}$$

where P is the partial pressure of each gaseous species and a is the activity of Ga_2O_3. In this calculation, the activity of solid phase species is defined as 1. The total pressure in this system is consisted of each partial pressure and described as follows;

$$P_{Tot} = P_{Ga} + P_{GaCl} + P_{GaCl2} + P_{GaCl3} + P_{(GaCl3)2} + P_{Cl2} + P_{GaO} + P_{Ga2O} + P_{O2} + P_{IG}$$

(8-15)

and, in this system, there is a constant amount of chlorine atom supplied for the generation of GaCl or $GaCl_3$ which is the source material of HVPE and THVPE, respectively. The relationship is described as follows;

$$xP^0_{GaClx} = P_{GaCl} + 2P_{GaCl2} + 3P_{GaCl3} + 6P_{(GaCl3)2} + 2P_{Cl2} \quad (8\text{-}16)$$

where P^0 is the input partial pressure of source materials, and x is 1 or 3 by HVPE and THVPE, respectively. Moreover, the relationship of stoichiometry of HVPE and THVPE is shown as follows:

$$\frac{1}{2}\left\{P^0_{GaClx} - \left(P_{Ga} + P_{GaCl} + P_{GaCl2} + P_{GaCl3} + 2P_{(GaCl3)2} + P_{GaO} + 2P_{Ga2O}\right)\right\}$$
$$= \frac{2}{3}\left\{P^0_{O2} - \left(P_{O2} + \frac{1}{2}P_{GaO} + \frac{1}{2}P_{Ga2O}\right)\right\} \quad (8\text{-}17)$$

This equation (7-17) shows the ratio of gallium and oxygen incorporated from gas phase to solid phase according to equations (7-7-1) and (7-7-2). Solving equation from (7-8) to (7-17), the partial pressure of each specie was obtained at equilibrium state. Furthermore, the driving force of HVPE and THVPE was described as follows:

$$\Delta P = P^0_{GaClx} - \left(P_{Ga} + P_{GaCl} + P_{GaCl2} + P_{GaCl3} + 2P_{(GaCl3)2} + P_{GaO} + 2P_{Ga2O}\right)$$
(8-18)

Then, the partial pressure and the driving force were drawn as a function of temperature, the ratio

of input partial pressure of group-VI and group-III (VI/III ratio), and the ratio of the supply partial pressure of the 2nd chlorine against that of the 1st at the generation of $GaCl_3$ (R_{2nd}) described as follows, respectively;

$$VI/III = \frac{2P^0_{O2}}{P^0_{GaClx}} \tag{8-19}$$

$$R_{2nd} = \frac{P^0_{2st\ Cl2}}{P^0_{1st\ Cl2}} = \frac{x - x_{1st}}{x_{1st}} \tag{8-20}$$

where x is a continuous value between 1 and 3, and x_{1st} is 1.

Figure 7.1. shows the dependence of the equilibrium constant of HVPE- and THVPE-Ga_2O_3 growth on the temperature. The equilibrium constant of Ga_2O_3 growth by HVPE is much larger than that by THVPE at any temperature. Furthermore, **figure 7.2.** shows the equilibrium partial pressure of gaseous species of HVPE and THVPE on the surface of the substrate. The change of partial pressure with increasing of the VI/III ratio is greatly different between HVPE and THVPE. In the case of HVPE, partial pressure changes drastically near the VI/III value of 1. On the other hand, in the case of THVPE, partial pressure changes gradually with increasing of the VI/III ratio. Then, the change of the driving force of HVPE and THVPE as a function of VI/III ratio also shows the different tendency (shown in **figure 7.3.**). According to these thermodynamic analysis, it seems that Ga_2O_3 growth by HVPE is superior to THVPE in terms of the driving force. However, a too large driving force of growth causes the gas-phase reaction before the raw molecules reach the substrate crystal. Generally, a critical nuclear radius depends on the driving force of crystal growth. This relationship is described as follows;

$$\Delta G = -\frac{4}{3}\pi r^3 \Delta P + 4\pi r^2 \sigma \tag{8-21}$$

where ΔG is the free energy of nucleation, ΔP is the driving force of growth, and σ is the surface energy. According to this equation, ΔG is a function of r and has a maximum value. Then, r^*, the critical radius of nucleation, which is the value of radius when ΔG has the maximum is defined as follows:

$$r^* = \frac{2\sigma}{\Delta P} \qquad (8\text{-}22)$$

According to this, r^* gets smaller with increasing $|\Delta P|$, namely, nucleation proceeds more likely in the gas phase. Therefore, due to the large driving force of β-Ga_2O_3 HVPE growth, it was found that GaCl and O_2 reacted in the gas phase as precursors of Ga_2O_3 growth, resulting in Ga_2O_3 particle formation. In order to suppress the Ga_2O_3 particle, it is thought THVPE having a relatively smaller and controllable driving force is suitable for Ga_2O_3 growth.

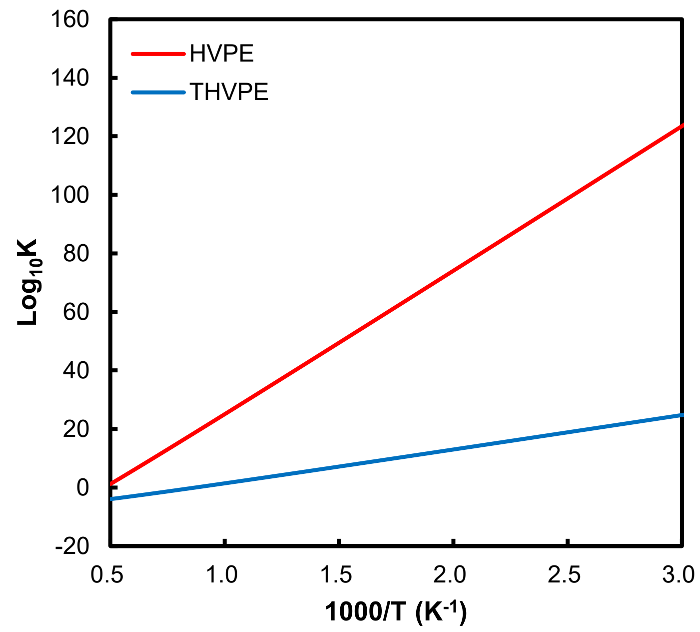

Figure 8.1. The dependence of equilibrium constant of HVPE- and THVPE-Ga_2O_3 growth on the temperature.[14]

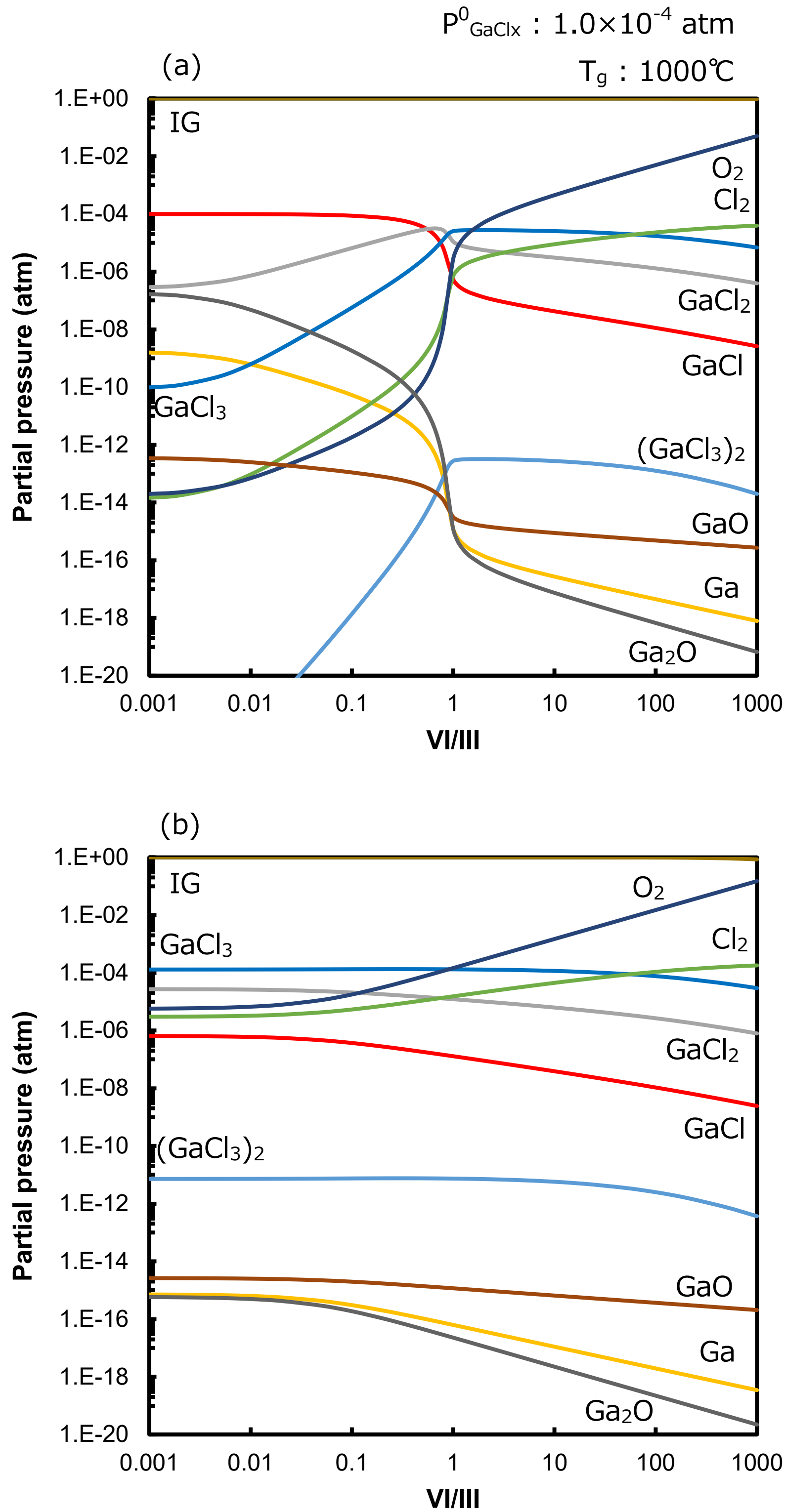

Figure 8.2. The dependence of equilibrium partial pressure of gaseous species on VI/III ratio compared with (a) HVPE[14] and (b) THVPE in the growth zone.

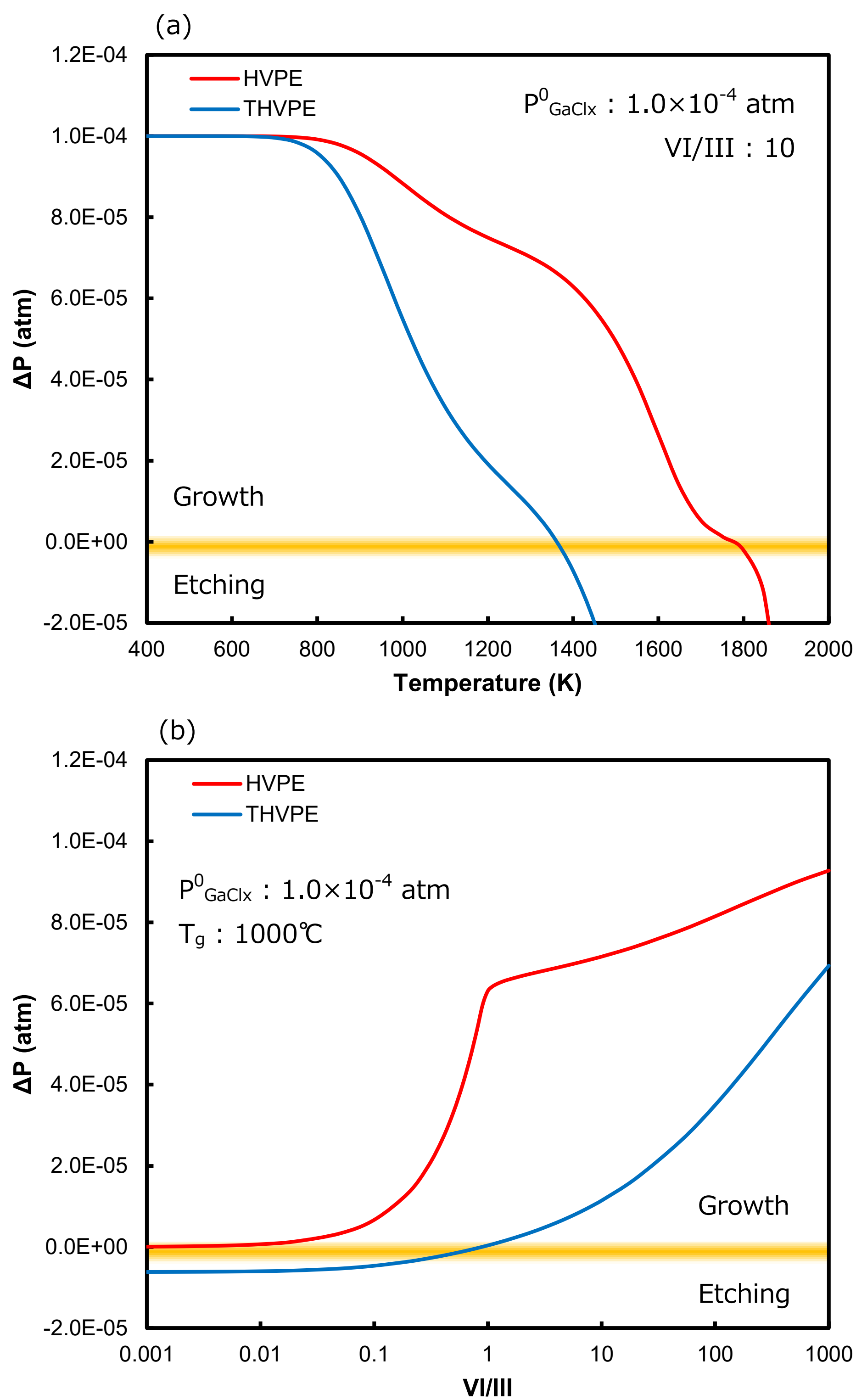

Figure 8.3. The driving force of growth by HVPE and THVPE vs. (a) growth temperature and (b) VI/III ratio.

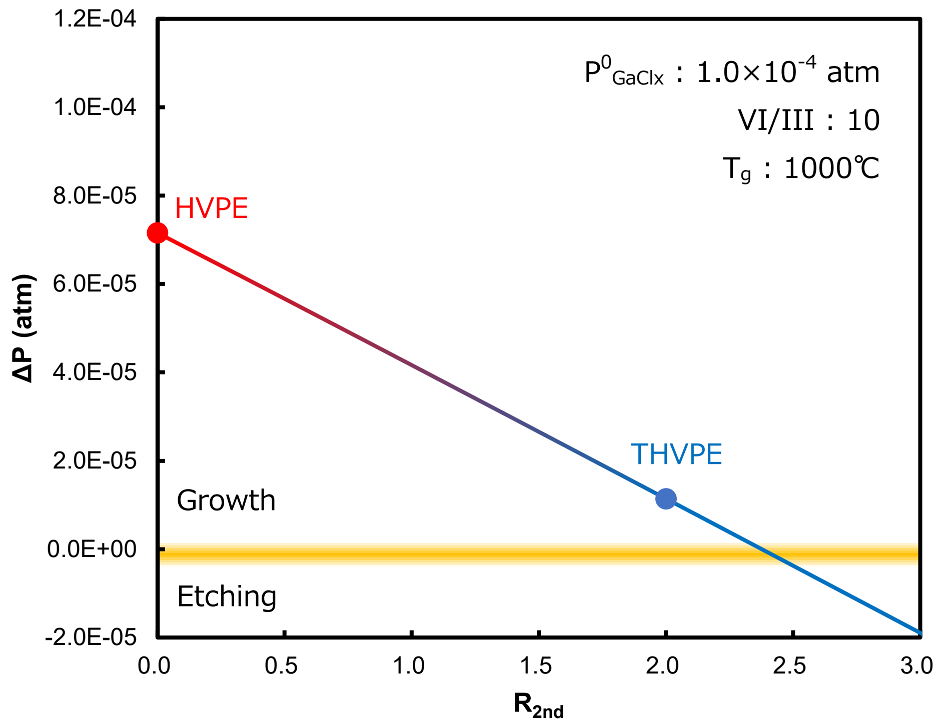

Figure 8.4. The driving force of growth by HVPE and THVPE vs. R_{2nd}.

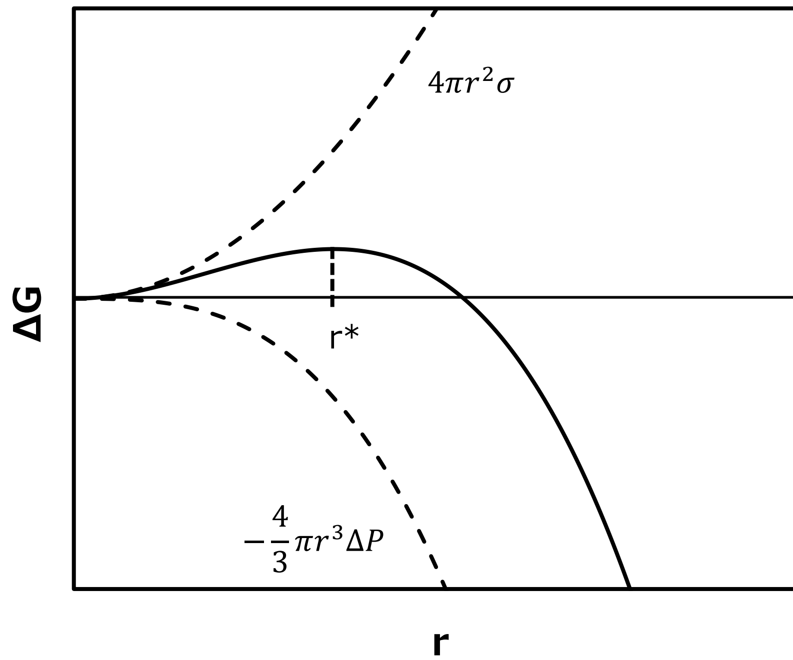

Figure 8.5. The critical nuclear radius estimated by the relationship between ΔG and r.

8.3. Consideration by thermodynamics for generation of the sources of THVPE

Figure 7.5. shows the schematics of the generation of Ga precursors by a one-step reaction, and **figure 7.6.** shows the thermodynamics analysis of the temperature dependence of the partial pressure of possible gaseous species in the source zone. In the case of the one-step reaction, it is clearly found that the main product is the gallium mono-chlorides almost the entire temperature. A certain amount of gaseous gallium is produced from the surface of the liquid metals as followed by the vapor pressure of them. Therefore, input Cl_2 reacted with gaseous Ga priority, and gallium mono-chloride is generated without generation of gallium tri-chlorides from the reaction between gallium mono-chloride and Cl_2. Therefore, by the one-step reaction, it is impossible that gallium trichlorides are obtained. On the other hand, **figure 7.7.** shows the schematics of the generation of Ga precursors by a two-step reaction using two separated chambers, one contains metallic gallium and is supplied 1st chlorine and the other is only supplied 2nd chlorine. **Figure 7.8.** shows the thermodynamic analysis of the reaction for gallium tri-chlorides generation compared with a one-step reaction and a two-step reaction in the source zone. However, in the case of a two-step reaction, it is found that the main products are the gallium tri-chlorides at the temperature between 400°C and 900°C. In the 1st chamber, gallium mono-chloride is generated via reaction of Ga and Cl_2, and only gallium mono-chloride is introduced into the 2nd chamber. Next, in the 2nd chamber, gallium tri-chloride is generated by the reaction of gallium mono-chlorides and 2nd Cl_2. The reactions occurring in the source zone are as follows:

$$\mathrm{Ga} + \frac{1}{2}\mathrm{Cl_2} \rightarrow \mathrm{GaCl} \qquad (8\text{-}23)$$

$$GaCl + Cl_2 \rightarrow GaCl_3 \qquad (8\text{-}24)$$

In addition, thermodynamic analysis shows $GaCl_3$ is prior to GaCl the entire temperature till 1200℃. Therefore, the author adopted the temperature of 860℃ at the source zone in InGaN growth .

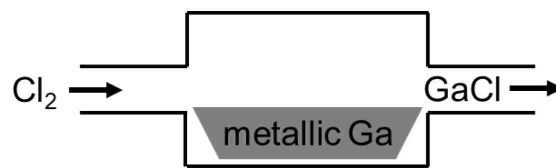

Figure 8.5. The schematics of one-step reaction of the generation of gallium precursor.

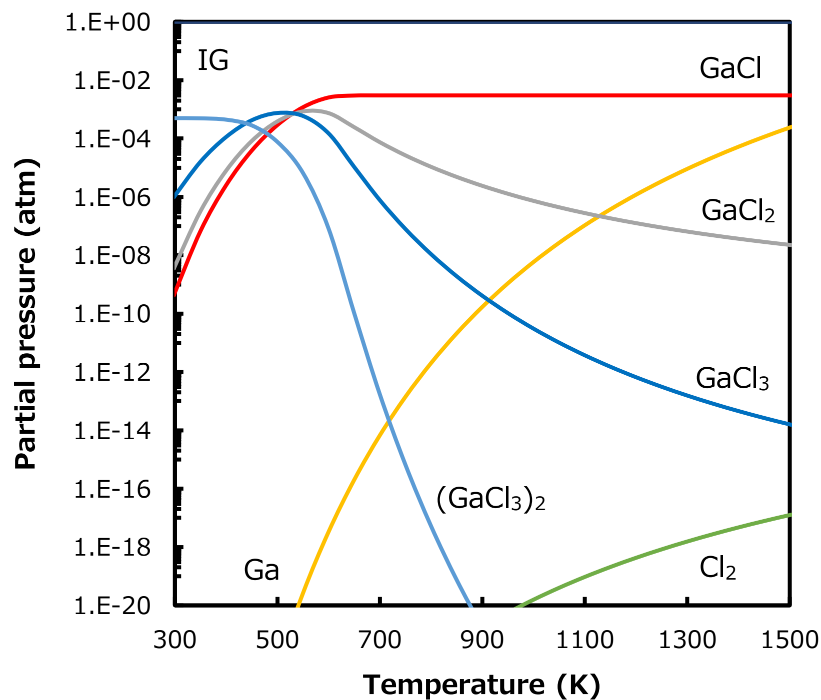

Figure 8.6. The temperature dependence of partial pressure of each gaseous species by one-step reaction of the generation of gallium precursor.

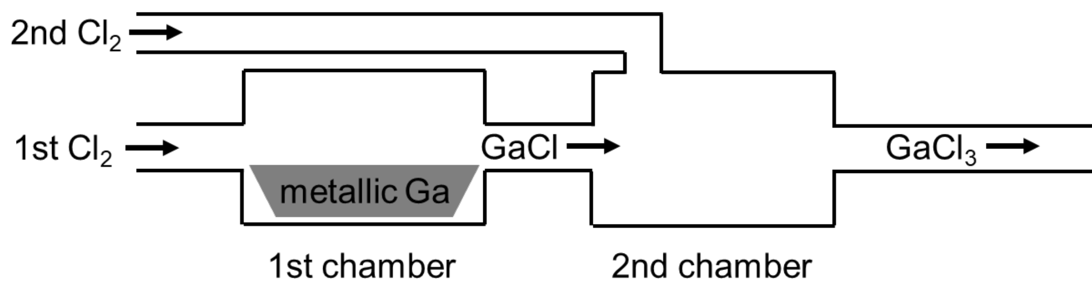

Figure 8.7. The schematics of two-step reaction of the generation of gallium precursor.

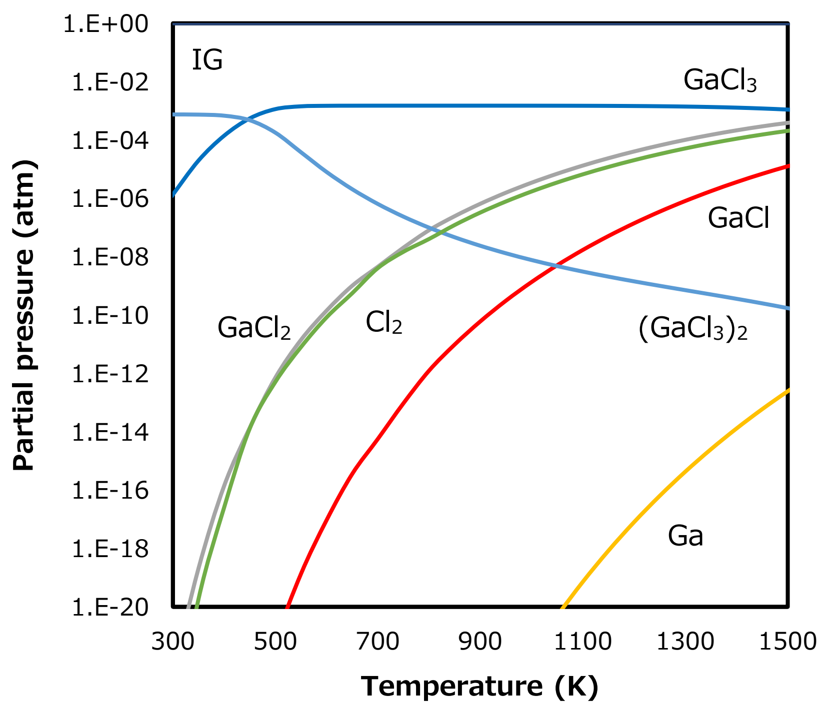

Figure 8.8. The temperature dependence of partial pressure of each gaseous species by two-step reaction of the generation of gallium precursor.

Reference

[1] E.G. Villora, K. Shimamura, Y. Yoshikawa, K. Aoki, N. Ichinose, J. Cryst. Growth **270**, 420 (2004).

[2] N. Ueda, H. Hosono, R. Waseda, H. Kawazoe, Appl. Phys. Lett. **70**, 3561 (1997).

[3] K. Hoshikawa, E. Ohba, T. Kobayashi, J. Yanagisawa, C. Miyagawa, Y. Nakamura, J. Cryst. Growth **447**, 36 (2016).

[4] Y. Tomm, P. Reiche, D. Klimm, T. Fukuda, J. Cryst. Growth **220**, 510 (2000).

[5] Z. Galazka, R. Uecker, D. Klimm, K. Irmscher, M. Naumann, M. Pietsch, A. Kwasniewski, R. Bertram, S. Ganschow, M. Bickermann, ECS J. Solid State Sci. Technol. **6**, Q3007 (2017).

[6] A. Kuramata, K. Koshi, S. Watanabe, Y. Yamaoka, T. Masui, S. Yamakoshi, Jpn. J. Appl. Phys. **55**, 1202A2 (2016).

[7] K. Sasaki, M. Higashiwaki, A. Kuramata, T. Masui, S. Yamakoshi, J. Cryst. Growth **392**, 30 (2014).

[8] M. Baldini, M. Albrecht, A. Fiedler, K. Irmscher, R. Schewski, G. Wagner, J. Mater. Sci. **51**, 3650 (2016).

[9] R. Wakabayashi, K. Yoshimatsu, M. Hattori, A. Ohtomo, Appl. Phys. Lett. **111**, 162101 (2017).

[10] H. Murakami, K. Nomura, K. Goto, K. Sasaki, K. Kawara, Q.T. Thieu, R. Togashi, Y. Kumagai, M. Higashiwaki, A. Kuramata, Appl. Phys. Express **8**, 015503 (2014).

[11] K. Goto, K. Konishi, H. Murakami, Y. Kumagai, B. Monemar, M. Higashiwaki, A. Kuramata, S. Yamakoshi, Thin Solid Films **666**, 182 (2018).

[12] M. Higashiwaki, K. Konishi, K. Sasaki, K. Goto, K. Nomura, Q.T. Thieu, R. Togashi, H. Murakami, Y. Kumagai, B. Monemar, A. Koukitu, A. Kuramata, S. Yamakoshi, Appl. Phys. Lett. **108**, 133503 (2018).

[13] Q.T. Thieu, D. Wakimoto, Y. Koishikawa, K. Sasaki, K. Goto, K. Konishi, H. Murakami, A. Kuramata, Y. Kumagai, S. Yamakoshi, Jpn. J. Appl. Phys. **56**, 110310 (2017).

[14] K. Nomura, K. Goto, R. Togashi, H. Murakami, Y. Kumagai, A. Kuramata, S. Yamakoshi, A. Koukitu, J. Cryst. Growth **405**, 19 (2014).

[15] K. Konishi, K. Goto, R. Togashi, H. Murakami, M. Higashiwaki, A. Kuramata, S. Yamakoshi, B. Monemar, Y. Kumagai, J. Cryst. Growth **492**, 39 (2018).

[16] T. Hirasaki, K. Asano, M. Banno, M. Ishikawa, F. Sakuma, H. Murakami, Y. Kumagai, A. Koukitu, Jpn. J. Appl. Phys. **53**, 05FL02 (2014).

[17] K. Iso, N. Takekawa, K. Matsuda, K. Hikida, N. Hayashida, H. Murakami, A. Koukitu, Appl. Phys. Express **9**, 105501 (2016).

Chapter 9. Homo- and hetero-epitaxial growth of β-Gallium Oxide via $GaCl_3$-O_2-N_2 system

9.1. Introduction

Gallium oxide (Ga_2O_3) shows polymorphism having α-, β-, γ-, δ-, ε-, and κ-phases [1-4], where the β-phase is the most stable among them. β-Ga_2O_3 is expected to be applied to next-generation electronic devices, low-loss and high withstand voltage power devices [5-9], due to its excellent physical properties such as a large bandgap of 4.5 eV and a high breakdown electric field [10-13]. The growth technique of the β-Ga_2O_3 substrate crystal has already been established [14-19], and there are several reports that β-Ga_2O_3 shows promise as light-emitting devices or light-receiving devices, such as the substrate for blue light-emitting diodes (LEDs) or deep ultra-violet photodetectors [20,21].

Bulk β-Ga_2O_3 crystals are generally grown using melt growth techniques, for example, the floating zone method [14,15], vertical Bridgeman method [16], Czochralski method [17,18], and edge-defined film-fed growth (EFG) method [19]. On the other hand, a thin film of β-Ga_2O_3 was grown by molecular beam epitaxy [5,22], metal-organic vapor phase epitaxy [23], pulsed laser deposition [24], and halide vapor phase epitaxy (HVPE) [25-29]. Thermodynamic analysis predicted high temperature and high-speed growth of Ga_2O_3 by HVPE [30,31], and we have succeeded in the homoepitaxial growth of high purity β-Ga_2O_3 by HVPE using the GaCl-O_2-N_2 system at 1000°C [25]. We have also succeeded in the fabrication of vertical β-Ga_2O_3 Schottky

barrier diodes with excellent Schottky characteristics using an HVPE-grown drift layer [5] and linear control of the n-type carrier density in the range of 10^{15} to 10^{18} cm^{-3} by changing the Si concentration [26]. However, generally, a critical nuclear radius depends on the driving force of crystal growth, and due to the large driving force of β-Ga_2O_3 HVPE growth, it was found that GaCl and O_2 reacted in the gas phase as precursors of Ga_2O_3 growth, resulting in Ga_2O_3 particle formation. Furthermore, many particles were deposited on the substrate, which affects the growth mode change from two-dimensional to three-dimensional. On the other hand, tri-halide vapor phase epitaxy (THVPE), another halide vapor phase epitaxy using $GaCl_3$ as a source of group III, has a relatively small driving force compared to HVPE [30], and it is expected that β-Ga_2O_3 is grown with suppressing the gas-phase reaction. For β-Ga_2O_3 growth, it is expected that the thickness control or surface morphology are improved by THVPE due to the unique adsorption behavior of $GaCl_3$, known as N-polar GaN growth [32,33]. However, β-Ga_2O_3 growth has not been carried out by THVPE in the high-temperature region, which is optimal for β-phase growth. In this study, β-Ga_2O_3 growth on sapphire substrates was performed, and its dependence on the ratio of O_2 input partial pressure against $GaCl_3$ (VI/III) in β-Ga_2O_3 growth by THVPE was investigated. Furthermore, homoepitaxial growth of β-Ga_2O_3 by THVPE was also carried out.

9.2. Experimental

Ga_2O_3 was grown in a hot-wall type quartz reactor by THVPE using $GaCl_3$ and O_2 as group III and group VI sources, respectively. In the source zone, $GaCl_3$ was selectively generated by a two-step reaction between metallic Ga and Cl_2 with two chambers [34] at a fixed temperature of 860°C. In the first chamber, GaCl was generated via the reaction of metallic Ga and Cl_2. Next, in

the second chamber, $GaCl_3$ was generated by the reaction of GaCl and second Cl_2. The schematic was shown in **Figure 8.1.** The reactions occurring in the source zone are as follows:

$$\mathrm{Ga} + \frac{1}{2}\mathrm{Cl_2} \rightarrow \mathrm{GaCl} \qquad (9\text{-}1)$$

$$\mathrm{GaCl} + \mathrm{Cl_2} \rightarrow \mathrm{GaCl_3} \qquad (9\text{-}2)$$

According to the stoichiometric coefficient of these equations, the supply partial pressure of the second chlorine is theoretically two times more than that of the first chlorine. In the growth zone, $GaCl_3$ was reacted with O_2 on the substrate crystals. The reactions occurring in the growth zone are as follows:

$$2\mathrm{GaCl_3} + \frac{3}{2}\mathrm{O_2} \rightarrow \mathrm{Ga_2O_3} + 3\mathrm{Cl_2} \qquad (9\text{-}3)$$

β-Ga_2O_3 was grown on the c-plane sapphire substrate at a fixed growth temperature of 1000°C or the same duration time, and the input group VI/III ratio was changed to 15, 30, and 60 under the fixed P^0_{GaCl3} of 1.3×10^{-3} atm. Furthermore, to investigate the driving force of THVPE β-Ga_2O_3 growth compared with that of HVPE, the ratio of the supply partial pressure of the second chlorine against that of the first on the growth of β-Ga_2O_3 (R_{2nd}) was changed between 1.75 and 2.05 under the fixed condition of P^0_{GaCl3} of 1.3×10^{-3} atm and VI/III = 60. Homoepitaxial growth was performed on a tin-doped β-Ga_2O_3 (001) substrate (10 × 10 mm) prepared by an EFG method [19] under the condition of VI/III = 60 and R_{2nd} = 2.00, which are optimized conditions for growth on sapphire substrates.

The surface morphologies of β-Ga_2O_3 epilayers were observed by Nomarski differential interference contrast (NDIC) microscopy. Crystalline quality was characterized by X-ray diffraction (XRD), and secondary ion mass spectrometry (SIMS) was carried out to evaluate impurity concentration levels in the β-Ga_2O_3 epilayer grown by THVPE.

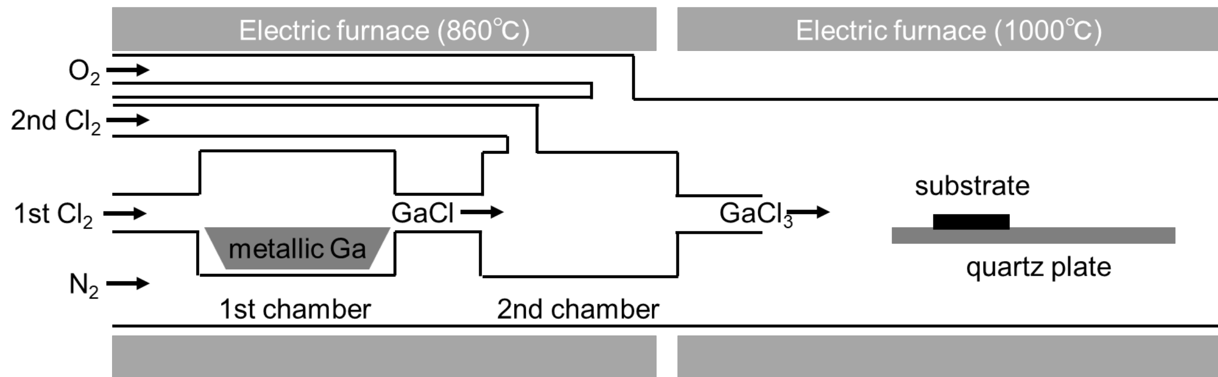

Figure 9.1. Schematic of THVPE β-Ga_2O_3 reactor. In the 1st chamber, GaCl was generated via reaction of metallic Ga and 1st Cl_2. Next, in the 2nd chamber, $GaCl_3$ was selectively generated by the reaction of GaCl and 2nd Cl_2. The temperature of both chambers was fixed at 860°C.

9.3. Results and discussion

9.3.1. Dependence of the VI/III ratio and R_{2nd} on the growth of β-Ga_2O_3 by THVPE

Ga_2O_3 was grown on c-plane sapphire substrates by THVPE by changing the VI/III ratio between 15 and 60 at a fixed R_{2nd} = 2.00. **Figure 8.2.** shows the XRD 2θ-ω profile of each sample. Peaks appearing around 18.9, 38.4, 59.1, and 82.3 degrees were assigned to β-Ga_2O_3 $\bar{2}01$, $\bar{4}02$, $\bar{6}03$, and $\bar{8}04$, respectively, and it was found that the single phase of β-Ga_2O_3 was successfully obtained in each sample by THVPE. The growth rate of each sample is shown in **Figure 8.3.** As the VI/III ratio increased, it was found that the growth rate also increased linearly, which is almost the same result as predicted by thermodynamic analysis [30]. Besides, it was also confirmed by X-ray rocking curve (XRC) measurement that the crystalline quality of the β-Ga_2O_3 epilayer was improved with increasing the VI/III ratio, which indicated that a higher VI/III ratio was preferred for β-Ga_2O_3 growth by THVPE, note that it was also considered that the crystalline quality was

improved with increasing the thickness of the β-Ga_2O_3 epilayer.

Furthermore, the dependence of the supply partial pressure of the second chlorine against that of the first (R_{2nd}) on the growth of β-Ga_2O_3 by THVPE was investigated. β-Ga_2O_3 was grown on c-plane sapphire substrates by THVPE with varying R_{2nd} values between 1.75 and 2.05 at a fixed VI/III ratio of 60. Under conditions of $R_{2nd} < 2.00$, GaCl and $GaCl_3$ were contained in the reaction system due to the lack of second chlorine, while at $R_{2nd} = 2.00$, it was considered that only $GaCl_3$ was contained in the reactor, and under conditions of $R_{2nd} > 2.00$, excess Cl_2 existed based on the stoichiometric coefficients of equations (1) and (2). **Figure 8.4.** shows the growth rate change of β-Ga_2O_3 linearly decreasing with increasing R_{2nd} between 1.75 and 2.05. In the region containing GaCl as a precursor of gallium, the growth rate of β-Ga_2O_3 was large, and as the ratio of GaCl in the gallium source increased, the growth rate also increased. Experimentally, it was indicated that the driving force of the THVPE β-Ga_2O_3 growth was smaller than that of HVPE, which was almost the same as the result predicted by thermodynamic analysis [30]. Moreover, under conditions of $R_{2nd} = 2.05$, which is an excess Cl_2 state, the growth rate decreased more. The equilibrium constant of the Ga_2O_3 generation by THVPE at 1000°C was relatively small compared with that by HVPE [30], and under conditions of a small equilibrium constant, excess Cl_2 greatly affects Ga_2O_3 generation, as shown by equation (3). Therefore, it is an important factor for Ga_2O_3 growth by THVPE to prevent GaCl contamination without decreasing the growth rate by controlling R_{2nd} values. For the results above, β-Ga_2O_3 homoepitaxial growth was performed under conditions of VI/III ratio of 60 and $R_{2nd} = 2.00$.

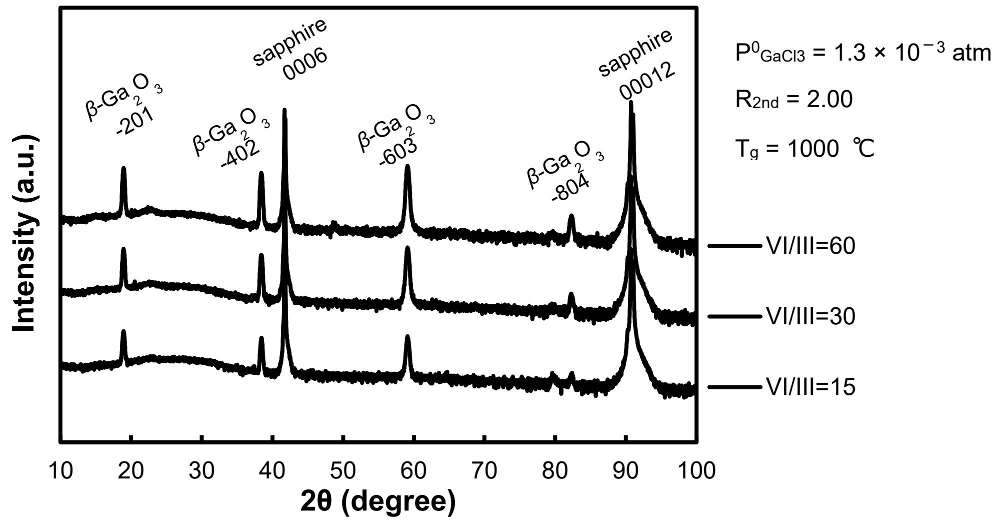

Figure 9.2. XRD 2θ-ω profiles of three samples of Ga_2O_3 grown on c-plane sapphire substrates for 1 hour by THVPE by changing the VI/III ratio from 15 to 60. Peaks appearing around 18.9, 38.4, 59.1, and 82.3 degrees were assigned to β-Ga_2O_3 $\bar{2}01$, $\bar{4}02$, $\bar{6}03$, and $\bar{8}04$, respectively.

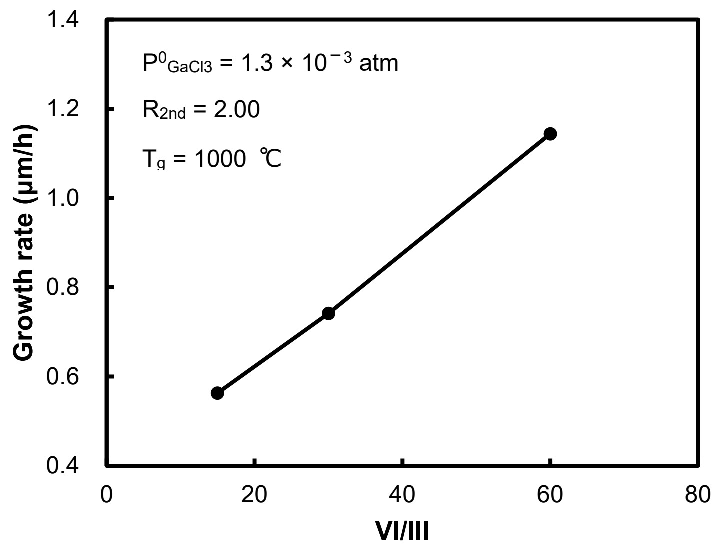

Figure 9.3. Growth rate as a function of VI/III ratio of β-Ga_2O_3 grown on sapphire substrates for 1 hour by THVPE. The growth rate linearly increased with increasing VI/III ratio.

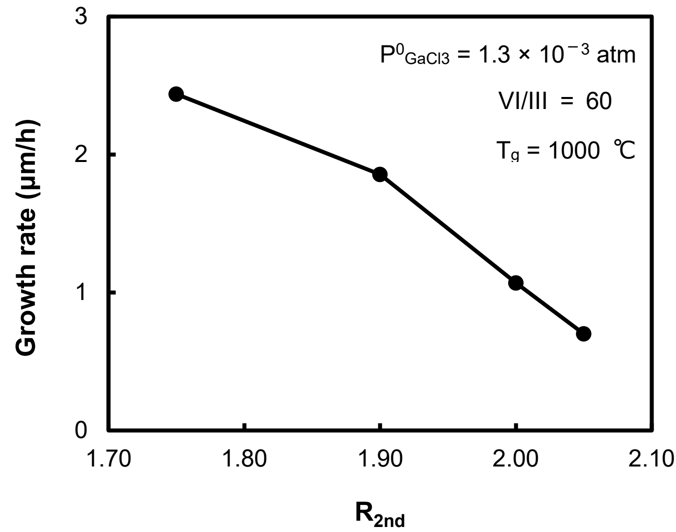

Figure 9.4. Dependence of the growth rate of β-Ga_2O_3 for 1 hour by THVPE on the R_{2nd} at a fixed VI/III ratio of 60. The β-Ga_2O_3 growth rate linearly decreased with increasing R_{2nd}.

9.3.2. Homoepitaxial growth of β-Ga_2O_3 by THVPE

β-Ga_2O_3 homoepitaxial growth by THVPE was performed under conditions of VI/III = 60 and R_{2nd} = 2.00 at 1000°C on a tin-doped β-Ga_2O_3 (001) substrate (10 × 10 mm) prepared by the EFG method. **Figure 8.5.** shows overviews of the β-Ga_2O_3 grown by HVPE and THVPE under the same growth conditions except for the R_{2nd} value. There are many particles on the surface of the crystal grown by HVPE, but no particles were observed in the sample grown by THVPE. The NDIC microscopic images of β-Ga_2O_3 homoepitaxial layers by HVPE and THVPE are shown in **Figure 8.6.** The samples shown in Fig. 6 (a) and (b) were grown under the same condition except for the R_{2nd} value, which was the same sample shown in Fig. 5. Due to the large driving force of β-Ga_2O_3 growth by HVPE compared to that by THVPE [30], the reaction of GaCl and O_2 was immediately carried out in the gas phase in the case of HVPE. In contrast, for THVPE, the reaction of $GaCl_3$ and O_2 was dominantly carried out on the surface of the β-Ga_2O_3 substrate.

The samples shown in Fig. 6 (c) and (d) were grown with the same growth rate of approximately 6 μm/h by changing input partial pressure (both of $GaCl_3$ and O_2) at a fixed VI/III ratio of 100, which was higher VI/III ratio than the other two (Fig. 6 (a) and (b)). Under a high VI/III condition, it was indicated the particle generation was effectively suppressed by THVPE. The surface of each β-Ga_2O_3 layer grown by HVPE and THVPE shows striations that are parallel to the [010] direction. However, the number of striations observed in THVPE was less than that in HVPE, indicating the surface morphology also improved via THVPE.

Figure 8.7. shows the XRC profiles around the 002 symmetrical reflection and 400 skew-symmetrical reflection of the β-Ga_2O_3 epilayers grown under the condition of VI/III = 60 and R_{2nd} = 2.00 and the seed substrate. The FWHM values of XRC for the epilayer and substrate were 28.7 and 26.9 arcsec around 002, respectively, and 27.4 and 25.6 arcsec around 400, respectively. It was found that the epilayer formed by THVPE had almost the same crystalline quality as the seed substrate, the pits observed in the surface of the epilayer originated from the substrate, and the epilayer was grown without any newly generated dislocations [35]. Therefore, the β-Ga_2O_3 epilayer grown by THVPE had almost the same crystalline quality as that of the β-Ga_2O_3 seed substrate.

The impurity concentrations measured by SIMS in the β-Ga_2O_3 layer homoepitaxially grown by THVPE are shown in Table I. The chlorine concentrations were approximately one order of magnitude more than the background levels (1×10^{15} cm^{-3}). The origin of chlorine impurity is attributed to $GaCl_3$ as a source of gallium. This result was slightly larger than that by HVPE (1×10^{16} cm^{-3}) with a growth rate of approximately 5 μm/h [25], and it was considered the increment of chlorine concentration was caused by the stoichiometric increase of chlorine atoms in the group III precursor. It was reported that Cl substituted on the O site acts as a donor [36]. However, it might be possible that chlorine concentration decreased by optimizing growth conditions, such

as the growth temperature. On the other hand, the carbon, nitrogen, and silicon concentrations were under background levels, and the tin concentrations were under the detection limit. Therefore, the concentration of high purity homoepitaxial β-Ga_2O_3 layer grown by THVPE was equivalent to that as obtained by HVPE [25].

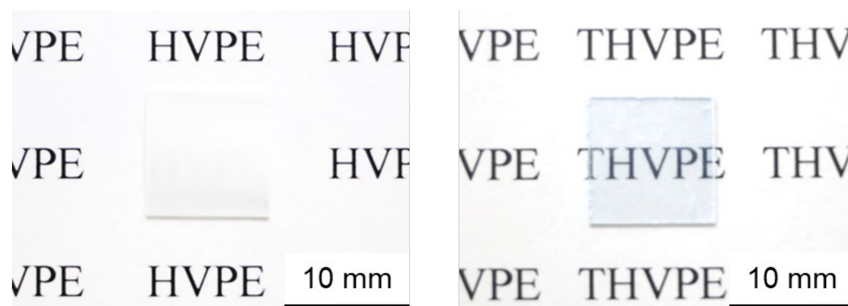

Figure 9.5. Overview of β-Ga_2O_3 homoepitaxial growth by HVPE and THVPE under the same conditions. Many particles were observed on the epilayer surface by HVPE, but no particles were observed by THVPE.

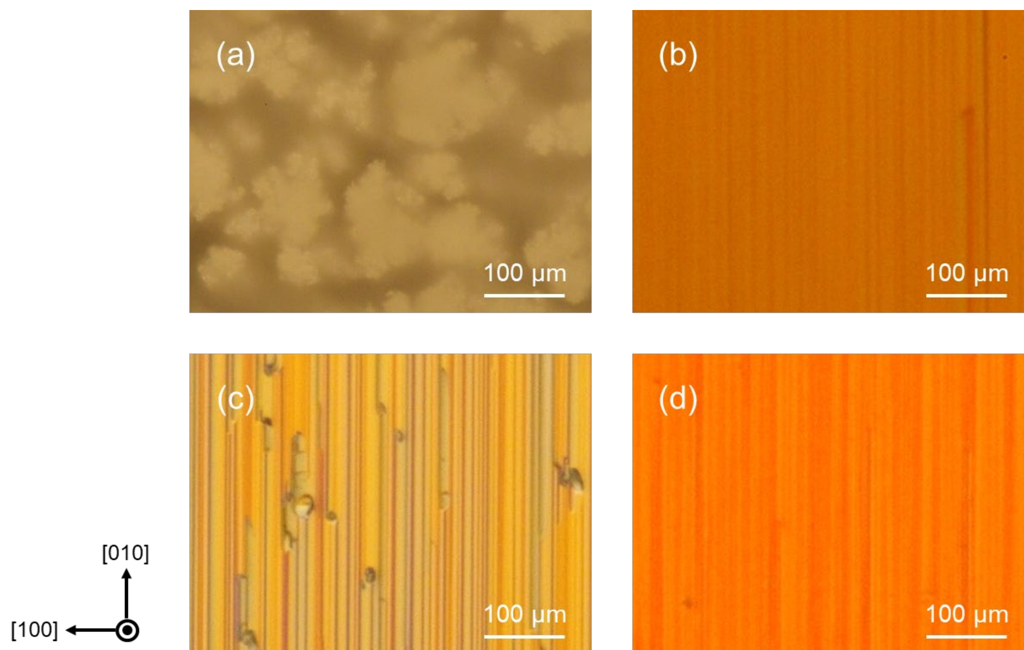

Figure 9.6. NDIC image of the β-Ga_2O_3 homoepitaxial layers grown under the same conditions

by (a) HVPE and (b) THVPE, and with the same growth rate of approximately 6 μm/h grown by (c) HVPE and (d) THVPE. Many particles were observed in (a), and a few particles were also observed in (c). However, there were no particles in (b) and (d). Striations parallel to the [010] direction were observed on the surface of each epilayer.

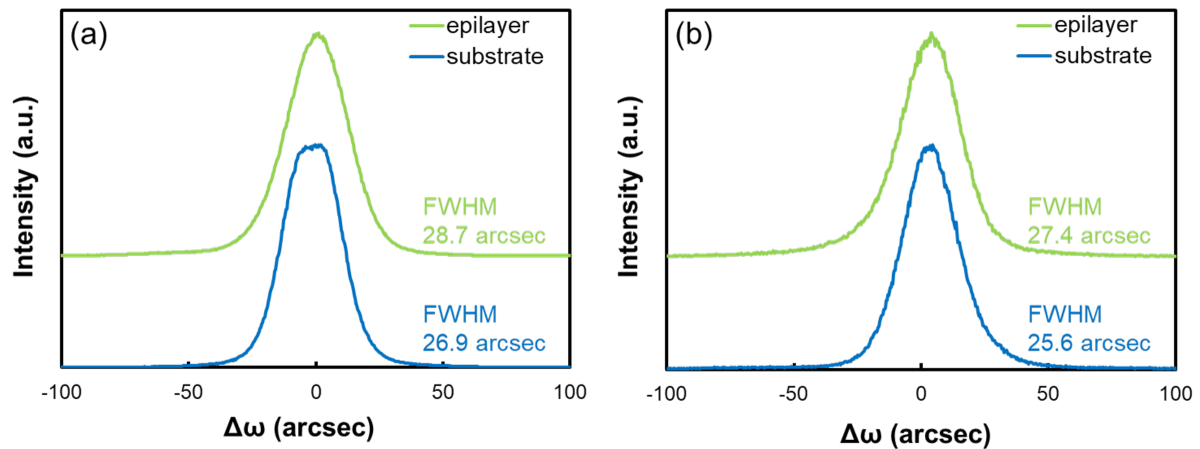

Figure 9.7. XRC profiles around (a) 002 symmetric reflection and (b) 400 asymmetric reflection of homoepitaxial β-Ga_2O_3 with the thickness of 3.1 μm by THVPE. The FWHM values of each measurement were 28.7 and 27.4 arcsec, respectively, which are similar to the 26.9 and 25.6 arcsec values of the β-Ga_2O_3 substrate, respectively.

Table 9.1. Impurity concentrations measured by SIMS in the homoepitaxial layer of β-Ga_2O_3 grown by THVPE.

Elements	Impurity concentration (cm^{-3})	Background levels (cm^{-3})
C	$< 6\times10^{16}$	6×10^{16}
N	$< 1\times10^{16}$	1×10^{16}
Si	$< 2\times10^{16}$	2×10^{16}
Cl	3×10^{16}	1×10^{15}
Sn	$< 3\times10^{15}$	3×10^{15}

9.4. Conclusion

β-Ga_2O_3 growth on sapphire substrates was carried out, and the dependence of the VI/III ratios on β-Ga_2O_3 growth by THVPE was investigated. It was found that a single phase of β-Ga_2O_3 was successfully obtained in each sample by THVPE. By changing R_{2nd} values during $GaCl_3$ generation, it was experimentally indicated that the driving force of THVPE β-Ga_2O_3 growth was smaller than that of HVPE. Furthermore, homoepitaxial growth of β-Ga_2O_3 by THVPE was performed. No particles were observed in the sample grown by THVPE with a growth rate of approximately 3 μm/h by adjusting the value of R_{2nd}, and the β-Ga_2O_3 epilayer had almost the same crystalline quality as that of the β-Ga_2O_3 seed substrate.

9.5. Acknowledgments

The authors thank Mr. N. Ogawa and Ms. R. Nagano of Tokyo University of Agriculture and Technology (TUAT) for their assistance with the experiments. Part of this work was supported by a Grant-in-Aid for Scientific Research on Innovative Areas (No. 16H06417) from the Japan Society for the Promotion of Science and by the Institute of Global Innovation Research, TUAT, Japan.

Reference

[1] R. Roy, V.G. Hill, E.F. Osborn, J. Am. Chem. Soc. **74** (1952) 719. DOI: https://doi.org/10.1021/ja01123a039

[2] H. He, R. Orlando, M.A. Blanco, R. Pandey, E. Amzallag, I. Baraille, M. Rérat, Phys. Rev. B **74** (2006) 195123. DOI: https://doi.org/10.1103/PhysRevB.74.195123

[3] S.I. Stepanov, V.I. Nikolaev, V.E. Bougrov, A.E. Romanov, Rev. Adv. Mater. Sci. **44** (2016) 63.

[4] I. Cora, F. Mezzadri, F. Boschi, M. Bosi, M. Čaplovičová, G. Calestani, I. Dódony, B. Pécz, and R. Fornari, Cryst. Eng. Comm. **19** (2017) 1509. DOI: https://doi.org/10.1039/C7CE00123A

[5] K. Sasaki, A. Kuramata, T. Masui, E.G. Víllora, K. Shimamura, S. Yamakoshi, Appl. Phys. Express **5** (2012) 035502. DOI: https://doi.org/10.1143/APEX.5.035502

[6] M. Higashiwaki, K. Sasaki, A. Kuramata, T. Masui, S. Yamakoshi, Appl. Phys. Lett. **100** (2012) 013504. DOI: https://doi.org/10.1063/1.3674287

[7] M.H. Wong, K. Sasaki, A. Kuramata, S. Yamakoshi, M. Higashiwaki, IEEE Electron Device Lett. **37** (2016) 212. DOI: https://doi.org/10.1109/LED.2015.2512279

[8] K. Konishi, K. Goto, H. Murakami, Y. Kumagai, A. Kuramata, S. Yamakoshi, M. Higashiwaki, Appl. Phys. Lett. **110** (2017) 103506. DOI: https://doi.org/10.1063/1.4977857

[9] K. Sasaki, D. Wakimoto, Q.T. Thieu, Y. Koishikawa, A. Kuramata, M. Higashiwaki, S. Yamakoshi, IEEE Electron Device Lett. **38** (2017) 783. DOI: https://doi.org/10.1109/LED.2017.2696986

[10] H.H. Tippins, Phys. Rev. **140** (1965) A316. DOI: https://doi.org/10.1103/PhysRev.140.A316

[11] M. Mohamed, C. Janowitz, I. Unger, R. Manzke, Z. Galazka, R. Uecker, R. Fornari, J.R. Weber, J.B. Varley, C.G. Van de Walle, Appl. Phys. Lett. **97** (2010) 211903. DOI: https://doi.org/10.1088/1367-2630/13/8/085014

[12] H. Peelaers, C.G. Van de Walle, Phys. Status Solidi B **252** (2015) 828. DOI: https://doi.org/10.1002/pssb.201451551

[13] T. Onuma, S. Saito, K. Sasaki, T. Masui, T. Yamaguchi, T. Honda, M. Higashiwaki, Jpn. J. Appl. Phys. **54** (2015) 112601. DOI: https://doi.org/10.7567/JJAP.54.112601

[14] E.G. Villora, K. Shimamura, Y. Yoshikawa, K. Aoki, N. Ichinose, J. Cryst. Growth **270** (2004) 420. DOI: https://doi.org/10.1016/j.jcrysgro.2004.06.027

[15] N. Ueda, H. Hosono, R. Waseda, H. Kawazoe, Appl. Phys. Lett. **70** (1997) 3561. DOI: https://doi.org/10.1063/1.119233

[16] K. Hoshikawa, E. Ohba, T. Kobayashi, J. Yanagisawa, C. Miyagawa, Y. Nakamura, J. Cryst. Growth **447** (2016) 36. DOI: https://doi.org/10.1016/j.jcrysgro.2016.04.022

[17] Y. Tomm, P. Reiche, D. Klimm, T. Fukuda, J. Cryst. Growth **220** (2000) 510. DOI: https://doi.org/10.1016/S0022-0248(00)00851-4

[18] Z. Galazka, R. Uecker, D. Klimm, K. Irmscher, M. Naumann, M. Pietsch, A. Kwasniewski, R. Bertram, S. Ganschow, M. Bickermann, ECS J. Solid State Sci. Technol. **6** (2017) Q3007. DOI: https://doi.org/10.1149/2.0021702jss

[19] A. Kuramata, K. Koshi, S. Watanabe, Y. Yamaoka, T. Masui, S. Yamakoshi, Jpn. J. Appl. Phys. **55** (2016) 1202A2. DOI: https://doi.org/10.7567/JJAP.55.1202A2

[20] Y. Kokubun, K. Miura, F. Endo, S. Nakagomi, Appl. Phys. Lett. **90** (2007) 031912. DOI: https://doi.org/10.1063/1.2432946

[21] T. Oshima, T. Okuno, S. Fujita, Jpn. J. Appl. Phys. **46** (2007) 7217. DOI: https://doi.org/10.1143/JJAP.46.7217

[22] K. Sasaki, M. Higashiwaki, A. Kuramata, T. Masui, S. Yamakoshi, J. Cryst. Growth **392** (2014) 30. DOI: https://doi.org/10.1016/j.jcrysgro.2014.02.002

[23] M. Baldini, M. Albrecht, A. Fiedler, K. Irmscher, R. Schewski, G. Wagner, J. Mater. Sci. **51** (2016) 3650. DOI: https://doi.org/10.1149/2.0081702jss

[24] R. Wakabayashi, K. Yoshimatsu, M. Hattori, A. Ohtomo, Appl. Phys. Lett. **111** (2017) 162101. DOI: https://doi.org/10.1063/1.5027005

[25] H. Murakami, K. Nomura, K. Goto, K. Sasaki, K. Kawara, Q.T. Thieu, R. Togashi, Y. Kumagai, M. Higashiwaki, A. Kuramata, Appl. Phys. Express **8** (2014) 015503. DOI: https://doi.org/10.7567/APEX.8.015503

[26] K. Goto, K. Konishi, H. Murakami, Y. Kumagai, B. Monemar, M. Higashiwaki, A. Kuramata, S. Yamakoshi, Thin Solid Films **666** (2018) 182. DOI: https://doi.org/10.1016/j.tsf.2018.09.006

[27] M. Higashiwaki, K. Konishi, K. Sasaki, K. Goto, K. Nomura, Q.T. Thieu, R. Togashi, H. Murakami, Y. Kumagai, B. Monemar, A. Koukitu, A. Kuramata, S. Yamakoshi, Appl. Phys. Lett. **108** (2018) 133503. DOI: https://doi.org/10.1063/1.4945267

[28] Q.T. Thieu, D. Wakimoto, Y. Koishikawa, K. Sasaki, K. Goto, K. Konishi, H. Murakami, A. Kuramata, Y. Kumagai, S. Yamakoshi, Jpn. J. Appl. Phys. **56** (2017) 110310. DOI: https://doi.org/10.7567/JJAP.56.110310

[29] Y. Oshima, E.G. Víllora, K. Shimamura, J. Cryst. Growth **410** (2015) 53. DOI: https://doi.org/10.1016/j.jcrysgro.2014.10.038

[30] K. Nomura, K. Goto, R. Togashi, H. Murakami, Y. Kumagai, A. Kuramata, S. Yamakoshi, A. Koukitu, J. Cryst. Growth **405** (2014) 19. DOI:

https://doi.org/10.1016/j.jcrysgro.2014.06.051

[31] K. Konishi, K. Goto, R. Togashi, H. Murakami, M. Higashiwaki, A. Kuramata, S. Yamakoshi, B. Monemar, Y. Kumagai, J. Cryst. Growth **492** (2018) 39. DOI: https://doi.org/10.1016/j.jcrysgro.2018.04.009

[32] T. Hirasaki, K. Asano, M. Banno, M. Ishikawa, F. Sakuma, H. Murakami, Y. Kumagai, A. Koukitu, Jpn. J. Appl. Phys. **53** (2014) 05FL02. DOI: https://doi.org/10.7567/JJAP.53.05FL02

[33] K. Iso, N. Takekawa, K. Matsuda, K. Hikida, N. Hayashida, H. Murakami, A. Koukitu, Appl. Phys. Express **9** (2016) 105501. DOI: https://doi.org/10.7567/APEX.9.105501

[34] K. Hanaoka, H. Murakami, Y. Kumagai, and A. Koukitu, J. Cryst. Growth **318** (2011) 441. https://doi.org/10.1016/j.jcrysgro.2010.11.079

[35] S. Masuya, K. Sasaki, A. Kuramata, S. Yamakoshi, O. Ueda, M. Kasu, Jpn. J. Appl. Phys. **58** (2019) 055501. DOI: https://doi.org/10.7567/1347-4065/ab0dba

[36] J.B. Varley, J.R. Weber, A. Janotti, C.G. Van de Walle, Appl. Phys. Lett. **97** (2010) 142106. DOI: https://doi.org/10.1063/1.4940444

Chapter 10. Conclusion of Part II

In this study, the capability of THVPE-β-Ga_2O_3 growth was investigated. Thermodynamic analysis revealed the difference in the tendency of the driving force vs. growth temperature, VI/III ratio, and R_{2nd} of Ga_2O_3 growth between by HVPE and by THVPE. The diving force of THVPE-β-Ga_2O_3 growth is lower than that of HVPE at any conditions, and gradually increases with increasing VI/III ratio. Moreover, the driving force of HVPE and THVPE was described by R_{2nd}, and linearly decreases with increasing R_{2nd}. Furthermore, experimentally, it was confirmed the driving force of THVPE was relatively smaller than that of HVPE by changing the R_{2nd} value for the β-Ga_2O_3 growth on the sapphire substrate. Moreover, high crystalline quality and high purity of β-Ga_2O_3 epilayer was obtained by homoepitaxial growth by THVPE. Therefore, THVPE-β-Ga_2O_3 growth was one of the desirable method.

Chapter 11. Discussion throughout Part I and Part II

11.1. Reactivity of raw materials

In chapter 9, the dependence of the VI/III ratio on the growth of β-Ga_2O_3 by THVPE was described, and it was confirmed not only theoretically but also experimentally that the driving force of β-Ga_2O_3 growth by THVPE increased with increasing the VI/III ratio. On the other hand, Hirasaki et al. reported the influence of NH_3 input partial pressure on N-polarity InGaN growth by THVPE.[1] According to this, the growth rate of InGaN by THVPE rarely changed as the V/III ratio increased from 20 to 160. The reactivity of raw materials explains this difference in the tendency on V/III or VI/III. In the InGaN growth by THVPE, the V/III ratio of several decades was enough for raw materials to react. However, in β-Ga_2O_3 growth by THVPE, the VI/III ratio of 60 may not be enough for raw materials to react, and a higher VI/III ratio may be superior to grow β-Ga_2O_3 by THVPE because the growth rate still increases at the VI/III ratio of 60; note that too high VI/III ratio causes the particle generation like HVPE. In the case of applying THVPE for the growth of other compound semiconductors, the reactivity of raw materials must be concerned.

11.2. Adsorption behavior of metal trichloride

Previous studies reported that the bulkiness of metal trichloride, especially gallium trichloride, affects adsorption on the substrate.[2] THVPE-GaN growth has plane selectivity due to the

bulkiness of gallium trichloride, and GaN hardly grows on the Ga-polar substrate but grows on the N-polar substrate.[3] Figure 11.1. shows the crystal structure of GaN having wurtzite. In the case of the GaN growth by THVPE on the Ga-polar substrate, N atoms on the surface of the substrate have three dangling bonds in the *c* direction. According to Hirasaki et al., when one $GaCl_3$ molecule adsorps on the N atom and fills one dangling bond, the other two are hardly adsorped other $GaCl_3$ molecules due to the bulkiness of the $GaCl_3$. On the other hand, in the growth of GaN by THVPE on the N-polar substrate, N atoms on the surface of the substrate have one dangling bond and are free from steric hindrance, resulting in GaN growing only N-polar by THVPE. A similar phenomenon may occur in the case of β-Ga_2O_3 growth by THVPE. β-Ga_2O_3 grows oriented to $(\bar{2}01)$ direction on a sapphire substrate. Under the O-rich condition, the surface of the crystal is covered with O atoms. Ga sites above the surface of the crystal covered with O atoms have two kinds of states; one is the tetrahedral Ga site, and the other is the octahedral Ga site. Moreover, the tetrahedral site has two polarities, tetrahedral-1 and tetrahedral-2 in figure 11.2. (a), like Ga-polar and N-polar of the N site in GaN having a wurtzite structure. If the adatoms of THVPE-β-Ga_2O_3 growth are incorporated in the surface as the same mechanism as THVPE-GaN growth, it is considered that adatoms are hardly incorporated in tetrahedral-1 but easily incorporated in tetrahedral-2 due to the bulkiness of gallium trichloride. On the other hand, it is considered that adatoms are also hardly incorporated in the octahedral site, which is similar to the Ga-polar N site of the wurtzite structure. Therefore, it was thought this structural characteristic, in addition to the driving force, causing the growth rate oriented to $(\bar{2}01)$ of THVPE-β-Ga_2O_3 on the sapphire substrate to be lower than that of HVPE.

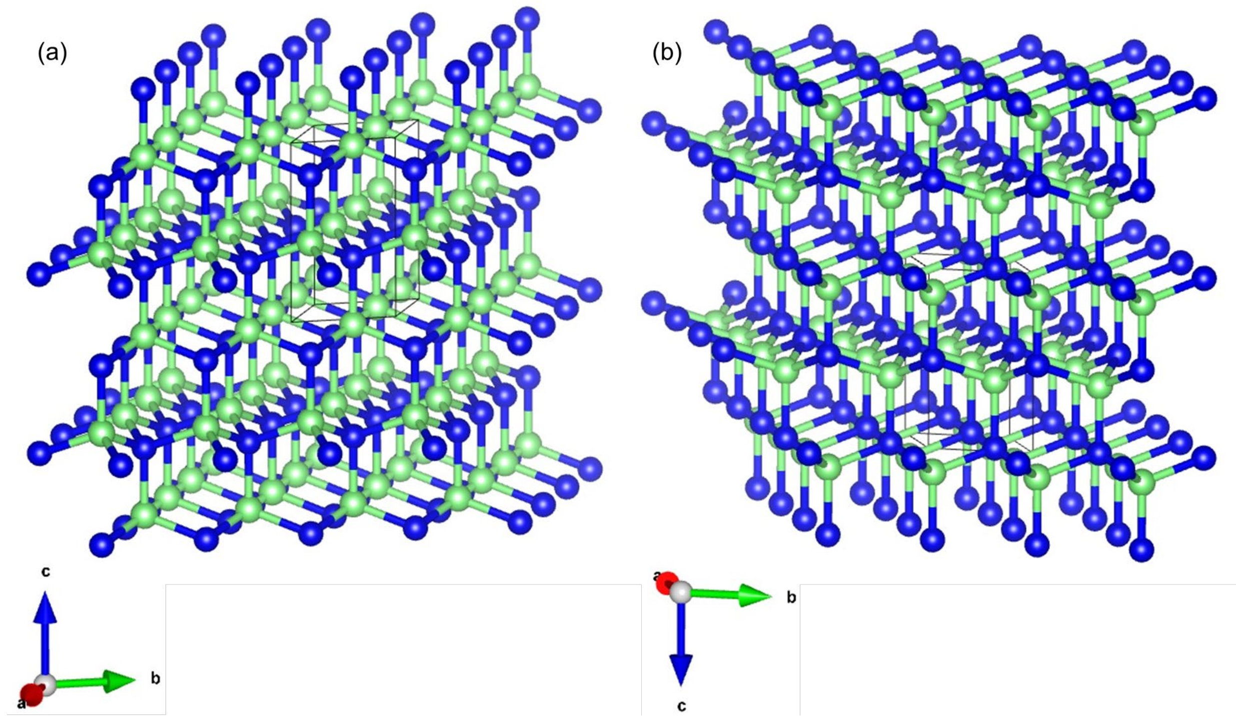

Figure 11.1. Crystal structure of (a) Ga-polar and (b) N-polar GaN. Green and blue ball shows gallium and nitrogen, respectively. The nitrogen atoms have three bond in *c* direction but one bonds in -*c* direction.

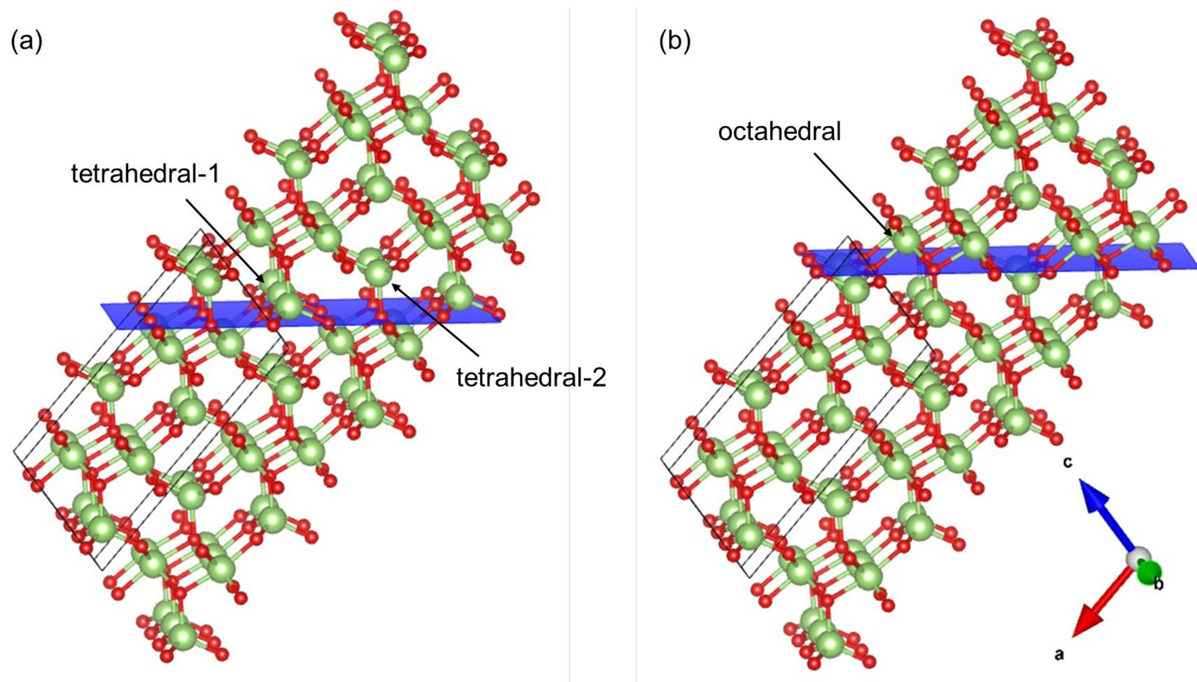

Figure 11.2. Crystal structure of β-Ga_2O_3. Green and red ball shows gallium and oxygen, respectively. Blue plane shows $(\bar{2}01)$ of β-Ga_2O_3. $(\bar{2}01)$ plane having O atoms on the surface next to the octahedral Ga site is shown in (a), and that next to the tetrahedral Ga site is shown in (b).

Reference

[1] T. Hirasaki, T. Hasegawa, M. Meguro, Q.T. Thieu, H. Murakami,Y. Kumagai, B. Monemar, and A. Koukitu, Jpn. J. Appl. Phys. **55**, 05FA01 (2016).

[2] T. Hirasaki, K. Asano, M. Banno, M. Ishikawa, F. Sakuma, H. Murakami, Y. Kumagai, and A. Koukitu, Jpn. J. Appl. Phys. **53**, 05FL02 (2014).

[3] K. Iso, N. Takekawa, K. Matsuda, K. Hikida, N. Hayashida, H. Murakami, and A. Koukitu Appl. Phys. Express **9**, 105501 (2016).

Chapter 12. Conclusion entire this thesis

In this thesis, the possibility of THVPE-InGaN and -Ga_2O_3 growth was investigated.

In Part I, the growth of the lattice relaxed thick InGaN was investigated. Our previous studies revealed the possibility of InGaN growth by THVPE using metal trichlorides, and high-speed InGaN growth was achieved. However, the InGaN epilayer was coherently grown on the N-polar GaN substrate. In this study, to obtain lattice relaxed thick InGaN layer, two approaches were carried out. One is the partially relaxed double intermediate InGaN layer to control lattice relaxation for the growth of fully relaxed $In_{0.05}Ga_{0.95}N$, and by controlling the thickness of the 1st InGaN layer, the lattice relaxation of the 2nd InGaN layer can be controlled. The other is the use of the PSS having a larger lattice mismatch than the GaN substrate to occur lattice relaxation easily, and by inserting the GaN intermediate layer between the InGaN epilayer and the PSS, lattice relaxed thick $In_{0.08}Ga_{0.92}N$ layer with high crystalline quality was obtained.

In Part II, the growth of Ga_2O_3 by THVPE was investigated to suppress the gas-phase reaction using gallium trichloride and O_2 as precursors having low driving force than HVPE. Compared with HVPE, it was revealed that THVPE-Ga_2O_3 growth could decrease particle generation by suppressing the gas-phase reaction at the condition of a higher VI/III ratio.

Throughout Part I and Part II, It was revealed that the THVPE method using metal trichloride had excellent potential to be applied to other compound semiconductors which are hardly grown by HVPE. The scheme of generation of metal trichloride for InGaN growth was able to be also

used for Ga_2O_3 growth. However, the reactivity of raw materials is different even if the same precursor of Group-III is utilized, and the tendency on the V/III or VI/III ratio of THVPE is also distinct for each compound semiconductor. Moreover, the bulkiness of metal trichlorides affects the adsorption of adatoms, especially in the case of being many dangling bonds on the surface of the crystal, and it seems the same tendency between THVPE-InGaN and -β-Ga_2O_3 growth. In order to utilize the THVPE method for more compound semiconductors, it is necessary to consider these reactivity and adsorption behavior which are unique in the THVPE growth.

Acknowledgments

I am glad to acknowledge a number of people who have made it possible to complete this thesis. I would like to express my profound thanks to Professor Hisashi Murakami for his supervision, guidance, support, continuous discussions, helpful suggestions, and encouragement throughout this work. I also would like to express my deepest gratitude to Professor Akinori Koukitu for his supervision, guidance, and support including finances. I am deeply grateful to Professor Yoshinao Kumagai for his beneficial comments and valuable discussion. I also would like to thank Dr. Ken Goto and Nao Takekawa for their help and discussion.

I also express my gratitude Professor Katsuhiko Naoi, Professor Kazuyuki Maeda, and Professor Etsuro Iwama of Department of Applied Chemistry, and Professor Tomo Ueno of Department of Electrical and Electronic Engineering of Tokyo University of Agriculture and Technology for their fruitful comments and helpful suggestions.

I would particularly like to thank Dr. Takahide Hirasaki for his beneficial discussion and encouragement. I could learn a lot of things from him, such as instruction on experimental apparatus design.

I would also like to offer my special thanks to Mr. Tomoyasu Hasegawa, Ms. Misaki Meguro, Mr. Naoya Matsumoto, Ms. Rio Uei, Ms. Mitsuki Kawabe, Mr. Ryohei Hieda, Mr. Naoyuki Ogawa, Ms. Iori Kobaayshi, and Ms. Risa Nagano for their valuable assistance and discussion. I would like to thank Ms. Kimiko Tsuji for her help and warm encouragement. I would also like to thank all the members of Murakami and Kumagai laboratory for their kind support.

List of the papers related to this research

Chapter 3

Influence of intermediate layers on thick InGaN growth using Tri-Halide Vapor Phase Epitaxy

Kentaro Ema, Rio Uei, Hisashi Murakami, and Akinori Koukitu

Japanese Journal of Applied Physics **58**, SC1027 (2019).

Chapter 4

Growth of Lattice-Relaxed InGaN Thick Films on Patterned Sapphire Substrates by Tri-Halide Vapor Phase Epitaxy

Kentaro Ema, Ryohei Hieda, and Hisashi Murakami

Physica Status Solidi A

Chapter 8

Homo- and hetero-epitaxial growth of β-Gallium Oxide via GaCl3-O2-N2 system

Kentaro Ema, Kohei Sasaki, Akito Kuramata, and Hisashi Murakami

Journal of Crystal Growth **564** (2021) 126129.

List of international conference presentations

[1] (Oral) Influence of intermediate layers on thick InGaN growth using THVPE

Kentaro Ema, Rio Uei, Hisashi Murakami, and Akinori Koukitu

International Workshop on Nitride Semiconductors 2018 (IWN2018), Ishikawa, November 2018

[2] (Poster) Growth of lattice-relaxed InGaN thick films by tri-halide vapor phase epitaxy

Kentaro Ema, Rio Uei, Mitsuki Kawabe, Hisashi Murakami, Yoshinao Kumagai, and Akinori Koukitu

OPTICS & PHOTONICS International Congress 2019 (OPIC2019), Kanagawa, April 2019

[3] (Poster) Growth of lattice-relaxed InGaN thick films on patterned sapphire substrates by tri-halide vapor phase epitaxy

Kentaro Ema, Rio Uei, Mitsuki Kawabe, Hisashi Murakami, Yoshinao Kumagai, and Akinori Koukitu

13th International Conference on Nitride Semiconductors (ICNS13th), Seattle, July 2019

Other contributed presentations

[1] (Invited) Recent progress in tri-halide vapor phase epitaxy of GaN-related materials

Hisashi Murakami, Nao Takekawa, Kentaro Ema, Yoshinao Kumagai, and Akinori Koukitu

International Workshop on Nitride Semiconductors 2018 (IWN2018), Ishikawa, November 2018

Awards

[1] 若手ポスター賞

THVPE 法を用いた準安定相 Ga_2O_3 成長における Sapphire 基板面方位が与える影響

江間研太郎, 竹川直, 後藤健, 村上尚, 熊谷義直

第 42 回結晶成長討論会大阪、2019 年 8 月

[2] 講演奨励賞

トリハライド気相成長法による ε-Ga_2O_3 成長の sapphire 基板面方位依存性

江間研太郎、竹川直、後藤健、村上尚、熊谷義直

第 48 回結晶成長国内会議、大阪、2019 年 10 月

[3] 発表奨励賞

$GaCl_3$-O_2-N_2 系を用いた β-酸化ガリウム成長

江間研太郎、小川直紀、佐々木公平、倉又朗人、村上尚

第 12 回ナノ構造・エピタキシャル成長講演会、愛媛(オンライン)、2020 年 7 月